PURDUE UNIVERSITY
GRADUATE SCHOOL
Thesis/Dissertation Acceptance

This is to certify that the thesis/dissertation prepared

By Kyle Conrad

Entitled
A Physics-Based Compact Model for Thermoelectric Devices

For the degree of   Master of Science in Electrical and Computer Engineering

Is approved by the final examining committee:

Mark S. Lundstrom

Ali Shakouri

Timothy S. Fisher

To the best of my knowledge and as understood by the student in the Thesis/Dissertation Agreement, Publication Delay, and Certification/Disclaimer (Graduate School Form 32), this thesis/dissertation adheres to the provisions of Purdue University's "Policy on Integrity in Research" and the use of copyrighted material.

Mark S. Lundstrom

Approved by Major Professor(s): _____

Approved by: Michael R. Melloch   02/03/2015

Head of the Department Graduate Program   Date

A PHYSICS-BASED COMPACT MODEL FOR THERMOELECTRIC DEVICES

A Thesis

Submitted to the Faculty

of

Purdue University

by

Kyle Conrad

In Partial Fulfillment of the

Requirements for the Degree

of

Master of Science in Electrical and Computer Engineering

May 2015

Purdue University

West Lafayette, Indiana

I would like to dedicate this to alot of people:

Jeff, Lindy, Kevin, Wolf, Tor, Mark, Debbie, Brenden, Charley, Levi, Matt, Mike,

Nate, Tristan, and Tyler

ACKNOWLEDGMENTS

First, I would like to thank Professor Lundstrom for all that he has done to help me along the way. From the moment that I walked into his office asking "to get my feet wet" in a research project he has given me incredible opportunities and been a great teacher both inside and outside the classroom. He has always been there to help guide and motivate me along the way, and done so with an excellent attitude that has been a constant source of encouragement.

I would also like to give sincere thanks to Dr. Jesse Maassen. Jesse has been a constant help ever since I started working on my first project. He has been incredibly patient and taught me many things on how to be an efficient researcher. Without his help, encouragement, and guidance I am sure I would still be working on this project. Also, thanks to Dr. Xufeng Wang for his help, especially with using Sentaurus®.

I would like to thank Professor Shakouri, not only for being a member of my advisory comittee, but also for being a resource for discussion regarding thermoelectrics outside of the Lundstrom research group. Thanks also goes to the final member of my advisory comittee, Professor Fisher.

I would like to thank some of my professors from Colorado School of Mines as well. Thanks to Professor Abbud-Madrid, who was my first research advisor and one of the kindest people I have ever met. Thanks to Professor Toberer who introduced me to thermoelectricity and solid state physics for the first time, and whose confidence in me grew confidence in myself.

TABLE OF CONTENTS

LIST OF TABLES

LIST OF FIGURES

ABSTRACT

Conrad, Kyle M.S.E.C.E., Purdue University, May 2015. A Physics-Based Compact Model for Thermoelectric Devices. Major Professor: Mark S. Lundstrom.

Thermoelectric devices have a wide variety of potential applications including as coolers, temperature regulators, power generators, and energy harvesters. During the past decade or so, new thermoelectric materials have been an active area of research. As a result, several new high figure of merit (zT) materials have been identified, but practical devices using these new materials have not yet been reported. A physics-based compact model could be used to simulate a thermoelectric devices within a full system using SPICE-compatible circuit simulators. If such a model accepts measured or simulated material parameters, it would be useful in exploring the system level applications of new materials. In this thesis, the ground work for such a compact model is developed and tested. I begin with a discussion of thermoelectric transport theory within the Landauer formalism. The Landauer formalism is used as the basis of the tool LanTraP, which uses full band descriptions to calculate the distribution of modes and thermoelectric transport parameters, which can serve as the input to a compact model. Next, an equivalent circuit model is presented, explained, and tested using a simple Bi_2Te_3 thermoelectric leg. The equivalent circuit is shown to perform well under a variety of DC, transient, and AC small signal operating conditions. With the equivalent circuit it is easy to determine the maximum cold side temperature drop, the maximum cold side heat absorbed, the temperature profile within the leg, the temperature response to a pulsed current, and impedance over a range of frequencies. Finally, Sentaurus®, a computer program that solves the thermoelectric transport equations numerically, is used to compare and benchmark some of the results of the equivalent circuit when considering Si as the thermoelectric material. The equivalent

circuit and Sentaurus® simulations produce similar results in DC and transient cases, but in the AC small signal case the two simulations produce slight differences. The results of this work establishes a baseline compact model for thermoelectric devices whose accuracy and capabilities can be extended.

1. INTRODUCTION

Thermoelectric materials are able to create an electric potential from a temperature difference, or create a temperature difference from an electric current. Thermoelectric effects are present in every solid-state material, but in good thermoelectrics, the coupling between thermal and electrical characteristics is appreciable and may be used in devices to achieve a variety of goals [1]. Historically thermoelectric devices were limited to niche applications due to their low electro-thermal energy conversion efficiency compared to other technologies. Recently there has been a great deal of interest and progress in increasing the efficiency of thermoelectric devices. With increased device efficiency, thermoelectrics have the potential to be used in a wide variety of applications and make a large impact on the advancement of society as a whole.

Many applications of thermoelectrics are in conjunction with electronic systems, so a consistent design approach would be valuable. For electronic systems, compact models succinctly describe the physics of a device in a way which is compatible with circuit simulation programs like SPICE. Such models not only enable system design, but can also illuminate device physics if they are strongly grounded in physics. Accordingly, a specific goal of this thesis is to develop a physics-based compact model for thermoelectric devices. More generally, this thesis aims to provide a general study of thermoelectric devices in an end-to-end approach, spanning materials and applications.

1.1 Thermoelectricity

Thermoelectric effects refer to a combination of a few phenomena, the discovery and understanding of which began in the 1800s. Thomas Johann Seebeck was the first
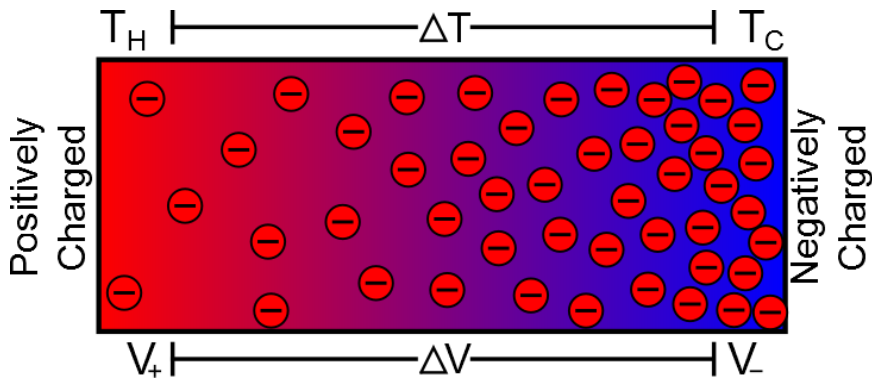
Fig. 1.1. Illustration of the Seebeck effect in an n-type material. Electrons diffuse from the hot side to the cold side, developing a voltage difference.

to present the discovery of a thermoelectric effect in 1820. Seebeck used a loop created by joining two different metals and held the junctions at different temperatures [2]. When a compass needle was brought close to this loop, the needle deflected causing Seebeck to believe that the temperature difference created a magnetic field [3]. Understanding of Ampere's law brought the realization that the temperature difference created a voltage (this phenomena is called the Seebeck effect), which drove a current that induced the observed magnetic field [4].

By maintaining the temperature difference between the ends of a material the more energetic charge carriers on the hot side diffuse to the cold side, which creates the Seebeck voltage (see Fig 1.1) [5]. The ratio of the open-circuit voltage to the applied temperature difference is defined as the Seebeck coefficient (s), an intrinsic material parameter [6].

$$\Delta V = -s\Delta T \tag{1.1}$$

The sign of the Seebeck coefficient depends on charge carrier type in a material: a positive s for holes, and a negative s for electrons. The Seebeck effect is the basis for temperature measuring thermocouples as well as thermoelectric generators (TEGs).

A second important thermoelectric effect was discovered in 1834 when Jean Charles Athanase Peltier found that when a current flowed between two dissimilar metals, heat

was emitted or absorbed at the junction [7]. For a pair of materials heat is emitted when current flows in one direction, and heat is absorbed when current flows in the opposite direction. The rate of heat is proportional to the current flowing through the junction.

$$Q = (\pi_A - \pi_B)I = I\Delta\pi \tag{1.2}$$

The constant of proportionality between the rate of heat absorbed/emitted at a junction (Q) and current is the difference in Peltier coefficients (π), or the difference in the amount of heat carried per charge, for the two materials. If a current is applied in the appropriate direction, the Peltier effect can be used to create a thermoelectric cooler (TEC).

In 1851 William Thomson (who was eventually named Lord Kelvin) observed another thermoelectric effect, which is often referred to as the Thomson effect [8]. As current flows through a spatial temperature gradient within a homogenous conductor, heat is absorbed or released along the length of the conductor. Using thermodynamics Thomson showed how all of the thermoelectric effects can be expressed in terms of the Seebeck coefficient using a set of expressions called the Kelvin relations. The Peltier and Seebeck coefficients are simply related by the temperature.

$$\pi = Ts \tag{1.3}$$

The Thomson effect is a continuous form of the Peltier effect, caused by the temperature dependence of the Seebeck coefficient. The Seebeck coefficient is temperature dependent in most materials, though the Thomson effect is often insignificant [9].

The thermoelectric effects are not the only phenomena occurring within thermoelectric devices. Other processes that often need to be taken into account in a thermoelectric include the Joule effect (also referred to as Ohmic or Joule heating) and heat conduction as described by Fouriers law [8]. Joule heating is the generation of heat as a current I flows through a material of resistance R (where σ is electrical conductivity, L and A are the length and area of the material respectively).

$$Q = I^2R = I^2\frac{L}{\sigma A} \tag{1.4}$$

Fourier's law relates the applied temperature gradient to the heat current density (q) via the thermal conductivity κ.

$$\vec{q} = -\kappa \vec{\nabla} T \tag{1.5}$$

Joule heating and Fourier conduction aren't often considered as thermoelectric effects as they exist appreciably in every electronic material, unlike the thermoelectric effects.

The effects described above can be condensed into a few equations that describe thermoelectric transport in bulk materials for the 1D case [10]. By forcing a current $I_x = A J_x$ (J_x is the current density) through a thermoelectric leg which has a temperature difference between the two ends, a voltage difference can be measured and related to the electric field.

$$E_x = \frac{1}{\sigma} J_x + s \frac{dT}{dx} \tag{1.6}$$

The heat current density can be expressed as a combination of the heat carried by the current (the Peltier effect), and Fourier's law, where the overall thermal conductivity (κ) is the sum of the lattice (κ_l) and electronic (κ_e) thermal conductivities (1.7).

$$q_x = \pi J_x - (\kappa_l + \kappa_e) \frac{dT}{dx} \tag{1.7}$$

These basic equations of thermoelectricity (Eqs. (1.6) and (1.7)) demonstrate how temperature differences produce voltage differences through the Seebeck effect, and how current flow produces temperature differences through the Peltier effect. Another take away is that the thermoelectric equations are all reversible: if the temperature difference or the current flow direction is reversed, the contribution from these effects is reversed as well. Though Eq. (1.7) does not show it, it is important to include the Joule effect contribution to heat flow. When the Joule effect is included, Eq. (1.7) is no longer a linear equation and is no longer reversible.

1.2 Thermoelectric Devices and Applications

Thermoelectric devices are created by connecting a p-type and an n-type thermoelectric legs (also called thermoelements) electrically in series and thermally in parallel
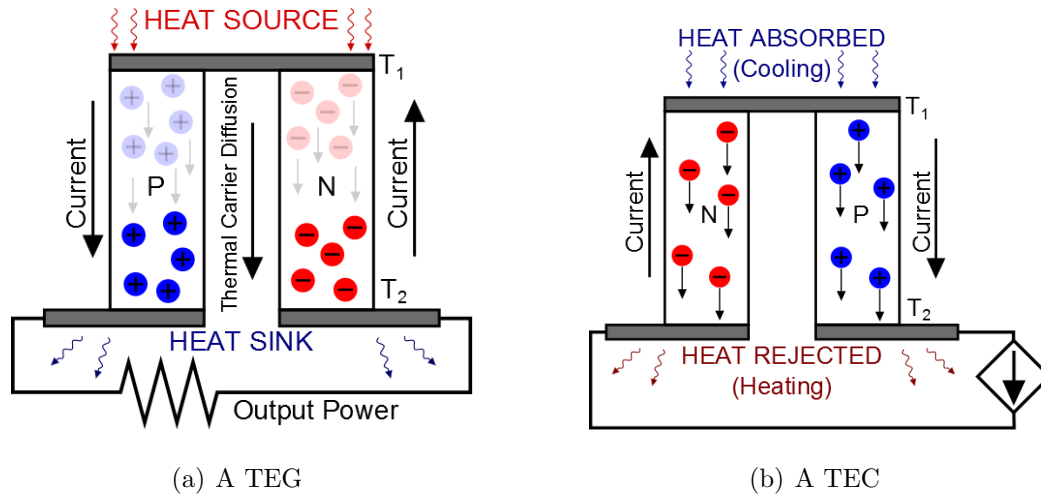
(a) A TEG

(b) A TEC

Fig. 1.2. Illustration of basic thermoelectric devices. **(a)** A TEG operates by the Seebeck effect creating a current which, when connected electrically in series to a load, allows power to be generated. **(b)** A TEC utilizes the Peltier effect where a current drives the charge carriers which carry heat from the top (cold side) to the bottom (hot side).

to form a thermocouple. Combining multiple thermocouples together (again electrically in series and thermally in parallel) creates a thermoelectric module (TEM), which is the common design for most practical devices [5]. In a TEG (Fig. 1.2(a))) a heat source produces a voltage due to the Seebeck effect between the p- and n-type thermoelements. By connecting a resistive load in series with the electrical circuit, the Seebeck voltage delivers power to the load [3]. In a TEC (Fig. 1.2(b)), an external source drives current through the thermoelements. Due to the Peltier effect, the hot side emits heat (often connected to a heat sink) while the cold side absorbs heat (causing cooling).

Simple expressions for device efficiency may be developed by examining a general thermocouple, neglecting the electrical and thermal resistances due to the metallic interconnects, and assuming constant material parameters [11]. The coefficient of

6

performance (COP) for a TEC is the ratio of heat removed at the cold side (Q_C) to the input power (P_{in}), which can be expressed as

$$\text{COP} = \frac{Q_{C,removed}}{P_{in}} = \frac{Z\frac{T_1^2}{2} - (T_2 - T_1)}{ZT_2T_1} \tag{1.8}$$

where T is the temperature shown in Fig 1.2 and Z is dependent only on the p-type and n-type material parameters when the leg dimensions are optimized.

$$Z = \frac{(s_p - s_n)^2}{\left(\sqrt{\frac{\kappa_p}{\sigma_p}} + \sqrt{\frac{\kappa_n}{\sigma_n}}\right)^2} \tag{1.9}$$

Using the same assumptions, the efficiency (η) of a TEG is the ratio of output power (P_{out}) to the input heat (Q_{in}) which can be shown to be

$$\eta = \frac{P_{out}}{Q_{in}} = \frac{(T_1 - T_2)}{T_1} \frac{\left(\sqrt{1 + ZT_m} - 1\right)}{\left(\sqrt{1 + ZT_m} + \frac{T_2}{T_1}\right)} \tag{1.10}$$

where T_m is the mean temperature between the hot and cold side. It is important to notice that both the efficiency of a TEG and the COP of a TEC are related to the same quantity Z. Z is typically multiplied by temperature and ZT is called the unitless thermocouple figure of merit [11]. In order to increase device efficiency it is important to maximize ZT. Often times research focuses on improving a single material at a time, rather than both the p- and n-type materials that make up a thermocouple. For a single material a unitless thermoelectric figure of merit is defined as zT, which is independent of the other material in the thermocouple.

$$zT = \frac{s^2\sigma}{\kappa}T \tag{1.11}$$

After the discovery of the thermoelectric effects, the initial device application was for temperature measurement. It wasn't long before TEGs and TECs were envisioned, and focus shifted to realizing these applications. A first macroscopic model of thermoelectric devices was developed by Edmund Altenkirche by assuming that the Seebeck coefficient, electrical conductivity, and the thermal conductivity were constant values throughout the device [8]. With this assumption Altenkirche was able

to predict the efficiency of a TEG (in 1909) and the COP of a TEC (in 1911). Using transport parameters of metals (the only available material at the time) Altenkirche predicted low efficiency for generators and an inefficient COP for cooling [3]. Because they are solid-state devices and therefore incredibly reliable, durable, and scalable, TEGs were especially desirable devices [12]. Despite the low generator COP metallic thermoelectric generators were being designed for military applications by the 1920s, though the efficiencies never exceeded 0.6% [3].

In 1929 Abram Fedorovich Ioffe (the developer of modern thermoelectric theory based around the figure of merit shown above) proposed using semiconductors as opposed to metals as thermoelectric materials [8]. At the time semiconductors were a new class of material, and Ioffe predicted an efficiency of 2.5 to 4% by using semiconducting thermoelements in a TEG [3]. PbS was an initial candidate material and in 1940 a PbS TEG reached 3% efficiency. The first application of the PbS TEG was powering a USSR military radio station, supplying 12 W for 400 hours.

Ioffe also showed that using semiconductors TEC efficiency became large enough for practical application. In the 1950s Ioffe organized a group to develop and successfully manufacture TECs by exploring applications with PbTe. The TECs developed by Ioffe's group would last for 20 years before failing [8], an early demonstration of thermoelectric reliability. Along with the development of PbTe in the USSR, in England Julian Goldsmid developed Bi_2Te_3 materials which are still a standard material for thermoelectric devices [13].

Goldsmid and Ioffe used materials with initial $zT \approx 0.5$ and developed them (often through alloying with other metals) to have $zT \leq 1$, creating optimism for the application of thermoelectric devices. But with no increases beyond $zT = 1$ and material discovery lacking, the field stagnated by the 1970s [1]. Although thermoelectrics were not efficient enough to replace their established commercial counterparts, they were used in certain niche applications. The advent of sub 0 ^{o}C cooling [4] created some use in home refrigeration as well as coolers for infrared sensors [1]. TEGs found some use in places where a constant reliable power generation was required. One of the

most common and consistent uses for TEGs since the 1960s has been in Radioisotope Thermoelectric Generators (RTG). In RTGs thermoelectric legs surround a radioactive element (typically plutonium) and create a steady source of power from the heat emitted. RTGs have been used a great deal in satellites and rovers for space exploration, such as the Voyager satellite missions (1977) and the Mars Curiosity Rover (2009) [14].

Present day thermoelectric devices are used to keep laser diodes at constant temperatures, thermally cycle enzyme reactions for DNA testing, vehicle seat climate control, and powering remote data systems [7]. Using thermoelectric generators in automobile exhaust has been prototyped and is considered to be one of the most promising advances for cars in the future [15]. As higher zT materials become available, existing device applications become more efficient, as well as new applications becoming practical.

Standard semiconductor processing techniques allow small scale thermoelectric fabrication with short thermal response times, creating unique applications to be explored. Thermoelectric devices may be included in integrated circuits as hot-spot coolers, which can provide thermal management allowing for faster clock speeds and longevity in microprocessors [7].

Another potential application for thermoelectrics is in biomedical devices. Thermoelectrics have already found biomedical applications in DNA testing, portable medicine coolers, and imaging devices. The previously pursued biomedical devices used thermoelectrics for their solid-state advantages, not necessarily thermoelectric efficiency. Now the efficiency of thermoelectric devices and advances in biomedical engineering are at a place for thermoelectric energy harvesters to power wireless sensors and implantable devices [16]. Using the temperature difference between skin and the air, for example, a TEG is able to create an output of 1.2 V [17].

Developing higher performance thermoelectric energy harvesters for a sustainable energy future is a major focus of present day materials research. About 78% of energy production in the United States is from fossil fuels [18] and over 60% of en-

ergy produced from these sources is lost as waste heat [19]. Applying thermoelectric devices to recover waste heat from energy generation, home heating, or other industrial processes could provide a clean source of alternative electricity. Other proposed energy applications are to use thermoelectric devices as co-generators, such as in a photovoltaic/thermoelectric system.

Though high zT materials have been achieved, few have made impact on mass produced thermoelectric devices. Most of the delay in moving high zT materials to market has been due to difficulties in scaling materials, which are often thin films, to bulk [1]. While industry waits for high zT material production and application to be profitable, another method to increase device efficiency is to optimize design to reduce parasitic losses [7]. By creating efficient materials and devices, thermoelectric devices may find widespread application in the modern, and future, world.

1.3 Modern Thermoelectric Materials

It is easy to examine (1.11) and realize that increasing electrical conductivity and Seebeck coefficient, or decreasing thermal conductivity will increase the figure of merit. As simple as it sounds, improving zT is actually a difficult task, as s, κ, and σ are all interrelated [12]. Parameters such as effective mass, carrier concentration, and electron thermal conductivity need to be balanced to create an optimum thermoelectric material. To illustrate these issues, consider the expression for Seebeck coefficient in a parabolic band degenerate semiconductor

$$s = \frac{8\pi^2 k_b^2 m^* T}{3eh^2} \left(\frac{\pi}{3n}\right)^{2/3} \tag{1.12}$$

where m^* is the effective mass and n is the carrier concentration [12]. The Seebeck coefficient is large with small carrier concentration, and increases with effective mass. Examining the Drude expression for conductivity (Eq. (1.13)) shows an opposite behavior compared to s: increasing the carrier concentration and/or decreasing the effective mass increases the electrical conductivity [20].

$$\sigma = \frac{ne^2\tau}{m^*} \tag{1.13}$$

The other parameter to consider in zT is thermal conductivity, which is the sum of lattice and electronic thermal conductivities. Electrical conductivity and the electronic thermal conductivity are related by the Wiedmann-Franz relationship, showing that both are related through the temperature and the Lorenz number L_0, which is nearly constant in many cases [6].

$$\kappa_e = L_0 \sigma T \qquad (1.14)$$

Typically in semiconductors, the lattice thermal conductivity (due to phonons) is larger than the electronic thermal conductivity. By minimizing the lattice contribution to thermal conductivity the overall material zT increases, but it is important not to hinder electron transport too much in the process. This leads to the idea that an ideal thermoelectric material behaves as a "phonon-glass electron-crystal", where phonon transport is difficult (as in a glass) while the electrons are easily transported (as in a crystal) [21].

After decades of stagnation thermoelectric research received a boost in 1993 when Hicks and Dresselhaus predicted large increases in zT by creating quantum-well superlattices [22]. This prediction focused on improving the electronic performance by utilizing quantum confinement effects. While a high zT material originating from this idea has not been conclusively demonstrated, nano-structured materials have shown great advances. This success has been mainly achieved through a reduction in thermal conductivity [12], which is prominent in small-material structures. The tone of thermoelectric research had changed: rather than exploring traditional bulk thermoelectric materials, nano-engineering could be used to design better thermoelectric materials.

Though not as effective, bandstructure engineering to improve the electronic performance has still increased zT in some materials. Current methods of bandstructure engineering include converging multiple valleys, distorting the density of states near the Fermi level with dopants, and by minimizing bipolar transport. The goal of these methods is to increase the power factor ($s^2\sigma$) through modifications of the electronic structure [19].

A common feature of high zT materials is a low lattice thermal conductivity. The lattice thermal conductivity can be further reduced by enhancing phonon scattering. The more phonons that are scattered, the lower the thermal conductivity will become. The most common method of scattering is by point defects, such as doping or alloying, which scatters short wavelength phonons. Nanoparticles embedded in a host thermoelectric material can also act as scatterers, and affect the low to mid wavelength phonons depending on the coherence between the particles and the lattice. Meso-scale scattering occurs at grain boundaries and scatters the long wavelength phonons. Combining bandstructure engineering with phonon scattering at all relevant length scales is called the panoscopic approach, and has lead to some of the highest reported zT values to date [19].

This panascopic approach was successfully demonstrated with a PbTe-based thermoelectric material. PbTe-based systems reached $zT = 1.8$ purely through the bandstructure engineering techniques mentioned above, with no intentional reductions to lattice thermal conductivity [19]. It has been shown that nearly 25% of PbTe lattice thermal conductivity is due to phonons with less than 5 nm mean free paths, 55% by phonons with between 5 and 100 nm mean free paths, and about 20% by 0.1 to 1 μm mean free paths. By scattering phonons at these lengths, thus invoking the panascopic approach, a PbTe-based thermoelectric material reached zT of about 2.2 [19].

1.4 Discussion

The field is currently focused on creating high zT materials at a range of temperatures to enable a variety of applications. Recently a new high zT of 2.6 was experimentally demonstrated at 923 K in bulk SnSe crystals, a material which had been overlooked as a thermoelectric until recently [23]. This work, like most other experimental work, focuses only on the material itself. It is important to optimize design and minimize the parasitic resistances that arise at the device level [7].

It is important to note that thermoelectric material parameters are temperature dependent, so certain materials are better suited for a certain temperature range than others. The temperature ranges typically considered are the cryogenic range (4 to 250 K), near room-temperature (250 to 500 K), mid temperature (500 to 900 K), and high temperature (those greater than 900 K) [19]. Thermoelectric material selection for devices varies based on the temperature range the device will operate in. It is important not just to have a large zT, but a large zT in the temperature range of interest for efficient devices.

Theoretical work in thermoelectrics is often focused on first principles calculations of material properties. First principle calculations are helpful to predict material properties and guide experimental research for new and existing materials. The benefits of the theoretical calculations is evident, however such approaches are not commonly connected to higher level device and system performance metrics.

Often times, thermoelectric devices are embedded within electric circuits. Especially in the cases of automotive exhaust generators (where the generator powers some of the electronics of a car), optoelectronic coolers, microprocessor hot spot cooling, and biomedical energy harvesters the thermoelectric device is linked with a potentially complex circuit. To efficiently incorporate thermoelectric devices the device and circuit should be co-optimized.

SPICE (Simulation Program with Integrated Circuit Emphasis) is a circuit simulation framework that is often used in system design as well as to check circuit behavior. SPICE is an industry standard to verify performance before committing to the cost of manufacturing a complex integrated circuit. A compact model captures the complicated behavior of a device, and makes it simple to include into a SPICE circuit simulation. A physics based, SPICE compatible, compact model for thermoelectric devices would be useful to address the gap between current thermoelectric research and system level device performance. Such a compact model would make circuit and device co-design simple and predict how effective a variety of applications may become.

1.5   Organization of Thesis

In this Thesis, I will present a study of thermoelectric devices in an end to end approach. The goal is to aid and expedite the transition from thermoelectric materials research to device performance to overall system optimization. The organization of this Thesis is as follows:

In Chapter 2, thermoelectric theory will be explained. The theoretical approach used is based on the Landauer formalism which will be briefly described in the context of an elastic resistor. Thermoelectric effects will then be considered within this formalism. The overall thermoelectric performance will be explained in a physical picture.

Chapter 3 will introduce the nanohub tool LanTraP, which is used to calculate transport coefficients from a dispersion relation. LanTraP is similar to the program BoltzTraP, though the calculation is done in the Landauer formalism. An advantage of Lantrap is that it is free to use and can be simply accessed through a web browser.

In Chapter 4 a SPICE-compatible equivalent circuit which can model thermoelectric devices will be presented. The individual components of the equivalent circuit will be explained and related to the physical picture of a thermoelectric device. The model will be tested using a Bi_2Te_3 thermoelement under DC, transient, and small signal AC bias to prove its validity.

Chapter 5 will provide a benchmark for the equivalent circuit using Sentaurus® device simulator. The equations Sentaurus® solves and how to prepare a constant material parameter simulation is explained. Sentaurus® will be used to simulate a thermoelement under the same biasing as the equivalent circuit, and the results will be compared.

2. THERMOELECTRIC THEORY

In this Chapter, we present a synopsis of thermoelectric theory within the Landauer approach for electron and phonon transport [24]. There are many books and review articles that discuss thermoelectric transport theory (e.g. [10] and [25]). The advantages of the Landauer approach are physical clarity, applicability to both electron and phonon transport, applicability from the diffusive to ballistic limits, and its clear connection to other approaches to the Boltzmann Transport Equation for semiclassical transport and to the non-equilibrium Greens function approach to quantum transport [26]. Expressions for the thermoelectric parameters will be presented. The origin of the thermoelectric effects and the physical significance of the expressions for the thermoelectric transport parameters will be discussed. For a more extensive discussion, see Ref. [24] and the online course, *Thermoelectricity: From Atoms to Systems* [27]. The goals of this chapter are to help readers develop a clear understanding of the physics of thermoelectricity and the expressions used to relate the thermoelectric parameters in the SPICE-compatible equivalent circuit (presented in Chapter 4) to the properties of the thermoelectric material.

2.1   The Landauer Approach for Electrons

By considering a simple, elastic resistor and the Landauer-Boltzmann expression for current, key concepts for thermoelectric transport can be explained. This approach is sometimes called the bottom-up approach, since the explanation begins by considering a nanoscale device. After the picture of a nanoscale device becomes clear the device is made larger so the concepts can be extended and applied to a bulk device. The following discussion will focus on the conduction band electrons inside a device, but it is important to realize that the same principles can be applied to valence
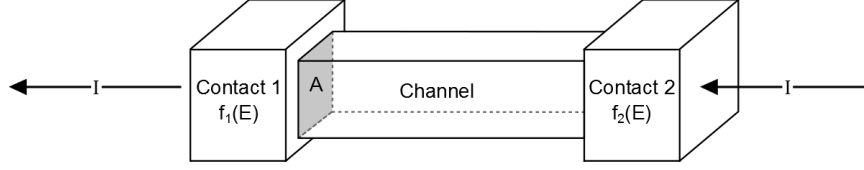
Fig. 2.1. An electronic Landauer device. The two contacts are defined by their equilibrium Fermi function which is determined by the Fermi level and temperature within each contact.

band electrons (holes). (The expressions used to describe thermoelectric conduction and valence bands are identical.)

The device to be considered in this chapter is a resistor (Fig. 2.1), with two contacts on either side of a channel. The contacts are large and dominated by inelastic scattering so that they maintain thermodynamic equilibrium. Each contact therefore has a well defined Fermi level (E_{F1} for contact 1 and E_{F2} for contact 2) which, along with temperature, defines the electron occupancy at an energy E through the Fermi function f (k_B is Boltzmann's constant, and T is the temperature of each contact).

$$f_0(E) = \frac{1}{1 + e^{\frac{E - E_F}{k_B T}}} \tag{2.1}$$

Both contacts are assumed to be perfectly absorbing, meaning that any electron that reaches a contact will enter the contact and instantly scatter to equilibrate with the Fermi level in the contact.

The channel itself is dominated by elastic scattering: the electrons don't change energy as they travel from one contact to another. Changes in momentum may occur, but the momentum changes do not change the total energy of the electron. The channel is characterized by its band structure $E(k)$.

The Landauer expression for current can be written as

$$I = \frac{2q}{h} \int \bar{T}(E) M(E) (f_1 - f_2) \mathrm{d}E, \tag{2.2}$$

where the symbol $\bar{T}(E)$ is the transmission and $M(E)$ is the number of modes. The transmission is the probability that an electron entering the channel from one contact,

leaves the channel through the other contact. With L being the length of the channel and $\lambda(E)$ being the mean-free-path for backscattering (how far an electron travels before scattering in the opposite direction), the transmission can be written as

$$\bar{T}(E) = \frac{\lambda(E)}{\lambda(E) + L}. \tag{2.3}$$

The transmission is a value between 0 and 1, and represents how diffusive or ballistic the movement of electrons is at each energy level. In the ballistic case, the mean-free-path is much larger than the length of the channel so $\bar{T}(E) \approx 1$. In the diffusive case, the channel length is much larger than the mean free path, so the transmission tends toward $\frac{\lambda}{L}$, which is very small.

The number of modes (also called the number of conducting channels) is proportional to the density of states (the number of available states per unit energy) and the average forward moving velocity in the transport direction.

$$M(E) = \frac{h}{4}\Big\langle v_x^+(E)\Big\rangle D(E) \tag{2.4}$$

Both the density of states and the velocity are determined by the dispersion relation in the channel. Qualitatively, the number of modes is analogous to the number of lanes on a highway. The more modes, the more channels for electrons to flow at an energy E. The number of modes is also the number of electron half wavelengths that can fit in the dimensions perpendicular to transport. With this last explanation of the number of modes, it makes sense that larger devices will have a larger number of modes, and that dimensionality (1D, 2D, or 3D) will also change the number of modes.

Equation (2.2) shows that current flows due to a difference in Fermi functions between the two contacts. This can be interpreted as follows. The contact with the higher Fermi energy has a larger, or equal, Fermi function at the energy of interest, E. This contact tries to fill states at energy E, in the channel up with electrons. The other contact, which has a smaller Fermi function, also tries to fill the channel according to its Fermi function. Since the second contact has a smaller Fermi function

at certain energies, this contact empties the states in the channel. Current occurs from the constant filling of states from the first contact and the emptying of states into the second contact. In the case where the difference in Fermi levels is due to an applied voltage (and temperature is held constant), and the voltage is small, the difference in Fermi levels may be approximated by Eq. (2.5).

$$f_1 - f_2 \approx -\frac{\partial f_0}{\partial E} qV \tag{2.5}$$

Similarly, the difference in Fermi functions may be approximated for small temperature difference by Eq. (2.6).

$$f_1 - f_2 \approx -\left(-\frac{\partial f_0}{\partial E} \right) \frac{E - E_F}{T} \Delta T \tag{2.6}$$

In both these approximations the so-called Fermi window $\left(-\frac{\partial f_0}{\partial E} \right)$ replaces the difference in Fermi functions in Eq. (2.2). The Fermi window represents the energy range within which electrons are able to flow. The difference between good and bad conductors is the number of modes that are available within the Fermi window.

Plots of Fermi function difference as a result of an applied voltage is shown in Fig. 2.2(a), while the difference as a result of a temperature difference is shown in Fig. 2.2(b). By applying a voltage the Fermi level of one of the contacts moves relative to the other. The sign of the difference in Fermi functions between the two contacts is therefore always either positive or negative in the applied voltage case. By applying a temperature difference, the width in energy of the Fermi function transition between one and zero is different for the two contacts. As a result the difference in Fermi functions changes sign on either side of the Fermi energy. The sign of the difference in Fermi functions is what causes n-type materials to have a negative, and p-type to have a positive, Seebeck coefficient.

The Landauer formalism gives an accurate view of how current flows. Thus far no assumptions need to be made about dimensionality or transport regime. The number of modes is impacted by the variability in dimensionality (1D nanotube, 2D thin film,

(a) Applied ΔV (b) Applied ΔT
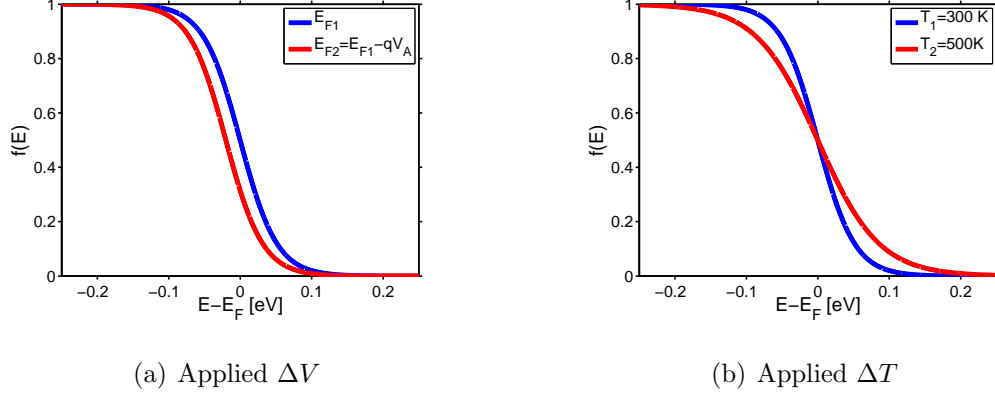
Fig. 2.2. The Fermi function differences with applied voltage and temperature difference. **(a)** An applied voltage creates a constant difference in Fermi functions, **(b)** while a temperature difference creates both a positive and negative region for Fermi function difference.

or 3D bulk material). The transmission captures the type of transport, ranging from ballistic to diffusive. With this established formalism, expressions for the transport coefficients can be determined.

2.2 Thermoelectric Transport Parameters for Electrons

Within the linear response regime (i.e. $f_1 \approx f_2$) the conductance (G), Seebeck coefficient (s), and the electronic thermal conductance (K_e) can all be written in terms of an integral H of order j [28].

$$G = \frac{2q^2}{h} H_0 \tag{2.7}$$

$$s = -\frac{k_B}{q} \frac{H_1}{H_0} \tag{2.8}$$

$$K_e = \frac{2k_B^2 T}{h} \left(H_2 - \frac{H_1^2}{H_0} \right) \tag{2.9}$$

$$H_j = \int \left(\frac{E - E_f}{k_B T}\right)^j \bar{T}(E) M(E) \left(-\frac{\partial f_0}{\partial E}\right) dE \tag{2.10}$$

The inclusion of the integral H, though different orders are used, illustrates how interrelated these coefficients are, which is a major reason for the difficulty of making high zT thermoelectric materials.

Besides the transmission and the number of modes, the integral H is affected by the location of the Fermi level. Depending on the location of the Fermi level, both the heat carried by electrons and the position of the Fermi window changes. When the Fermi level is a few $k_B T$ below the conduction band (or above the valence band) the material is non-degenerate (this is often the case for a semiconductor). When the Fermi level is deep inside a band, the material is degenerate (this is the case for a metal or a heavily doped semiconductor). In a semiconductor, the location of the Fermi level can be set by doping or by controlling the density of various defects (e.g. vacancies, anti-site defects, etc.). The location of the Fermi level can be deduced from carrier concentration measurements (e.g. Hall effect measurements). It is important to remember that it is the Fermi level that is fundamentally important in transport calculations, not the carrier concentration.

Examining a band diagram (Fig. 2.3) is useful to explain the Peltier effect, and consequently the Seebeck effect. Assuming an n-type material, then the states that are important to conduction, as defined by the Fermi window, are those near the bottom of the conduction band. In a non-degenerate semiconductor, the conduction band lies above the Fermi level, so for an electron to leave the contact, it must absorb energy. The energy absorbed by the electron is the difference between the average energy in the channel which current flows in and the Fermi level of the contact. This energy absorption is Peltier cooling, because energy is being drawn from the environment to allow a current to flow. At the other end of the device, the opposite effect occurs; the electrons are at an energy above the Fermi level in the 2nd contact and so they emit energy, therefore heating the surroundings. This is Peltier heating.
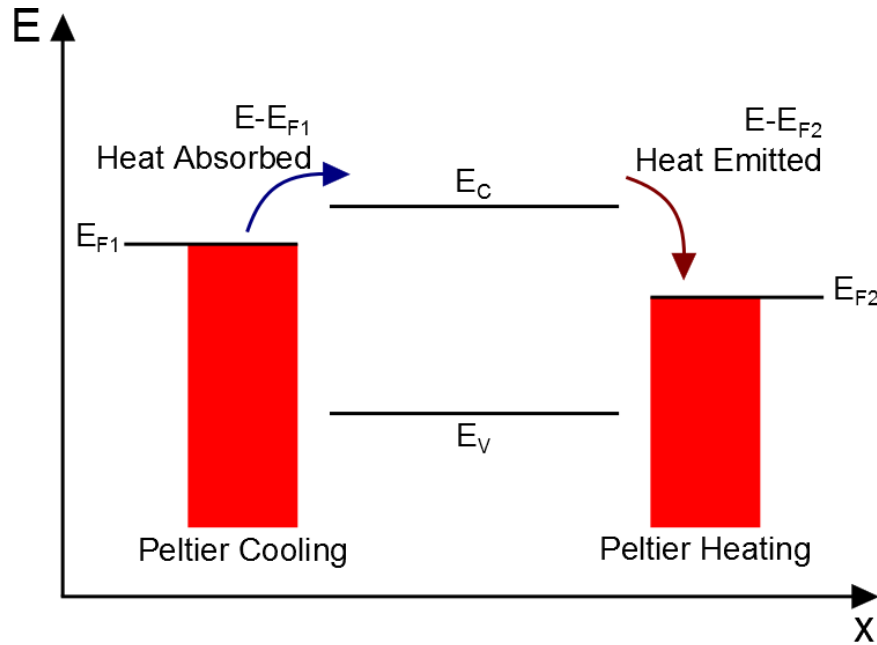
Fig. 2.3. The Peltier effect. Electrons need to absorb energy to move from the left contact into the channel of energy E. The electrons travel in this energy channel until they reach the right contact where they will emit energy to the contact.

Note that the effect is reversible if we change the sign of the applied bias, the location of the Peltier cooling and heating switches.

Examining Eqs. (2.8) and (2.10) shows that the Seebeck coefficient is the energy of electrons relative to the Fermi level, weighted and normalized by the conductance. The Seebeck coefficient is thus a measure of the average energy at which current flows relative to the Fermi level. The Fermi level is therefore important in determining the magnitude of the Seebeck coefficient, while the sign is dependent on the material type (n or p type). It is important in a thermoelectric material for current to flow predominantly above or below the Fermi level, which explains why metals are poor thermoelectrics. Metallic bands are degenerate, so the states available for transport are near the Fermi level, and the magnitude of the Seebeck coefficient is small as a result.

This discussion of the electronic contribution to thermoelectric parameters, has assumed electrons in the conduction band. Electrons in the valence band (holes) would behave in a similar way, the major difference being that the sign of the charge (and, therefore, the sign of the Seebeck coefficient) changes. In a case where both the electrons and holes contribute, Eqs. (2.7)-(2.10) still apply because the integrals are taken over all energy. Just as the density of states has an energy gap where no states exist, the number of conducting channels does as well. It is therefore mathematically equivalent to consider all energies at once, or to consider the conduction and valence bands separately, and then add the effects. The difference in sign between the two bands brings to light an important criterion in enhancing thermoelectric materials: bipolar transport must be suppressed. With both bands conducting, the total conductance increases and the total Seebeck coefficient decreases.

2.3   The Landauer Approach for Phonons

Thus far we have neglected the lattice in the thermoelectric effects. The lattice carries heat due to the lattice vibrations, which are treated as particles called phonons. For metals, the electrons carry most of the heat ($\kappa_e >> \kappa_l$), but for semiconductors and insulators it is the phonons which are responsible for the majority of the heat transport.

An important difference between electrons and phonons is that phonons are not fermions, and so the equilibrium occupation function is a Bose-Einstein distribution,

$$n_0(\hbar\omega) = \frac{1}{\mathrm{e}^{\frac{\hbar\omega}{k_B T}} - 1}. \tag{2.11}$$

Since phonons are bosons, there is no Fermi level in the occupation function, instead the distribution is only modified by temperature. Both electrons and phonons in a crystal are defined by a dispersion that is periodic in a Brillouin zone. The electron dispersion is a plot of electron energy vs. wavevector, and the phonon dispersion is a plot of phonon frequency vs. wavevector. The two are equivalent because $E = \hbar\omega$.

Similar to electron transport, phonon transport can be treated within the Landauer approach. Again the ideas will be made clear by thinking of a thermal resistor. The two contacts on both sides of the channel are each in equilibrium with their respective temperatures and can be described by the occupation functions, n_1 and n_2. The heat current for phonons is similar to electrical current for electrons, but rather than charge, the energy of oscillation ($\hbar\omega$) is transported. The lattice heat current, analogous to the electric current in Eq. (2.2) is given by

$$Q = \frac{1}{h} \int \hbar\omega \bar{T}_{ph}(\hbar\omega) M_{ph}(\hbar\omega)(n_1 - n_2)\mathrm{d}(\hbar\omega). \tag{2.12}$$

where Q depends on the phonon transmission and number of modes, which are functions of frequency (or energy). The electron modes are determined by the electron dispersion, and the phonon modes are determined by the phonon dispersion, which is different from the electron dispersion. Both electron and phonon transmission can be described by Eq. (2.3), but the mean-free-paths for electrons and phonons are different because they are, in general, determined by different scattering processes.

As for electron current, the heat current is driven by the differences in equilibrium occupation functions of the two contacts. In the linear response regime ($n_1 \approx n_2$, which means $T_1 \approx T_2$), the difference in Bose-Einstein distribution of the contacts can be approximated in a similar method as for electrons. We find

$$n_1 - n_2 \approx -\frac{\hbar\omega}{T}\left(-\frac{\partial n_0}{\partial(\hbar\omega)}\right)\Delta T. \tag{2.13}$$

The linear response regime for phonon transport also involves a window function, in this case $\left(-\frac{\partial n_0}{\partial(\hbar\omega)}\right)$. This is the frequency range in which phonon conduction will occur. By normalizing the window function (resulting in the term within curly brackets in Eq. (2.14)) and writing $Q = K_l \Delta T$, the thermal conductance for phonons (K_l) can be expressed as

$$K_l = \frac{\pi^2 k_B^2 T}{3h} \int \bar{T}_{ph}(\hbar\omega) M_{ph}(\hbar\omega)\left\{\frac{3}{\pi^2}\left(\frac{\hbar\omega}{k_B T}\right)^2\left(-\frac{\partial n_0}{\partial(\hbar\omega)}\right)\right\}\mathrm{d}(\hbar\omega). \tag{2.14}$$

One of the major differences between phonons and electrons is the width of the dispersion in energy. For electrons, the dispersion is several tens of eV wide, while the dispersion for phonons is several a tens of meV wide. The width of the window functions are very similar, so the window function for electrons at 300 K only involves states near the band edge while the window function for phonons at 300 K typically involves phonon states across the entire bandwidth. The number of channels available for conduction can often be accurately approximated for electrons with a parabolic band, but for phonons, a full band dispersion is often required.

2.4   Relating to Devices

Thermoelectric devices are typically composed of bulk materials where the length is many times longer than the mean free path. The transmission function for a diffusive material reduces to $\lambda(E)/L$, and rather than thinking of conductances, $G, K_e,$ andK_l, it is easier to think of conductivities, σ, κ_e, and κ_l. The bulk transport parameters can be written in terms of the differential conductivity, $\sigma'(E)$, as

$$\sigma'(E) = \frac{2q^2}{h}\lambda(E)\frac{M(E)}{A}\left(-\frac{\partial f_0}{\partial E}\right) \tag{2.15}$$

$$\sigma = G\frac{L}{A} = \int \sigma'(E)\mathrm{d}E \tag{2.16}$$

$$s = -\frac{1}{qT}\frac{\int(E-E_F)\sigma'(E)\mathrm{d}E}{\int \sigma'(E)\mathrm{d}E} \tag{2.17}$$

$$\kappa_e = K_e\frac{L}{A} = -T\sigma s^2 + \frac{1}{q^2T}\int(E-E_F)^2\sigma'(E)\mathrm{d}E \tag{2.18}$$

$$\kappa_l = K_l\frac{L}{A} = \frac{1}{h}\int\frac{(\hbar\omega)^2}{T}\lambda_{ph}(\hbar\omega)\frac{M_{ph}(\hbar\omega)}{A}\left(-\frac{\partial n_0}{\partial(\hbar\omega)}\right)\mathrm{d}(\hbar\omega). \tag{2.19}$$

Equations (2.16)-(2.19) are the thermoelectric transport parameters in a form that is typically used by the thermoelectric community.

The results presented here came from a Landauer formalism, though typically thermoelectric parameters are found by solving the Boltzmann Transport Equation. The Boltzmann Transport Equation relies on integrals similar to Eqs. (2.15)-(2.19), but uses a transport distribution function that lumps together the band structure information as well as scattering effects. In the Landauer approach, the transport distribution is replaced by the number of modes and the mean-free-path for backscattering. In the diffusive transport regime, under the relaxation time approximation the results from these two methods are equivalent, but the Landauer approach provides a simple, physical interpretation of the transport distribution is it simply the product of the number of channels at energy E, and the mean-free-path for backscattering at the same energy. It is particularly easy to compute $M(E)$ from a given band-structure (either an analytical one or an ab initio calculation). See Chapter 3 for a description of LanTraP, a tool for calculating Modes and transport paramaters from a bandstructure, that has been developed by the author and deployed on nanoHUB.org.

As shown in Chapter 1, thermoelectric device performance is determined by the efficiency of the materials used in the device. The material figure of merit, zT, was defined in Eq. (1.11). Examining the material figure of merit in the context of the transport parameter definitions above, we can specifically identify the factors that lead to better thermoelectric materials.

The power factor $(s^2\sigma)$ should be maximized to increase zT. Both conductivity and Seebeck coefficient are determined by the location of the Fermi level. In order to obtain a large conductivity, the Fermi window should overlap in energy where there are a large number of modes. For the Seebeck coefficient to be large, there should be a difference in the energy that the current flows at and the Fermi energy. Therefore the ideal location of the Fermi level to be just below (for n-type) or above (for p-type) the band edge. A qualitative plot of the power factor, Seebeck coefficient squared, and conductivity is shown in Fig. 2.4. In general the best band structure will have a large number of channels near the band edge without decreasing the mean free path.
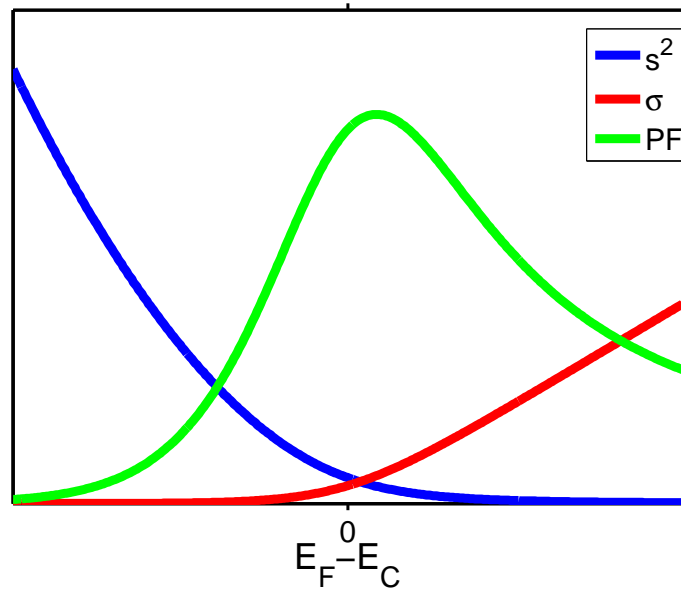
Fig. 2.4. A qualitative plot of power factor vs. Fermi level in the conduction band. The conductivity increases as the Fermi level gets further into the band, while the Seebeck increases as the Fermi level goes deeper into the band gap. Overall the power factor is maximized near the band edge.

Reducing dimensionality has been suggested as a method to ensure that there are a large number of modes near the band edge. By switching to lower dimensions, the maximum power factor occurs with a lower Fermi level, translating to a larger Seebeck coefficient. A 1D nanotube is able to increase s^2 by 40% compared to 3D, though in order for this to be realized the conductivity needs to be maintained [29]. To maintain a high conductivity the nano tubes would need to be densely packed, which is a difficult task. The advantages of reduced dimensionality have been difficult to realize in actual materials.

Since the total thermal conductivity is the sum of both the electronic and the lattice contributions and is typically dominated by the lattice contribution, increases to the electronic thermal conductivity that occur due to power factor enhancements are relatively unimportant. As discussed in Chapter 1, large enhances to zT have been

recently realized due to reductions in lattice thermal conductivity. For electrons, the transport parameters are highly influenced by the location of the Fermi level, but this isn't an option for the lattice. Instead the mean-free-path is lowered at different frequencies which creates an overall lower lattice thermal conductivity [19], [12]. By scattering phonons at a variety of frequencies it is possible to reduce the thermal conductivity without affecting that electronic transport.

2.5   Summary

In this chapter the basics of thermoelectric transport theory have been discussed. Using the Landauer formalism, a nanoscale resistor was used to explain concepts like Modes, Transmission, and Fermi level to describe why current flows. From this picture if current flow definitions for Seebeck coefficient, conductivity, thermal conductivity for electrons, and thermal conductivity for phonons were developed and their physical basis described. The transport definitions were then rewritten and described in a more common bulk form that is used for realistic devices. The next chapter will describe the online thermoelectric calculator LanTraP. LanTraP was developed to calculate transport properties of a material using several definitions presented within this chapter.

3. LANTRAP

Landauer Transport Properties (LanTraP) is an online tool developed to aid research and education. The tool utilizes band structure information to calculate the distribution of modes as well as the thermoelectric transport properties for both electrons and phonons. LanTraP is similar to BoltzTraP, but where BoltzTraP is based on the Boltzmann Transport Equation, LanTrap uses the Landauer formalism to perform calculations. Because LanTraP is built on the Landauer formalism, it is very easy to calculate the transport/TE parameters for ballistic, quasi ballistic, and diffusive transport [30]. The tool is available online at https://nanohub.org/tools/lantrap and may be used for free in an internet browser. This chapter will present a brief overview of the tool and its potential uses. For more information on LanTraP, the user manual is included in Appendix A.

3.1 Distribution of Modes

In order to perform any calculation, LanTraP must have information about the material in question. The user must upload either a dispersion relation or a distribution of modes. The distribution of modes (DOM) shows how the number of modes are distributed in energy. If a dispersion relation is uploaded the tool will calculate a distribution of modes via the band counting method before continuing. The band counting method examines the band structure in dimensions perpendicular to transport, and sums up the number of bands or branches with positive velocity, as expressed in Eq. (3.1) [27].

$$M(E) = \sum_{\vec{k}_\perp, n^+} \Theta\left(E - E_{\vec{k}_\perp}\right) \tag{3.1}$$
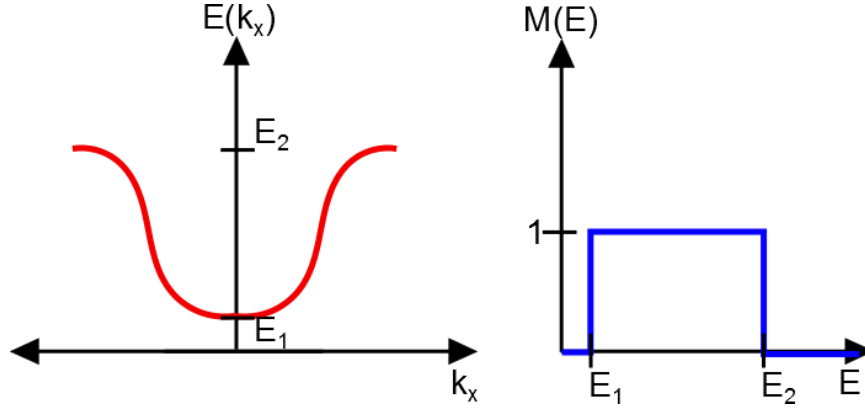
Fig. 3.1. The band counting method for counting modes. At each energy, the number of branches with positive velocity states adds one mode. The number of modes at a given energy is the distribution of modes.

In Eq. (3.1), Θ is the Heaviside function, showing that each branch contributes one mode (or conduction channel) for all energy within its range, as seen in Fig. 3.1. Computationally, the band counting method is very quick, as can be seen in Ref. [31].

For electrons, the band structure is often approximated to be parabolic near the bottom of the conduction band (or top of the valence band), and is fit by an effective mass. In the simple case of a 3 dimensional parabolic valance and conduction band, the distribution of modes is can be calculated analytically using Eq. (2.4):

$$M(E) = \frac{1}{2\pi\hbar^2}\left\{\left(g_C m_C^*(E - E_C)\Theta(E - E_C)\right) + \left(g_V m_V^*(E_V - E)\Theta(E_V - E)\right)\right\} \quad (3.2)$$

where g_C and m_C^* are the degeneracy and effective mass in the conduction band (g_V and m_V^* are the valence band counter parts). Analytically it is apparent that the modes will increase linearly with energy above the conduction band (or below the valence band). Since the number of modes is proportional to the product of density of states and velocity, both of which increase as the square root of kinetic energy, it makes sense for the result to increase linearly with energy. The results from a distribution of modes calculation in LanTraP confirms this result (as seen in Fig. 3.2). The distribution of modes is clearly linear, and the slope is dependent on the
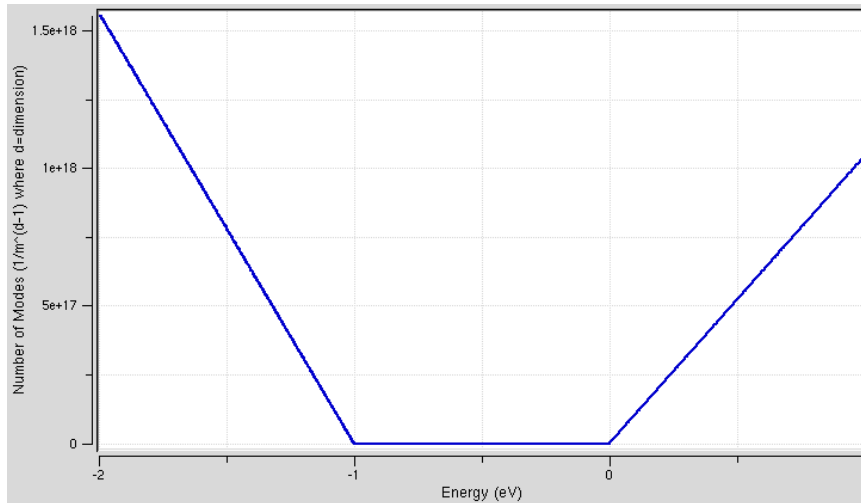
Fig. 3.2. The distribution of modes for a 3D parabolic conduction and valence band calculated by LanTraP. The band gap is 1 eV, the effective masses of the valence and conduction bands are 1.5 m_0 and 1 m_0, respectively. The valence band has a heavier effective mass, so the number of modes has a larger slope than in the conduction band.

effective mass of the band. In the examples shown in Fig. 3.2 $m_V^* = 1.5 \times m_0$ and $m_C^* = 1.0 \times m_0$.

The parabolic band is simple and analytic results are easy to calculate. The electronic structures of materials is often more complex, such as that for Bi_2Te_3 shown in Fig. 3.3(a). The band-counting method used by LanTraP is able to accurately determine the distribution of modes of this material in a matter of minutes. The resulting distribution of modes (Fig. 3.3(b)) shows that even though Bi_2Te_3 has a highly non-parabolic electronic dispersion, the distribution of modes is roughly linear near the band edges. Thus, an effective mass can be fitted from the full numerical solution, but should be done with care (the fit should be decent over several k_BT around the energy of interest). The full band method on the other hand is reliable for all energies.

The method to compute the distribution of modes of phonons is identical to that of electrons. Phonon dispersion relations are often approximated within the Debye model, where a linear dispersion is assumed. Phonons are not treated differently
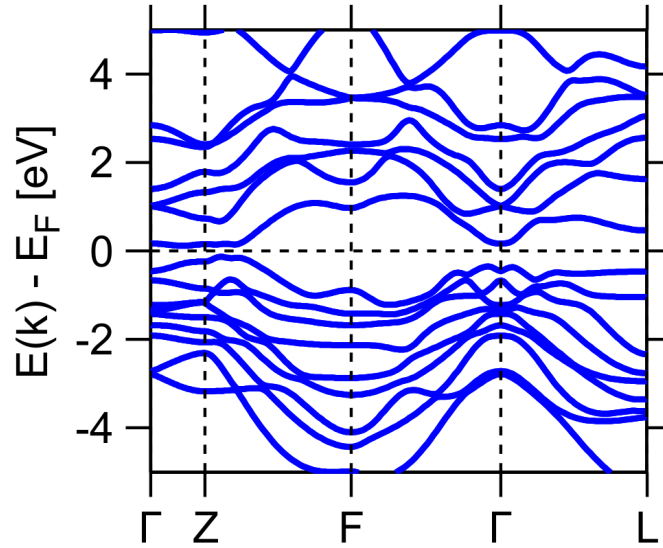
(a) Bi$_2$Te$_3$ Dispersion
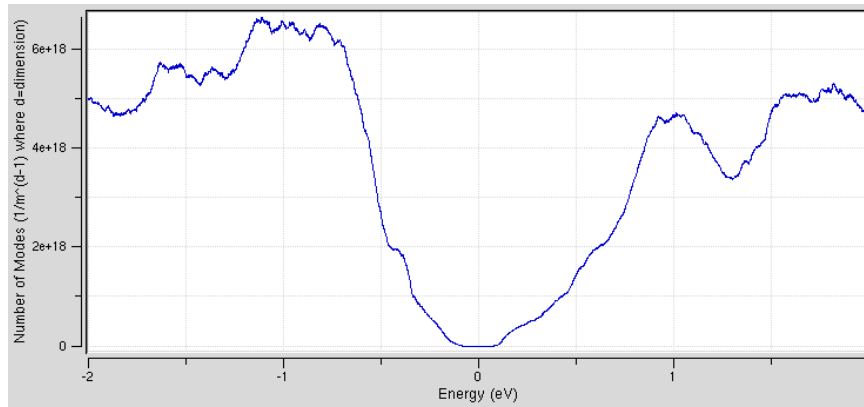
(b) Bi$_2$Te$_3$ Distribution of Modes

Fig. 3.3. The band structure and distribution of modes of Bi$_2$Te$_3$. **(a)** The dispersion is incredibly complex but **(b)** with LanTraP the complex dispersion is analyzed into a much simpler distribution of modes.

than electrons in calculating the distribution of modes, and the Debye model has an analytic solution (Eq. (3.3)) [10].

$$M_{ph}(\hbar\omega) = \frac{3(\hbar\omega)^2}{4\pi(\hbar v_D)^2} \tag{3.3}$$
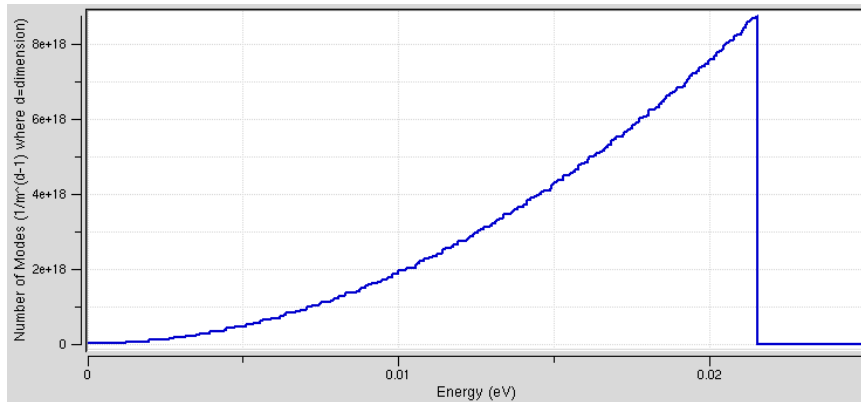
Fig. 3.4. The distribution of modes for Debye phonons. The dispersion is linear, but the distribution of modes is parabolic, until the end of the band.

In Eq. (3.3) v_D is the Debye velocity (or group/sound velocity), which plays a similar role to the effective mass in the parabolic band approximation.

The linear Debye phonon branch results in a parabolic distribution of modes as seen in Fig. 3.4. Using the full phonon band structure is important since the band width is on the order of $k_B T$, as was discussed in Section 2.3, and is often much more complicated than a simple Debye dispersion. The phonon band structure for Si is shown in Fig. 3.5(a), and the corresponding distribution of modes is shown in Fig. 3.5(b). It is clear that the Debye model does not capture the entire phonon dispersion (though it may work for the 0-10 meV range), and that a full band treatment is necessary to correctly determine the number of modes.

3.2   TE Coefficients

Once the distribution of modes is known by LanTraP, the transport coefficients are calculated by using the equations from Sections 2.2 - 2.4. LanTraP determines the transport parameters for a range of Fermi levels specified by the user. The transmission (Eq. (2.3)) is the last piece that needs to be determined before the transport parameters are calculated. Depending on the transport regime (ballistic,
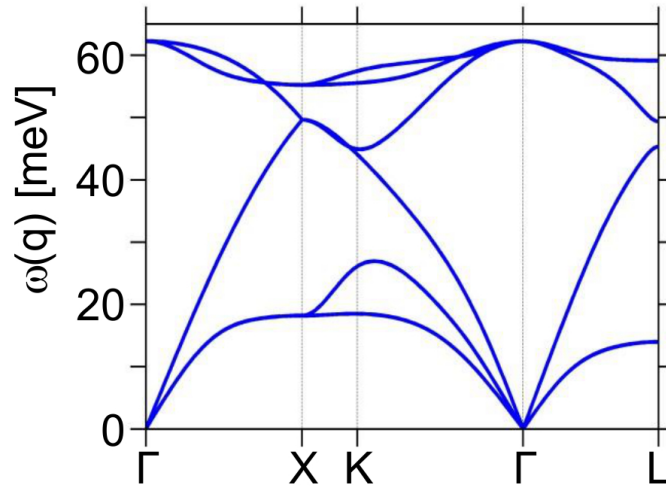
(a) Si Dispersion
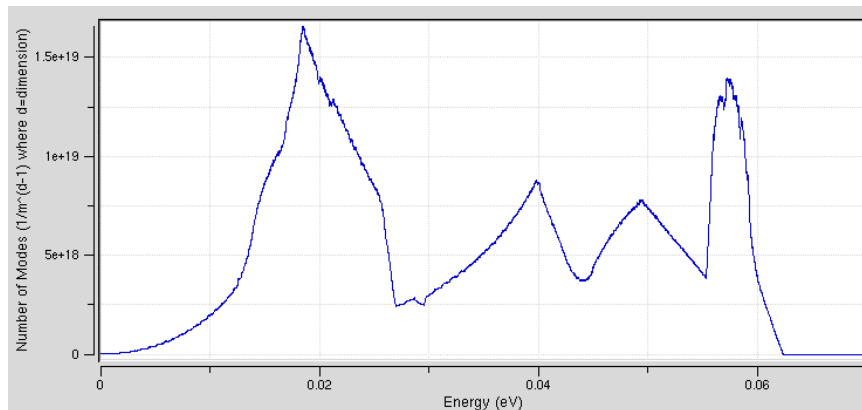
(b) Si Distribution of Modes

Fig. 3.5. The **(a)** band structure and **(b)** distribution of modes for phonons in Si. Note that the distribution of modes is similar to that of a Debye model for energies less than roughly 15 meV.

quasi-ballistic, or diffusive) the transmission requires different information. In the ballistic regime, $\lambda(E) >> L$ so the transmission is 1 and only the distribution of modes needs to be specified. For diffusive and quasi-ballistic transport the mean-free-path, in addition to the distribution of modes, is needed to calculate the transmission. LanTraP allows energy dependent mean-free-paths for a conduction and a valence band, which are expressed as a power law:

$$\lambda(E) = \lambda_0 \left(\frac{E_{kin}}{k_B T} \right)^r \tag{3.4}$$

In Eq. (3.4) r is the scattering parameter and E_{kin} is the kinetic energy of a particle in a band.

To account for different scattering mechanisms, the mean free path at each energy can be obtained using Mathiessen's rule:

$$\frac{1}{\lambda(E)} = \frac{1}{\lambda_1(E)} + \frac{1}{\lambda_2(E)} + \dots \tag{3.5}$$

Note that the energy dependent mean-free-path for the valance and conduction bands are treated separately from each other.

In the case of phonons, the mean free path can vary by many orders of magnitude. Under common conditions, the phonon mean-free-path can often be approximately described using a power law for the energy dependence. If a particular mean-free-path distribution is needed, then it is recommended that the TE coefficients be calculated by modifying the distribution of modes file to correctly include the scattering that occurs at each energy and then performing calculations in LanTraP under ballistic transport conditions. This method is also applicable to electrons.

For electrons in the ballistic regime, conductance, Seebeck coefficient, electronic thermal conductance, power factor, and electronic zT are calculated. For electrons in the quasi-ballistic or diffusive regime, conductivity and electronic thermal conductivity are calculated rather than conductance and thermal conductance. For phonons only the lattice thermal conductance in the ballistic regime and lattice thermal conductivity in the diffusive and quasi-ballistic regime are calculated. The results are plotted within the tool and may be downloaded in .txt format to be readily used in programs such as MATLAB.

3.3   Relating to SPICE

When running a SPICE simulation for a thermoelectric device, all the material parameters calculated by the TE LanTraP simulator can be used as input parameters for the SPICE model. It is therefore easy to check all of the inputs that are used in SPICE when verifying results. As well, if a temperature dependent material parameter SPICE simulation were needed, LanTraP could be used to determine all parameters at a variety of temperatures.

LanTraP could prove to be extremely useful when developing new thermoelectric materials. By only knowing the band structure information and the mean-free-path, the thermoelectric performance can be quickly and easily determined. Rather than relying on band edge approximations, LanTraP utilizes full band dispersions, leading to more accurate results.

The next chapter will be a discussion of a SPICE-compatible thermoelectric equivalent circuit. The information in this and previous chapters have presented the basic mechanisms and theory of thermoelectric materials and devices. Understanding the thermoelectric equations and how to determine material parameters will allow an easy transition into developing the equivalent circuit. In theory, LanTraP may be used as a first step toward simulating thermoelectric devices based on newer materials. The following chapters will focus on thermoelectric device simulation.

4. A THERMOELECTRIC EQUIVALENT CIRCUIT MODEL

This chapter will explain a thermoelectric equivalent circuit which is compatible with SPICE, initially developed by Mitrani et al. [32], [33]. The benefit of this physics-based model is that not only can it be used in conjunction with an electronic circuit, but also to help predict performance in unique or difficult situations. The chapter will begin by explaining the circuit and how it relates to the actual device physics. The model will then be tested against analytic results with DC bias. Two transient test cases are then simulated and the results discussed. A final set of simulations will be with an applied AC small signal as is done in impedance spectroscopy. All test cases were simulated using XYCE, an opensource SPICE-compatible circuit simulator [34]. Netlists for all test cases are included in Appendix B.

4.1   The Equivalent Circuit

A single thermoelement will be considered when initially developing the equivalent circuit, though it will be explained later how this simple case can be expanded to a full device. It is assumed that there are no sources of thermal or electrical resistance from anything but the thermoelectric material. These assumptions are only made to reach analytic results, though if desired other resistances may be easily added. It will also be assumed that the length is much larger than the width and thickness, so that the problem is one dimensional and that all heat and current flow are along the length of the leg.

The general expressions for energy balance (Eq. (4.1)) , heat flow (Eq. (4.2)), and electric field (Eq. (4.3)) are:

$$\frac{\partial}{\partial x}\left(\kappa(x)\frac{\partial T(x)}{\partial(x)}\right) + \frac{J^2}{\sigma(x)} - JT(x)\frac{\partial s(x)}{\partial x} = c\rho\frac{\partial T(x)}{\partial t}, \tag{4.1}$$

$$q(x) = Js(x)T(x) - \kappa(x)\frac{\partial T(x)}{\partial x}, \tag{4.2}$$

$$E(x) = \frac{J}{\sigma(x)} + s(x)\frac{\partial T(x)}{\partial x}. \tag{4.3}$$

There are usually approximations that must be made to solve these equations analytically, and even then they may still be difficult or impossible to solve, depending on the problem in question. These equations will be translated into the equivalent circuit, as will be seen in the DC case.

One of the benefits of this equivalent circuit is that it could easily be incorporated into another SPICE simulation, to simulate an entire circuit. This is particularly advantageous when a thermoelectric is incorporated into a complex circuit, such as a temperature regulator. It is easy to incorporate the equivalent circuit into other SPICE simulationss because the thermoelectric is modeled in a three port system as shown in Fig. 4.1. The bottom port connects to the electrical circuit, while the two side ports are thermal connections to the cold and hot sides. Each of these ports represents a necessary boundary condition for a working simulation. For the hot and cold ports the temperature or heat flow must be specified, and for the electrical port the voltage or current is needed.

The equivalent circuit is shown in Fig. 4.2. In order for the thermal effects to be represented in an electronic circuit, analogies are made to relate the two as summarized in Table 4.1. Voltage and current are used in the thermal circuit to represent temperature and heat flow respectively. Resistors, which are characterized by electrical conductivity, are used as thermal resistors to prevent heat flow (characterized by thermal conductivity). Capacitors are used in the thermal circuit to represent the storage of heat by the material, and is determined by the heat capacity (or specific heat and density) and volume of the material.
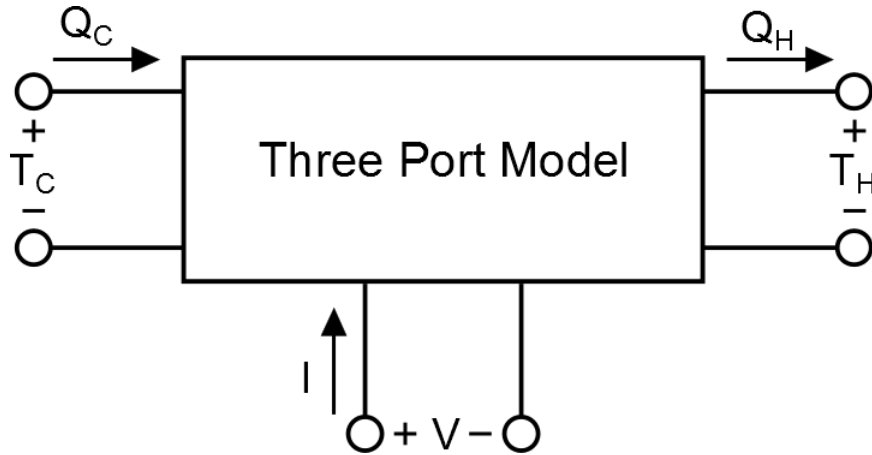
Fig. 4.1. Three port system. The equivalent circuit has three ports that connect the thermoelectric device to the environment. These ports are the hot side and cold side thermal ports, and the electrical port. All of the thermoelectric effects are included inside the box.

The equivalent circuit separates the electronic and thermal effects into two circuits, which influence each other through current and voltage dependent sources. The electrical circuit is the simpler of the two to understand. A current or voltage is applied at the electrical port and then experiences a resistor in series with a voltage source. The resistor is the resistance of the leg ($R = \frac{L}{\sigma A}$). The voltage source represents the Seebeck voltage that arises from the temperature difference ($V_S = s\Delta T$).

One issue to remember when simulating a thermal circuit in SPICE is that ground corresponds to 0 V, which is 0 K for a thermal circuit. At the edges of the thermal circuit are current sources Q_{PC} and Q_{PH}. The Q_P current sources represent Peltier heating and cooling with $Q_{PC} = sIT_C$ and $Q_{PH} = sIT_H$. The direction of the current sources represent heat being added (Q_{PH}) or taken away (Q_{PC}). The other current source in the thermal circuit is the Joule heating source $Q_J = I^2R$. The Joule heating arises throughout the entire length of the thermoelectric leg, and half of the heat goes to the cold side, while the other half goes to the hot side. The two resistors represent the thermal resistance of the leg $R_{TH} = \frac{L}{\kappa A}$, each resistor representing half of the

Table 4.1.
Thermal circuit analogies and the units associated with each. Each circuit element has an analogous meaning in a thermal circuit, which is summarized in this table.

Thermal Variable		Electrical Variable	
Heat Flow	W	Current	A
Temperature	V	Voltage	V
Thermal Resistance	K/W	Resistor	Ω
Thermal Mass	J/K	Capacitor	F
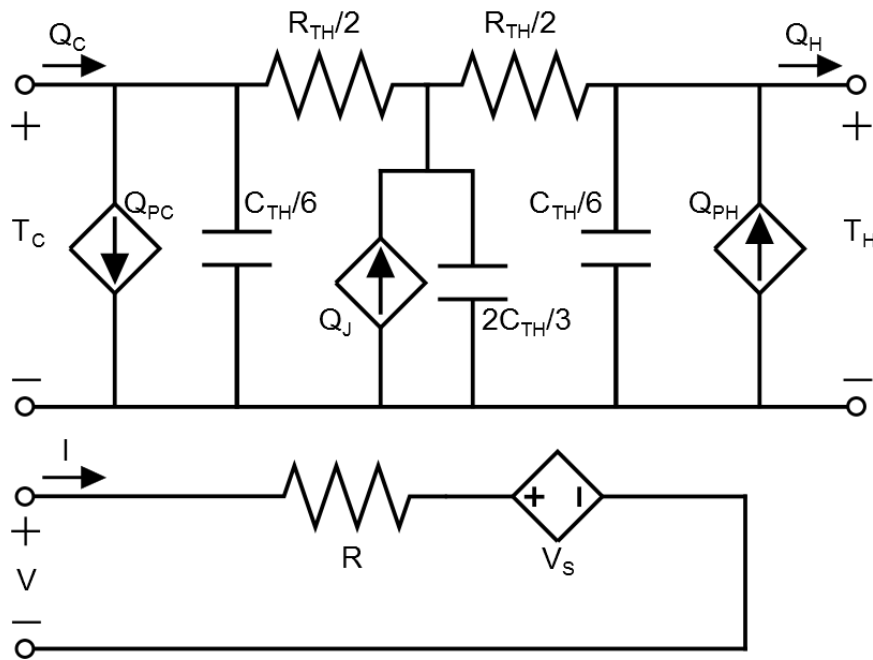
Fig. 4.2. The thermoelectric equivalent circuit. The circuit has a thermal circuit which connects the hot and cold sides (top), and an electronic circuit (bottom). The two circuits are related through current and voltage sources.

total resistance. All of the thermal capacitors $(C_{TH} = c_p \rho V)$ cause a time delay to temperature changes resulting from the heat sources heating the thermoelectric.

The equivalent circuit has been developed with an understanding of the physics of a single thermoelectric leg. If a thermocouple, or an entire thermoelectric device, were to be simulated, this model could still apply. If it is assumed that the ceramic shell and metal contacts between the thermoelectric legs add no electrical or thermal resistance, or thermal capacitance, then an entire module may be simulated with one circuit. The model can be expanded to a TEM by multiplying the Seebeck voltage, electrical resistance, thermal resistance, and thermal capacitance by the number of legs in the module. This also assumes that the n-type and p-type legs are of the same material, and that the only difference is opposite signs of the Seebeck coefficient. These assumptions are made to allow for simple simulation, but this method could also be applied to nearly any other situation. The approach used in this chapter can be used in nearly all cases: the material parameters don't need to be constant, n-type and p-type legs could be made of different materials, and other resistances may be added if desired.

4.2   DC Bias Simulation

The first, and simplest, case that the equivalent circuit will be tested against is the case of an applied DC bias. The leg will be operating as a cooler, so a current is applied. It is assumed that the material parameters do not change with position in the leg or with temperature.

As mentioned before, the DC case allows for analytic solutions. When assuming steady state and constant material parameters, Eqs. (4.1) - (4.3) can be arranged into the equations which describe a single thermoelectric leg [32].

$$\frac{\partial^2 T(x)}{\partial x^2} = -\frac{J^2}{\kappa\sigma} \tag{4.4}$$

$$q_C = q(x=0) = -\frac{J^2 L}{2\sigma} + JsT_C - \frac{\kappa(T_H - T_C)}{L} \tag{4.5}$$

$$q_H = q(x = L) = \frac{J^2 L}{2\sigma} + JsT_C - \frac{\kappa(T_H - T_C)}{L} \tag{4.6}$$

$$V = \frac{JL}{\sigma} - s(T_H - T_C) \tag{4.7}$$

where $T_C = T(0)$ and $T_H = T(L)$. The names "cold" and "hot" are fixed to these positions, though in some cases the cold contact may reach a higher temperature than the hot contact.

Equations (4.4)-(4.7) are the leg equations. Equation (4.4) can be solved for a temperature profile, while Eqs. (4.6) and (4.5) solve for the heat flux at the cold and hot ends. The voltage across the leg (Eq. (4.7)) is found by integrating the electric field, Eq. (4.3), across the length of the leg. These equations are all in terms of the material parameters and the current density, but it is the bulk parameters (such as current, and resistance) that are directly used and solved for in circuit simulations. Fortunately it is easy to change from the material parameters to bulk parameters using the dimensions of the leg. In the simple case that has been presented so far multiplying by area and the number of thermoelements, N, Eqs. (4.4)-(4.7) can be transformed into the module equations. The module equations (Eqs. (4.8)-(4.11)) apply in the specific case of constant material parameters, similar n-type and p-type legs, and no contact resistance or capacitance between thermoelements. Again, these are not necessary assumptions, but they are made to simplify the problem.

$$\frac{\partial^2 T(x)}{\partial x^2} = -\frac{I^2 R}{K} \tag{4.8}$$

$$Q_C = -\frac{I^2 R}{2} + IST_C - K(T_H - T_C) \tag{4.9}$$

$$Q_H = \frac{I^2 R}{2} + IST_H - K(T_H - T_C) \tag{4.10}$$

$$V = IR - S(T_H - T_C) \tag{4.11}$$

where S is the module Seebeck coefficient, R is the module resistance, K is the module thermal conductance, and C_{TH} is the module thermal capacitance.

$$S = Ns \tag{4.12}$$

$$R = N\frac{L}{A\sigma} \tag{4.13}$$

$$K = N\frac{\kappa L}{A} \tag{4.14}$$

$$C_{TH} = Nc_p\rho V \tag{4.15}$$

The module equations directly relate to the equivalent circuit. By using Kirchoff's laws, it can be easily verified that Eqs. (4.9) and (4.10) are exactly described by the thermal equivalent circuit in the DC case. Equation (4.11) can be verified by the same method, but in the electrical circuit. The circuit is therefore not only laid out in a physically significant way, but it also clearly replicates the analytic expressions.

The first exercise of the model will be to calculate how the cold side temperature, T_C, varies with current. Since Peltier cooling increases linearly with current, and Joule heating increases as the current squared, there is guaranteed to be a minimum T_C occurring at a current $I_{TC,Min}$. The goal of the first exercise is to find $T_{C,Min}$ and $I_{TC,Min}$.

In order to perform this simulation, the leg is assumed to be made of p-type Bi$_2$Te$_3$, with material parameters and device dimensions shown in Table 4.2 [35]. The hot side is assumed to have a perfect heat sink such that $T_H = 300$ K, and the cold side is assumed to absorb no heat from the surroundings so that $Q_C = 0$ W. The DC electrical current is swept, so that at each current a cold side temperature can be determined. A netlist for this example to run with XYCE is included in Appendix B.1. An analytic expression for T_C (Eq. (4.16)) and $I_{TC,Min}$ (Eq. (4.17)) can be solved by using Eq. (4.9) and the cold side boundary condition, $Q_C = 0$ W.

Table 4.2.

Material parameters for single Bi_2Te_3 leg simulations. These are the values assumed for the material parameters and device dimensions. These values completely specify the thermoelement in the equivalent circuit.

$s = 245$	$\mu V/K$	
$\kappa = 1.4$	$W/m \cdot K$	
$1/\sigma = 20$	$\mu \Omega/m$	
$\rho = 7.75 \times 10^6$	kg/m^3	
$c_p = 0.158$	$J/g \cdot K$	
$L = 5$	mm	
$A = 1$	mm^2	

$$T_C(I) = \frac{I^2 R + 2KT_H}{2IS + 2K} \tag{4.16}$$

$$I_{TC,Min} = \frac{\sqrt{KR(KR + 2S^2 T)} - KR}{RS} \tag{4.17}$$

Using the material and device parameters (see Table 4.2) in Eqs. (4.16) & (4.17) it is predicted that for this device $I_{TC,Min} = 0.585$ A, which produces $T_{C,Min} = 238.85$ K. The simulation results are plotted in Fig. 4.3 along with the analytic expression. There is clearly good agreement between our simulated results and the analytical expressions. Physically, Fig. 4.3 shows that as current is applied, the cold side temperature drops until $T_{C,Min}$. At these currents, Peltier cooling is greater than the Joule heating. With larger current the Joule heating increases until eventually T_C is greater than T_H. This occurs because T_H is fixed at 300 K, and so any additional heat produced must go to the cold side, causing T_C to become hotter than the denoted hot side. The Joule heat still goes to both contact equally, but the Fourier heat going to the "cold" contact increases to keep the "hot" contact at 300 K.
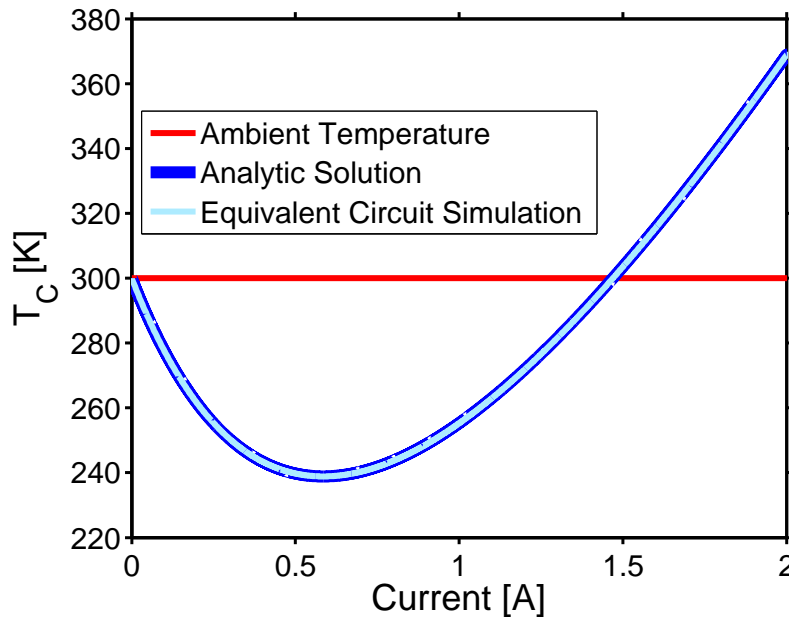
Fig. 4.3. Minimum T_C. The dark blue line is the analytic result, the light blue is the XYCE simulation results. The red line shows ambient temperature.

Another test case considered is to find the maximum heat absorbed at the cold side, $Q_{C,Max}$. Similar to the previous example, the combination of Peltier and Joule effects causes Q_C to change with I, with $Q_{C,Max}$ occuring at $I_{QC,Max}$. Equation (4.9) shows that $Q_{C,Max}$ occurs when the temperature difference between hot and cold side is zero. Under these conditions, $Q_{C,Max}$ and $I_{QC,Max}$ can be solved for.

$$Q_C(I) = -\frac{I^2 R}{2} + IST_C \tag{4.18}$$

$$I_{QC,Max} = \frac{ST_C}{R} \tag{4.19}$$

In order to run this simulation, the cold side boundary condition needs to be changed from $Q_C = 0$ W to $T_C = 300$ K. The material and device parameters from Table 4.2 are still used, and the netlist for this simulation is presented in Appendix B.2. The results of the XYCE simulation are shown in Fig. 4.4, and it can be seen
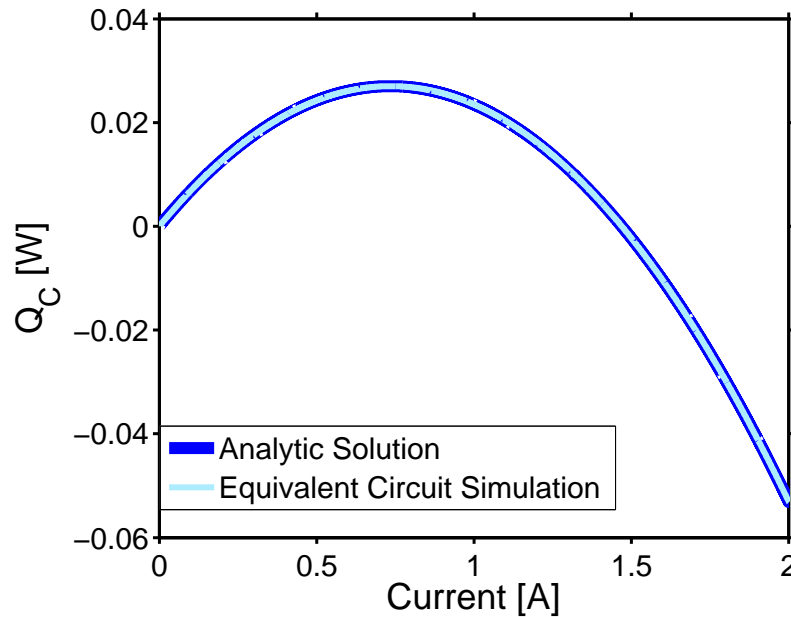
Fig. 4.4. Maximum Q_C. The dark blue line is the analytic result, the light blue is the XYCE simulation results.

that there is good agreement with the analytic results. Solving Eqs. (4.18) and (4.19) gives $I_{QC,Max} = 0.735$ A and that $Q_{C,Max} = 0.027$ W, the same result which is achieved by the equivalent circuit simulation. Examining Fig. 4.4 shows that as the current increases, the "cold" side is able to absorb more heat from the surroundings as a result of the Peltier effect. Eventually the current becomes large enough that the Joule heating within the leg begins to limit the amount of heat absorbed, and if a large enough current is applied, will begin to emit heat to the environment.

This model only produces results for the heat flow and temperature at the ends of the leg. In order to see the temperature within a thermoelement, the model needs to be switched from a lumped to a distributed model. This is done by expressing a thermoelement as smaller sections and then replicating the inside of the circuit to match these smaller sections, as shown in Fig. 4.5. The Peltier heating and cooling sources are not included in the sub-circuit because, with a constant Seebeck coefficient, they are equal and opposite and will cancel each other out. If the Seebeck

(a) Thermoelement

(b) Equivalent Circuit
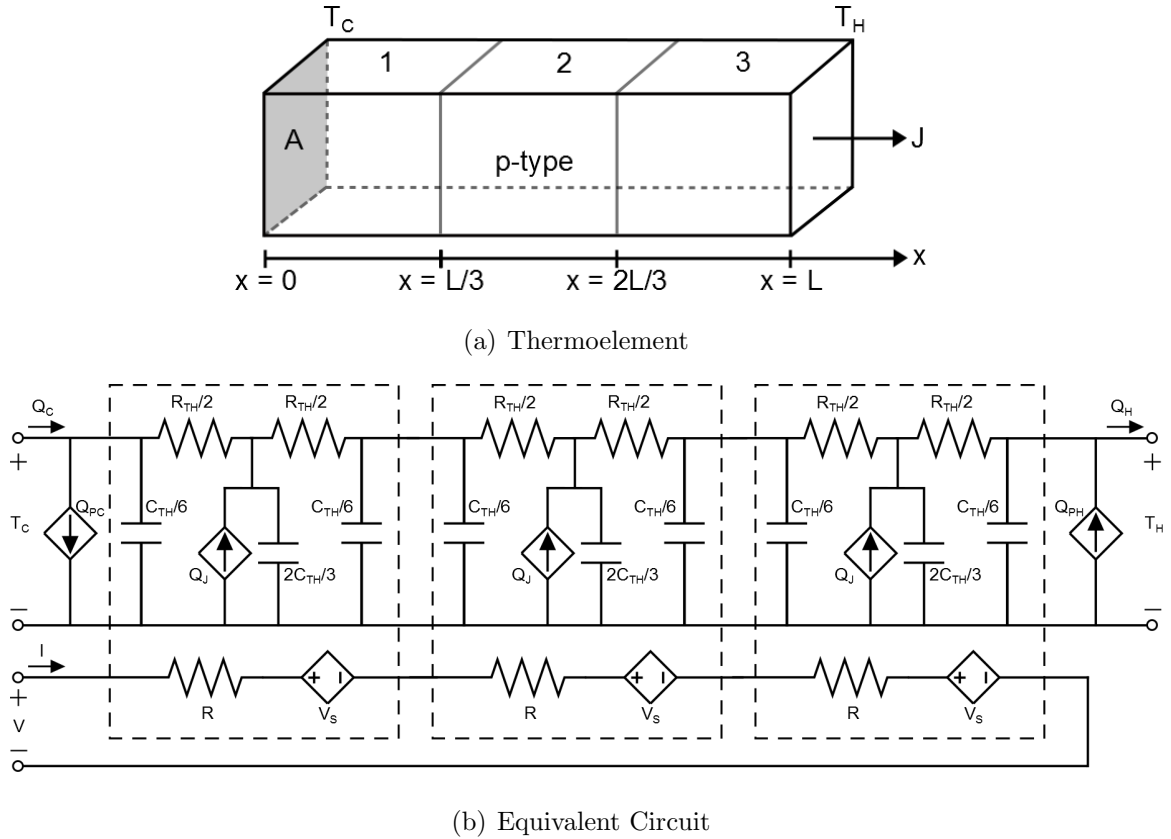
Fig. 4.5. Creating a distributed model. **(a)** The thermoelement is organized into sub-sections (in this case 3) which are reflected in **(b)** the creation of sub-circuits.

coefficient changes, these sources should be included with each sub-circuit. With this distributed circuit, the temperature and heat at the edges of each sub-section can be resolved. This distributed model also produces more accurate results in non-steady state cases, as will be seen in the next section.

Solving Eq. (4.8) for $T(x)$ gives the analytic solution for the steady state temperature distribution as

$$T(x) = -\frac{I^2 R}{2KL^2}x^2 + \left(\frac{T_H - T_C}{L} + \frac{I^2 R}{2KL}\right)x + T_C. \qquad (4.20)$$

Equation (4.20) is compared against a 10 element simulation for the two DC cases previously studied, and the temperature distribution is compared. The netlists for

(a) $T_{C,Min}$ Temperature Profile

(b) $Q_{C,Max}$ Temperature Profile
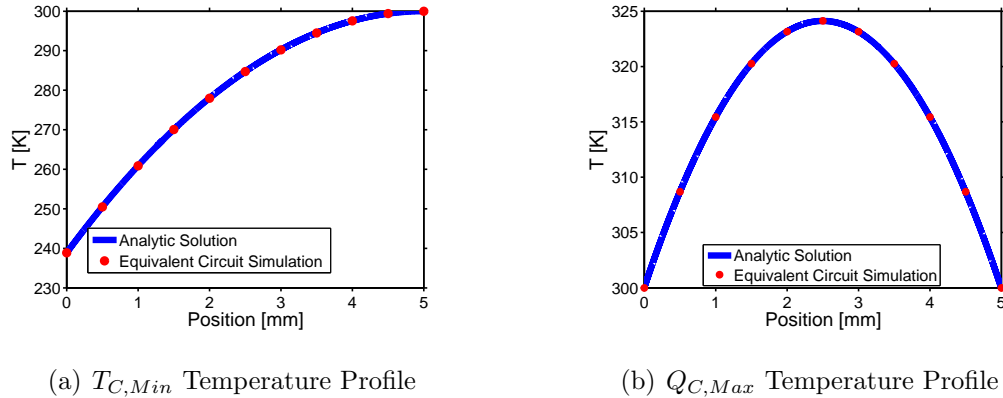
Fig. 4.6. Verifying the temperature distribution with 10 distributed elements. **(a)** When the current is at $I_{TC,Min}$ with no heat absorbed at the cold side and **(b)** when the current is at $I_{QC,Max}$ and $T_C = T_H$.

the $T_{C,Min}$ and $Q_{C,Max}$ simulations are found in Appendix B.3 and B.4 respectively. The temperature distribution in Fig. 4.6(a) corresponds to the $Q_C = 0$ W boundary condition and the current is $I_{TC,Min}$, while Fig. 4.6(b) shows the temperature distribution corresponding to the $T_C = 300$ K boundary condition and the current is $I_{QC,Max}$. There is good agreement between the simulation and the analytic results in both cases.

4.3 Transient Simulation

The next operating condition to test the equivalent circuit is under transient conditions. This is an important test to understand how a thermoelectric will behave during turn on and turn off conditions, or during situations of time dependent changes to the thermal or electrical environment [36]. To start the model will be tested in turn off conditions and a thermal time constant will be determined. Since this is the first test where the thermal capacitance is important, this test is designed to be certain that the capacitors are behaving correctly.

To simulate a thermoelectric under turn off conditions a variety of currents were applied to a leg and then turned off. The T_C response depends on the current used,

(a) Currents of Interest
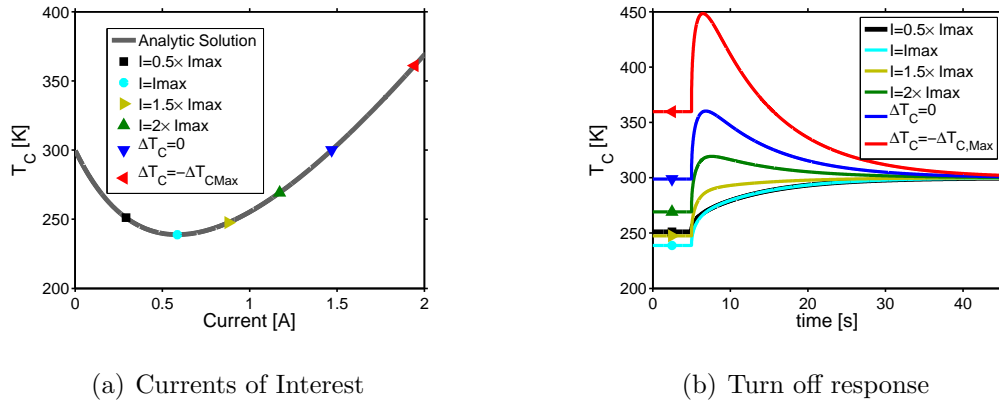
(b) Turn off response

Fig. 4.7. A thermoelement under turnoff conditions at a variety of currents. **(a)** The currents used, as shown on a plot of the steady state T_C vs I. **(b)**) The T_C response to turning off the current.

but will begin at a steady state temperature $T_{C,SS}$ determined by the current. Then when the current is turned off, all of the Peltier cooling present at the cold side will immediately be gone while the remaining Joule heat in the body takes time to reach the contacts. Due to the difference in time between the Joule and Peltier effects reaching the cold side, T_C begins to increase. Eventually the thermoelement will return to room temperature as the left over Joule heat exits the thermoelement.

The same device parameters from Table 4.2 are used in this simulation, with $T_H = 300$ K and $Q_C = 0$ W boundary conditions and using 25 distributions. The currents used in this simulation are shown on a plot of T_C vs I in Fig. 4.7(a) and the T_C response to turn off is shown in Fig. 4.7(b). An example netlist for this simulation is provided in Appendix B.5 (note that only the $I = I_{TC,Min}$ netlist is provided). As mentioned before, increasing the number of distributions creates more accurate results when it is important to resolve the spatial dependence of the temperature profile. Fig. 4.8 shows how the number of distributions affects the results in this simulation.

The temperature response in Fig. 4.7(b) resembles a capacitor discharging, and that analogy is used to analyze the results. Modifying the common expression for a capacitor discharging to this situation results in
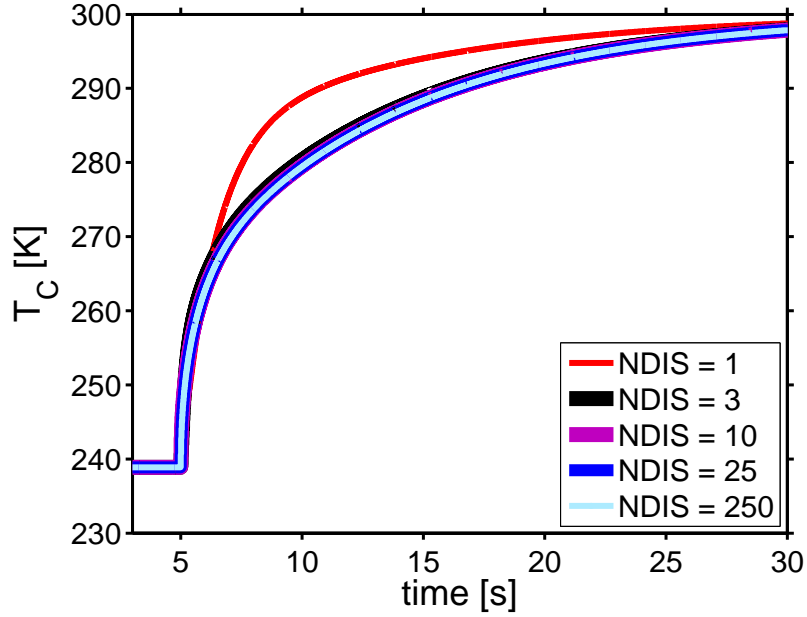
Fig. 4.8. The effect of the number of distributions on simulation results, only showing the $I = I_{TC,Min}$ case. For this case 25 distributions was a good balance of simulation accuracy (more distributions didn't affect results much) and simulation time.

$$\Delta T(t) = \Delta T(0) e^{\frac{-t}{\tau}}. \tag{4.21}$$

The temporal response of the thermoelectric is determined by a characteristic thermal time constant τ, which is related to the thermal diffusion coefficient α and the device length [37]

$$\tau = \frac{4L^2}{\pi^2 \alpha} = \frac{4L^2}{\pi^2} \frac{c_p \rho}{\kappa}. \tag{4.22}$$

To find τ, $\frac{d}{dt} \ln\left(\frac{\Delta T(t)}{\Delta T(0)}\right)$ is approximated from the results of each simulation and compared to Eq. (4.22) with the input material parameters used. Each current has the same time constant, $\tau = 8.9$ s, which matches the analytic time constant.

An application which requires transient thermoelectric device operation is pulsed cooling. With pulsed cooling the cold side of the leg becomes colder than possible in

steady state, but only for a short time. This enhanced cooling effect can be used to treat hot spot cooling when used in conjunction with microelectromechanical systems (MEMS) [38], or in any case where increased cooling is only necessary for a short period of time. A summary of studies on pulsed cooling can be found in *Encyclopedia of Thermal Packaging* [36].

With pulsed cooling an initial current of $I_{TC,Min}$ is flowing through the device, and is then increased in a square pulse to I_{Pulse} (which is much larger than $I_{TC,Min}$) for a short time, and then returns to $I_{TC,Min}$, as shown in Fig. 4.9(a). The result is a temporarily lower cold side temperature than could be achieved in steady state, followed by a large rise in T_C which eventually decays back to the steady state value. The reason for this response is that the Peltier cooling (which increases linearly with current) instantly cools the cold side. Joule heating (which increases as the square of current) occurs within the body of the leg and takes time to reach the cold side, but greatly increases the cold side temperature when it does.

The T_C response is determined by a few factors, and can be analyzed by looking at a few terms, which are labeled in Fig. 4.9(b). The difference between the steady-state minimum, $T_{C,SS}$, and the minimum T_C as a result of the current pulse is ΔT_{Pulse}, and occurs at a time t_{min} after the pulse. The time that it takes for T_C to return to the steady state temperature is t_{ret}. The maximum temperature achieved after the current pulse is $\Delta T_{PostPulse}$.

The pulsed cooling problem has no closed form analytic solution, but there are analytic approximations as well as experimental evidence provided by Snyder et al. [37]. Assuming constant material parameters, no heat absorbed at the cold side, a perfect heat sink at the hot side, and making a linear approximation to Eq. (4.1), ΔT_{Pulse} can be approximated using $\Delta T_{SS} = T_{Ambient} - T_{C,SS}$.

$$\Delta T_{Pulse} = \frac{\Delta T_{SS}}{2}\left(\frac{P-1}{P+1}\right) \tag{4.23}$$

where

$$P = \frac{I_{Pulse}}{I_{Min}} \tag{4.24}$$

(a) Current Pulse   (b) Qualitative Temperature Response
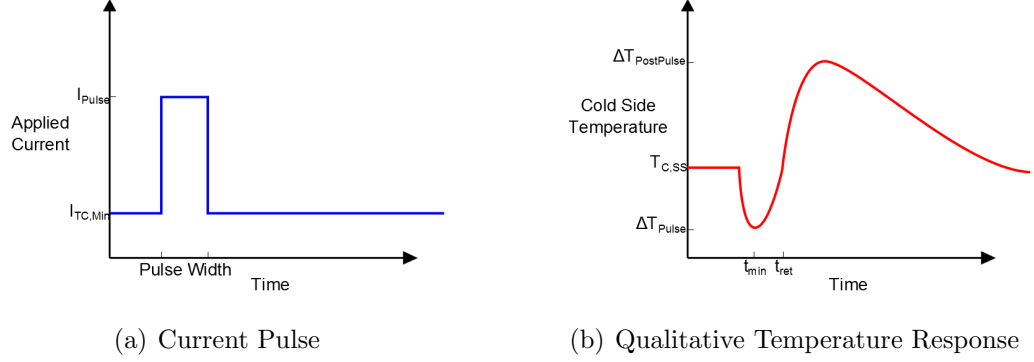
Fig. 4.9. A qualitative sketch of pulsed cooling. **(a)** The squarewave current pulse causing pulsed cooling. **(b)** The temperature response, with the points of interest that will be used to characterize the temperature response labeled.

The time constant and pulse magnitude predict t_{min} and t_{ret} by

$$t_{min} = \frac{t_{ret}}{4} = \frac{L^2}{4\alpha(P+1)^2} = \frac{\tau}{(P+1)^2} \tag{4.25}$$

The time constant in Eq. (4.25) is not the same as the time constant used in the turnoff case, though they are related.

To accurately model problems beyond steady state, a distributed model must be used. Fig. 4.10 shows how the number of distributed elements used in the simulation changes the results, with 25 elements seeming to be nearly as sufficient as any simulation using more elements. A p-type Bi_2Te_3 leg is simulated using the material parameters from Table 4.2, assuming $Q_C = 0$ W and $T_H = 300$ K, the netlist for which may be found in Appendix B.6. The pulse width is set to be t_{ret} (which is determined from previous simulations where the pulse width is very long) and $P = 2.5$ in order to match previous experimental and simulation results. Indeed Fig. 4.11 showing T_C vs. time has a similar response to the experimental results shown in Fig. 2 from Ref. [37].

Using Eqs. (4.23) - (4.25) the predicted $T_{C,Min} = T_{C,SS} - \Delta T_{Pulse}$ after pulse is 225.75 K and occurs at $t_{min} = 0.356$ s after the pulse, with $t_{ret} = 1.42$ s after the pulse. From the simulation $T_{C,min} = 224.93$ K, $t_{min} = 0.451$ s, and $t_{ret} = 2.13$ s.
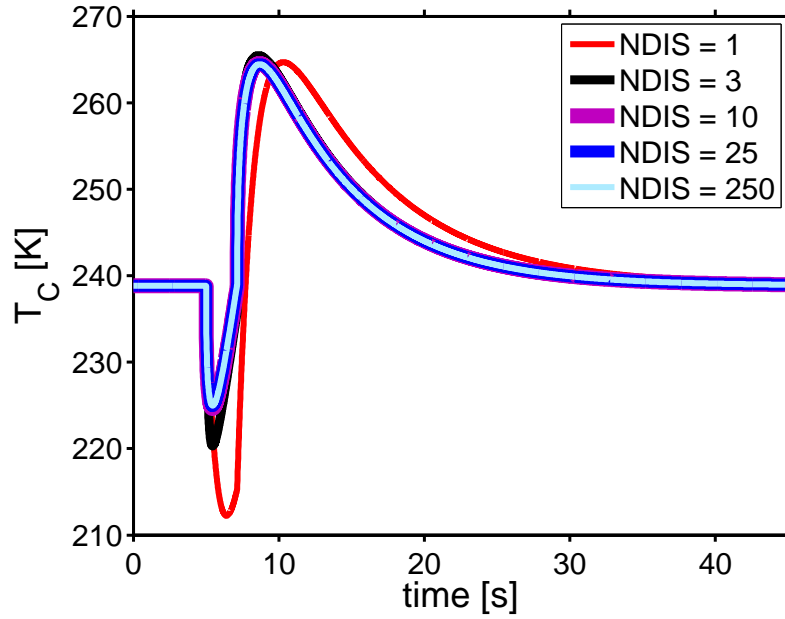
Fig. 4.10. The effect of the number of distributed elements on simulation results for pulsed cooling.
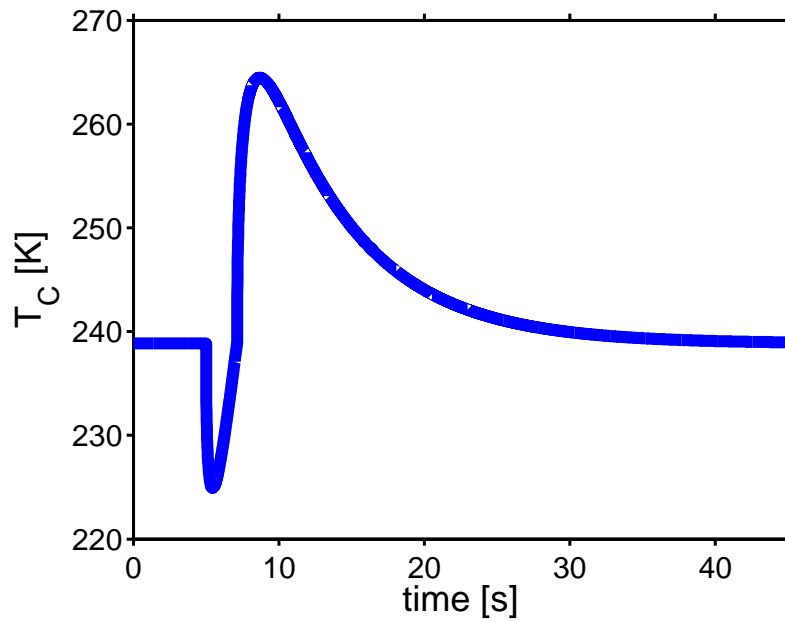
Fig. 4.11. Pulsed cooling simulation using 25 distributed elements.

4.4 AC Small Signal Simulation

Impedance spectroscopy will be explored in order to test the model under AC small signal conditions. Impedance spectroscopy is a measurement method that has been used to characterize a variety of materials and devices including photovoltaics and fuel cells [39]. When a small AC signal is applied at a variety of frequencies, processes within the device are distinguished from each other by the impedance response. The impedance spectrum is visualized on a plot of the real impedance against the imaginary impedance in a Nyquist plot. Faster process are able to occur at high frequency while slower processes are not, and so the impedance at each frequency varies based on the processes occurring. Impedance spectroscopy has recently been used to characterize thermoelectrics in a number of papers (such as Refs. [39] and [40]), making it an interesting case study for the equivalent circuit.

The impedance is given by the ratio of voltage to current across the thermoelectric leg.

$$Z = \frac{V}{I} = R + \frac{s(T_H - T_C)}{I} \tag{4.26}$$

Solving the heat equation (Eq. (4.1)) in the frequency domain, while neglecting the contacts, and the Joule effect (which is a reasonable assumption if the current is small) results in [39]

$$Z(j\omega) = R + \frac{s^2 T L}{\kappa A} \left(\frac{j\omega}{\omega_{TE}} \right)^{-1/2} \tanh \left\{ \left(\frac{j\omega}{\omega_{TE}} \right)^{1/2} \right\}' \tag{4.27}$$

where

$$\omega_{TE} = 2\pi f_{TE} = \frac{4\alpha}{L^2}. \tag{4.28}$$

Since low currents are used $T \approx T_{amb} = T_H$. A thermoelectric resistance

$$R_{TE} = \frac{s^2 T L}{\kappa A} \tag{4.29}$$

is defined, which has units of resistance and accounts for energetic losses due to the Seebeck effect. Examining the limits of Eq. (4.27) shows that at high frequency, the impedance is only due to the electrical resistance, R. As the frequency goes to 0, the

impedance is the sum of the thermoelectric resistance and the electrical resistance. This separation of effects in the frequency spectrum will be used in analyzing results.

One of the benefits of Impedance spectroscopy is that it allows for direct measurement of zT, similar to that of a modified Harman method. In the modified Harman method the resistance of device is measured under DC and AC conditions, and the ratio of the two results in $1 + zT$. Since impedance spectroscopy involves a sweep of a wide frequency range, it is simple to know the impedance at low frequencies (similar to a DC resistance measurement) and high frequencies (the AC resistance) [40]. Dividing the low frequency real impedance by the high frequency real impedance results in

$$\frac{R + R_{TE}}{R} = 1 + \frac{s^2 TL/\kappa A}{L/\sigma A} = 1 + \frac{s^2 \sigma}{\kappa}T = 1 + zT \qquad (4.30)$$

Using $Q_C = 0$ W and $T_H = 300$ K, the same Bi$_2$Te$_3$ thermoelement with parameters listed in Table 4.2 is simulated using Xyce with a 10 mV AC signal at a range of frequencies, the netlist for which is included in Appendix B.7. Again, this simulation requires a distributed model to improve the accuracy of the results (Fig. 4.12). The Nyquist plot is shown in Fig. 4.13. From the plot it can be determined that $R = 0.1$ Ω and $R_{TE} = 0.0643$ Ω, which are the same as the predicted results using the material parameters. Using these values of R and R_{TE}, $zT = 0.643$ by use of Eq. (4.30), the same as would be expected from the material parameters.

Experimental validation for this method was demonstrated by Cañadas and Min in Ref. [41] using a full thermoelectric module. This paper also provided the parameters of the device, and so can be used as inputs to the equivalent circuit and the results can be compared. As mentioned before, there are assumptions that are made in order to expand this single leg equivalent circuit to an entire module. The information about the TEM is displayed in Table 4.3.

A XYCE simulation of this TEM was performed using the material parameters in Table 4.3, $Q_C = 0$ W and $T_H = 300$ K boundary conditions, and a 10 mV AC voltage swept from 1 μHz to 1 MHz as described in the experiment (the netlist is found in Appendix B.8). Comparing the Nyquist plot created by the simulation
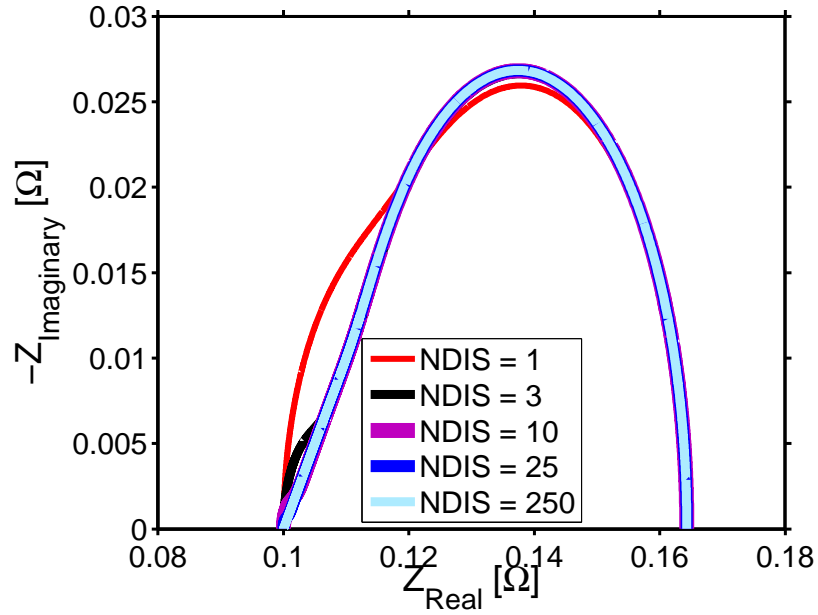
Fig. 4.12. The effect of the number of distributed elements on simulation results for AC simulation.

Table 4.3.

Material parameters for Bi_2Te_3 module simulations. These are the values assumed for the material parameters and device dimensions. These values completely specify the TEM in the equivalent circuit.

$s = 200$	$^{\mu V}/_K$
$\kappa = 1.5$	$^W/_{m \cdot K}$
$^1/_\sigma = 9.62$	$^{\mu \Omega}/_m$
$\rho = 7.7$	$^g/_{cm^3}$
$c_p = 0.17$	$^J/_{g \cdot K}$
$L = 1.5$	mm
$A = 1$	mm^2
$N = 245$	Number of thermoelements
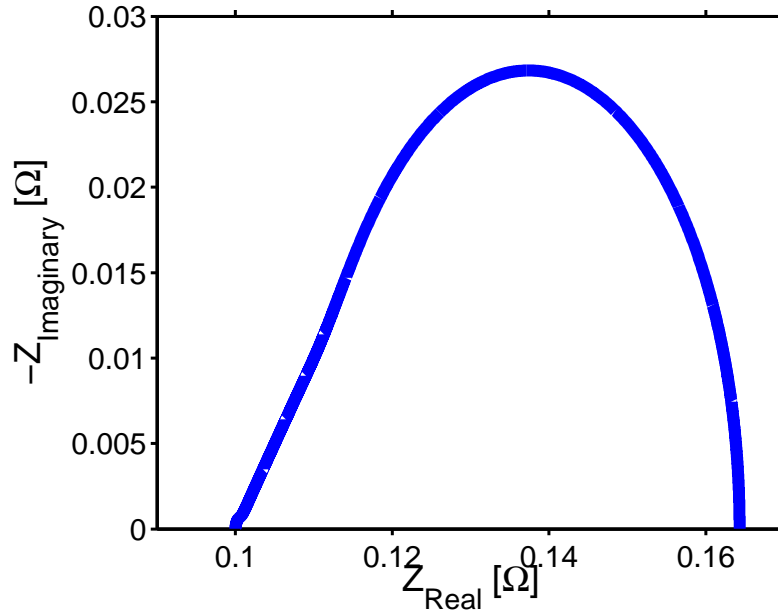
Fig. 4.13. The Nyquist plot from XYCE simulation of the equivalent circuit. The signal frequency increases from right to left, and the real intercepts are R (on the left) and $R + R_{TE}$ (on the right).

(Fig. 4.14) and Fig. 2 in Ref. [41], there are obvious differences. The simulation plot looks nearly identical to that of a single thermoelement, while the experimental result is nearly a perfect semi-circle. The differences in plots is attributed to the lack of ceramic plates and contacts, which have similar specific heats to the Bi_2Te_3 legs, in the simulation causing the imaginary impedance to increase. There is a small difference in experimental and simulated R_{TE}, but since the ceramic and contacts have larger thermal conductivity this difference is not as great as the imaginary impedance. The simulation gives $R = 3.66 \, \Omega$ and $R_{TE} = 3.05 \, \Omega$, which are the same as those predicted while ignoring the contacts and ceramic. This shows that in order for a full module to be simulated, both the ceramic and the contacts should be included.
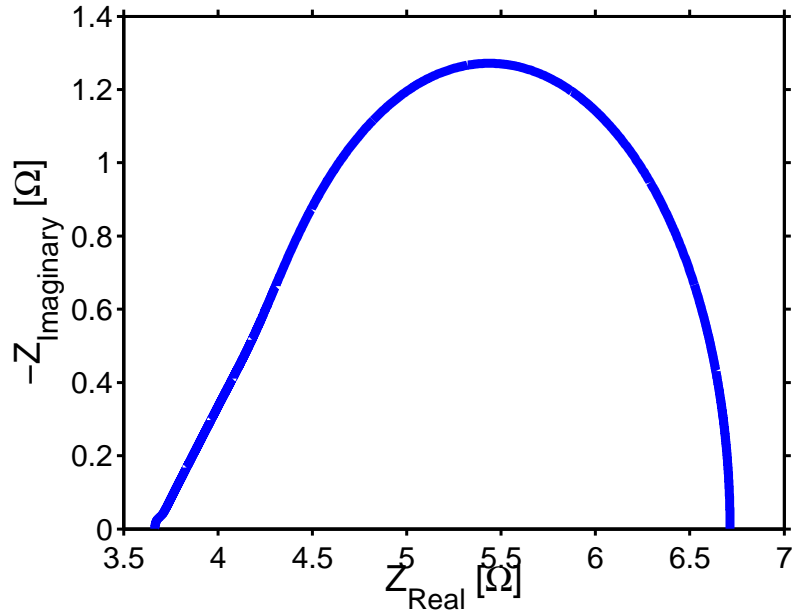
Fig. 4.14. The Nyquist plot from XYCE simulation of a full module. This plot can be compared to Fig. 2 in [41] to see the differences between experimental data and the simulation which neglects metal contacts and ceramic casing.

4.5 Conclusion

The equivalent circuit spice model has been tested under a variety of conditions. In DC the model was able to produce the same result as predicted by analytic expressions for cold side temperature and cold side heat absorbed at a variety of currents. Using a distributed model, the temperature within a thermoelement could be determined, and the result matched analytic expressions. Under transient conditions the model was able to match the turn off time constant for a variety of currents. As well, pulsed cooling was demonstrated, and showed similar results to published experimental results. Impedance spectroscopy was examined to test AC small signal operation, and the results were used to determine the material parameters used in the simulation. Experimental evidence of a full TEM was compared to simulation results and though similarities existed, it was determined that the model would need

to include the metal contacts and ceramic case to fully replicate results. Overall the model has stood up well to all of the test cases considered.

There are other envisioned tests for this model that have not been shown in this chapter, but have been considered. A simple test to perform would be to use the model in energy harvesting and power generation. Rather than applying a voltage or driving a current through the device, observe the electrical behavior resulting from a temperature difference.

The model presented in this chapter is a base for a variety of simulation conditions that could be used to model a variety of problems or to improve accuracy. To make the model more accurate, an n and a p leg could be modeled separately so that the assumption of identical legs (besides the Seebeck coefficient) would not be needed. Another problem that could be simulated would be to vary the material parameters throughout the leg (as performed in [42]). An important possible variant on the simulations performed thus far would be to consider temperature independent parameters [32]. Non-uniform heating of a module could also be modeled by changing the boundary conditions for different legs in the simulation.

The physics-based equivalent circuit model provides a fast and easy to understand model which may be used in system level design thanks to the XYCE simulation platform. In order to provide further benchmarking of this model, a thermoelectric leg will be simulated using Sentaurus, a widely used simulator for electronic devices, in the next chapter. Several of the tests performed on this equivalent circuit will be performed again, and the results will be compared.

5. SENTAURUS® SIMULATION OF A THERMOELECTRIC DEVICE

In this chapter a thermoelement will be simulated using Synopsis' Sentaurus® Workbench [43]. Sentaurus® Workbench is a collection of programs that can be used to design and simulate a variety of semiconductor devices. There are few examples of using Sentaurus® for thermoelectric devices (such as Refs. [44] and [45]), but it has been used to successfully model and simulate a variety of semiconductor devices including lasers, photovoltaics, and MOSFETs. The chapter will begin by describing the device setup and material parameters used in the simulation. Then the equations solved by the simulator will be presented, and the setup required for DC, transient, and AC small signal will be discussed. The simulation results from Sentaurus® will be presented and compared to the corresponding equivalent circuit results. The required files needed to run a simulation as discussed in this chapter are provided in Appendix C.

5.1 Device Setup and Parameter Definition

This section will describe the setup for the device used in simulation. First a device is created using Sentaurus® Structure Editor, and material parameters will be specified using Sentaurus® Device. Each of these programs has a command file associated with it, and will be referred to throughout this section.

A thermoelement is created using Sentaurus® Structure Editor [46]. With this tool, the physical device is defined, along with the real-space mesh and contacts. The mesh is used to break a structure into smaller sizes for an accurate solution. Devices may only be defined as 2D or 3D structures, but by defining the mesh properly, the simulation will act as though the properties don't change perpendicular to the direc-

tion of transport, similar to a 1D structure. This is important in order to correctly compare the results from the Sentaurus$^{\circledR}$ simulation to those of the equivalent circuit simulation. Contacts are created to allow electrical (where the contacts are called electrodes) and thermal (where the contacts are called thermode) stimuli, and act as boundary conditions in the simulation.

The device is a 5 mm x 1 mm^2 block of Si with a constant B doping of 1×10^{-19}cm^{-3}. Silicon was chosen as the material since it is the most thoroughly documented material within Sentaurus$^{\circledR}$, and more work is required to simulate higher efficiency thermoelectric materials. In order to decrease computation time, the simulation is performed on a 2D rather than a 3D object. In order to calculate values like current and resistance (quantities which are not densities and are bulk in nature) an area factor is used to multiply 2D results by. For this simulation, the area factor is 1 cm (the device is 5 cm long and 1 cm tall), and is defined in the Sentaurus$^{\circledR}$ Device command file. A cold contact at $x = 0$ and a hot contact at $x = L$ are also defined in the Sentaurus$^{\circledR}$ Structure Editor. In the structure editor, the contacts are only defined, the values and boundary condition declaration occurs in the device editor file. The structure editor command file may be found in Appendix C.1.

The Sentaurus$^{\circledR}$ Device command file is where the physics to include in the simulation, the equations to solve, and various stimuli are all specified [47]. In order to match the equivalent circuit simulation, the Sentaurus$^{\circledR}$ simulation must have constant material parameters. The material parameters are defined to be constant in a variety of ways, depending on the parameter in question. Some parameters can be made constant through the physics section in the Sentaurus$^{\circledR}$ Device command file, while others require writing a custom parameter file that can be read by Sentaurus$^{\circledR}$.

The Sentaurus$^{\circledR}$ Device command file and the parameter file (only the modified parts, not the entire file) are included in Appendix C.2 and C.3 respectively. The boundary conditions are specified in the device command file, and are associated with the contacts defined in the structure editor. The cold side of the device has an electrode with a voltage (the voltage changes depending on the simulation) and

a thermode with temperature of 300 K and 0 W power boundary condition. When two boundary conditions are defined (as is the case with the cold thermode), the temperature is taken as an initial guess when solving, and the power is the true boundary condition [47]. The cold side voltage starts at 0 V, but changes with time as will be discussed with the transient simulation. The hot side also has two contacts, the electrode with a 0 V boundary condition and the thermode with a 300 K boundary condition. Since only temperature is specified on the hot thermode, the temperature is kept fixed at 300 K, where as the cold side is kept at 0 W heat absorbed.

Sentaurus® calculates the conductivity rather than directly defining as is done in the equivalent circuit. Using the Drude expression for conductivity (Eq. (1.13)) along with the relationship between mobility and scattering time, $\mu = \frac{q\tau}{m^*}$, in order for the conductivity to remain constant, the mobillity and carrier concentration must be made constant. The carrier concentration is spatially constant as defined when the device was created, and the band gap narrowing is turned off in the general physics section as well. The mobility is kept constant with the constant mobility tag in the physics section of the Sentaurus® Device command file. The constant mobility tag references a line in the parameter file defining the hole mobility as 470.5 $^{cm^2}/_{V \cdot s}$. The other parameters that need to be constant are heat capacity, thermal conductivity, and Seebeck coefficient (called thermopower in Sentaurus®). Most of these material parameters are dependent on temperature according to a set expression, which can be made constant by setting some coefficients to 0.

The lattice thermal conductivity has two equations that may be used. Setting *Formula* = 1 in the parameter file means that the thermal conductivity is given by

$$\kappa = \kappa_a + \kappa_b T + \kappa_c T^2. \tag{5.1}$$

By setting $\kappa_b = \kappa_c = 0$, the thermal conductivity becomes independent of temperature and $\kappa = \kappa_a = 1.5$ $^W/_{cm \cdot K}$. The heat capacity is given by

$$c_v = c_{va} + c_{vb} T + c_{vc} T^2 + c_{vd} T^3. \tag{5.2}$$

Table 5.1.
Material parameters for a Si thermoelement used in Sentaurus®.

$s = 270$	$^{\mu V}/_K$	
$\kappa = 1.5$	$^W/_{cm \cdot K}$	
$c_v = 1.63$	$^J/_{cm^3 \cdot K}$	
$\mu = 470.5$	$^{cm^2}/_{V \cdot s}$	
$p = 1 \times 10^{19}$	cm^{-3}	
$L = 5$	mm	
$Height = 1$	mm	
$AreaFactor = 1$	mm	

The heat capacity becomes independent of temperature by setting $c_{vb} = c_{vc} = c_{vd} = 0$, so that $c_v = c_{va} = 1.63 \, ^J/_{K \cdot cm^3}$.

Unlike the other parameters, there is no simple way to define a constant Seebeck coefficient using predefined expressions in Sentaurus®. Sentaurus® does allow user defined expressions for physical models using a physical model interface (PMI) [47]. A PMI was written that allows for a single value to be defined for the Seebeck coefficient, with no dependence on any other parameter (the PMI is included in Appendix C.4). Using the PMI, the Seebeck coefficient for Sentaurus® was set to $270 \, ^{\mu V}/_K$. Now all important parameters are constant (summarized in Table 5.1) such that the device is identical to the one simulated by the equivalent circuit.

5.2   Equations and Simulation Setup

This section will focus on the physics included in the simulation, and the equations being solved. The physics options determine which phenomena occur in a device and change some terms in the solved equations. The physics options chosen here are to simplify the problem to be similar to the equivalent circuit model of the previous

chapter. Most of the physics is specified in a global physics section, such as constant mobility and area factor, which are described above.

The most important physics to include for a thermoelectric simulation is *thermodynamic*, which allows temperature to be included in calculations. The hole current density with the *thermodynamic* command is calculated as

$$\vec{J_p} = pq\mu_p \left(\nabla\Phi_p + s\nabla T \right) \tag{5.3}$$

where Φ_p is the quasi-Fermi potential of holes. The continuity equation for holes is given by

$$-\nabla \cdot \vec{J_p} = qR_{net} + q\frac{\partial p}{\partial t} \tag{5.4}$$

where R_{net} is the net recombination rate, which for this simulation is 0, since no recombination is allowed.

Both hot and cold contacts have additional physics to include the Peltier effect, which is included in a contact physics section rather than the global physics section. The *MSPeltier* command models the heat density from the Peltier effect for holes as

$$\dot{Q} = J_p \left(\alpha_p \Delta E_p + (1 - \alpha_p)\Delta\epsilon_p \right) \tag{5.5}$$

where

$$\Delta E_p = \Phi_M - \beta_p \left(\Phi_p + \gamma_p s_p T \right) + (1 - \beta_p)\frac{E_V}{q} \tag{5.6}$$

and α_p, β_p, γ_p and ϵ_p are fitting parameters, Φ_M and Φ_p are the Fermi potential of the metal and hole-doped TE material, respectively, and ΔE_p is the energy difference of holes across the interface [47]. With the fitting parameters set as $\alpha_p = \beta_p = \gamma_p = 1$ and $\epsilon_p = 0$ eV, Eq. (5.5) reduces to

$$\dot{Q} = J_p \left(\Phi_M - (\Phi_p + s_p T) \right) \tag{5.7}$$

Once the physics commands have been specified, the simulation begins to work on solving the desired equations. There are a couple of equations that need to be solved, and they are listed in the solve command in the Sentaurus® Device command

file. Initially, only the Poisson equation is solved. Then the Poisson equation is solved along with the electron and hole concentrations. Finally the Poisson equation is solved with the electron, hole, and temperature equations. The reason that these equations aren't solved together at once is to help Sentaurus® converge on a solution faster.

The Poisson equation is solved first as

$$\nabla \cdot \left(\epsilon \nabla \phi + \vec{P} \right) = -q(p - n + N_d - N_A) - \rho_{trap} \tag{5.8}$$

where ϕ is the electrostatic potential, $\vec{P}$ is the polarization, and ρ_{trap} is the trap density. The thermoelectric simulation has no traps, and no polarization. Then electron and hole concentration is solved using

$$n = N_C e^{\left(\frac{-q\Phi_n - E_C}{kT} \right)} \tag{5.9}$$

$$p = N_V e^{\left(\frac{E_V + q\Phi_p}{kT} \right)} \tag{5.10}$$

where N_C and N_V are the effective density of states for electrons and holes. The final equation to be solved is the temperature equation

$$\frac{\partial}{\partial t} c_L T - \nabla \cdot \kappa \nabla T = -\nabla \cdot \left[(s_n + T + \Phi_n) \vec{J}_n + (s_p + T + \Phi_n) \vec{J}_p \right] - \left(E_C + \frac{3}{2} k_b T \right) \nabla \cdot \vec{J}_n$$
$$- \left(E_V - \frac{3}{2} k_b T \right) \nabla \cdot \vec{J}_p + q R_{net} (E_C - E_V + 3k_b T) + \hbar \omega G_{opt} \tag{5.11}$$

which, using no recombination, no optical generation, the thermodynamic current density, constant material parameters, and assuming steady state conditions can be rewritten as

$$\frac{d^2 T(x)}{dx^2} = \frac{\vec{J}_n}{\kappa} \left(\frac{\vec{J}_n}{\sigma} \right) + \frac{\vec{J}_p}{\kappa} \left(\frac{\vec{J}_p}{\sigma} \right). \tag{5.12}$$

Equation (5.12) is the same equation that was being solved for by the equivalent circuit in the DC case (Eq. (4.4)), showing that the two simulators are both solving the same equation. Equations (5.8)-(5.11) are each solved during the simulation under a variety of stimuli. The stimuli for each test will be described in the next section, as well as the simulation results.

Table 5.2.
Material parameters for a Si thermoelement used in Xyce

$s = 270$	$\mu V/K$
$\kappa = 150$	$W/_{m \cdot K}$
$1/_\sigma = 13.2657$	$\mu\Omega/m$
$\rho = 1 \times 10^7$	g/cm^3
$c_p = 0.163$	$J/_{g \cdot K}$
$L = 5$	mm
$A = 1$	mm^2

5.3   Results

In this section the results of the simulations will be discussed, as well as how the stimuli for each simulation is created. All of the simulations are run using the same Sentaurus® Device command file (Appendix C.2).

Since the Sentaurus® simulation uses Si rather than Bi$_2$Te3, new equivalent circuit simulations must be performed as well. The only changes to the equivalent circuit simulations from Ch. 4 are the material parameters, which are shown in Table 5.2. The equivalent circuit netlists for Si are also included in Appendix C.

The first simulation is under DC bias, where the voltage on the cold contact is ramped up. This simulation is similar to the DC case for the equivalent circuit where the current is changed and the cold side temperature is examined. Voltage is ramped rather than current because in Sentaurus® the voltage boundary condition converges more easily than using the current as the boundary condition. The voltage ramping occurs in the solve section, with the *quasistationary* command. The cold side voltage is ramped from 0 to 0.2 V, and at each point during the ramp, the cold side temperature and current is measured. The hot side is kept at 0 V and 300 K.
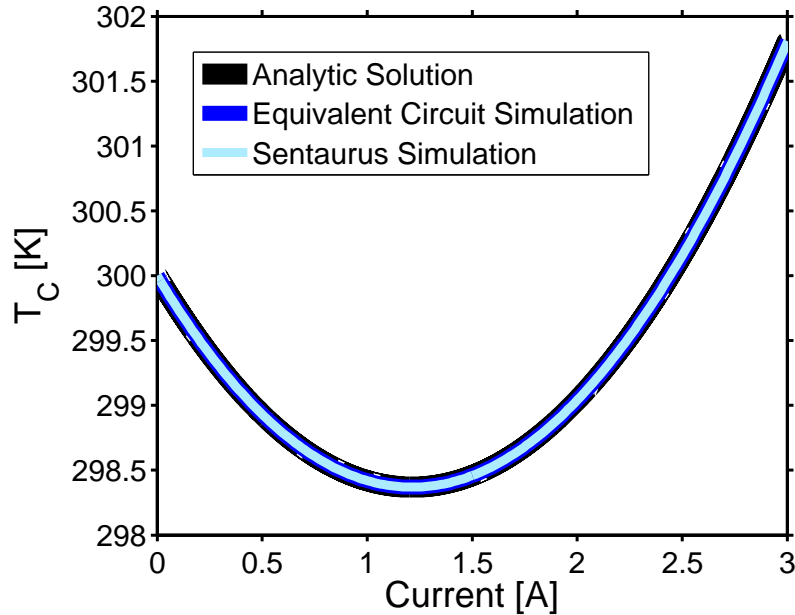
Fig. 5.1. T_C vs I for a Si thermoelement for a DC simulation. The analytic solution and both simulations have very good agreement with each other.

For the XYCE equivalent circuit simulation (the netlist is included in Appendix C.5) the voltage is also increased. The result of both simulations are shown in Fig. 5.1. Using Eqs. (4.16) and (4.17) predicts that $T_{C,Min} = 298.3693$ K and $I_{TC,Min} = 1.2146$ A. The analytic predictions are in good agreement with those found in the simulations ($T_{C,Min} = 298.3693$ K and $I_{TC,Min} = 1.2146$ A for both the Sentaurus® and XYCE simulations).

The pulsed cooling simulation from 4.3 is performed again with the Si thermoelement. The equivalent circuit netlist using 50 elements is presented in Appendix C.6. For this transient simulation the voltage rather than current is pulsed. The initial voltage is 0.081 V (the voltage that causes $T_{C,Min}$ in the DC case) and is pulsed to 0.2025 V (2.5 $\times$ the initial voltage) for 0.027 s (the length of time for the cold side temperature to return to $T_{C,Min}$), then returns to the initial voltage. In Sentaurus®, the voltage is pulsed within the contact definition by assigning a voltage to a time. When the voltage changes over time, Sentaurus® ramps the voltage linearly between
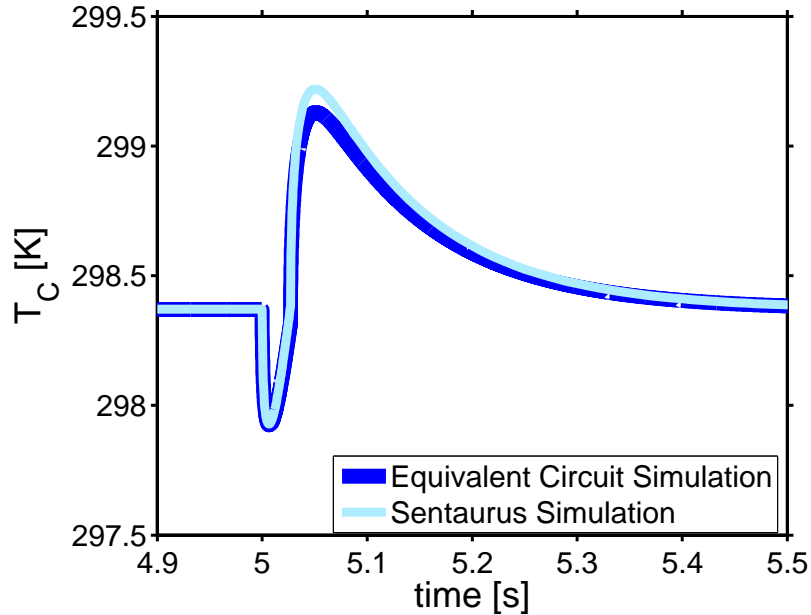
Fig. 5.2. T_C vs t for a pulsed cooling simulation. The two simulations have similar shape, though the Sentaurus® simulation does reach a higher temperature after the pulse is turned off.

the two points, which is undesirable when creating a square pulse. In order to make a square pulse, duplicate voltages are defined before and after voltage changes, so that no linear portions exist besides the rise and fall time. For both the equivalent circuit and Sentaurus® simulations the time and cold side temperature are recorded and plotted in Fig. 5.2. The shape of the temperature response is similar for both cases, though the Sentaurus® simulation has a slightly larger $\Delta T_{PostPulse}$ (hottest temperature reached after the pulse). The equivalent circuit simulation reaches a minimum cold side temperature of 297.9247 K 0.007 seconds after the pulse begins, while the Sentaurus® simulation reaches 297.9277 K 0.0065 s after the pulse begins. The difference in the temperature after the pulse is more pronounced, with the equivalent circuit reaching 299.1287 K 0.0512 s after the beginning of the pulse and the Sentaurus® simulation reaching 299.2195 K 0.0505 s after the beginning of the pulse.
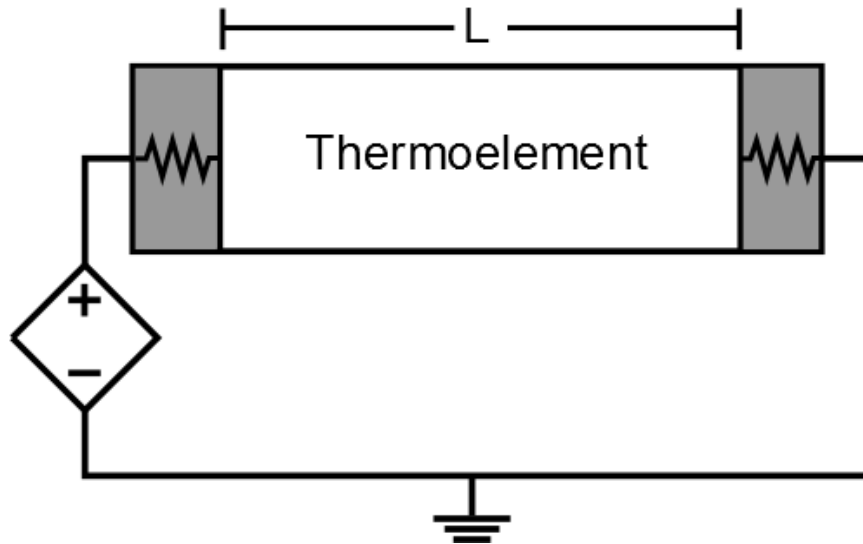
Fig. 5.3. The mixed mode circuit used in Sentaurus® simulation. There is a single voltage source in series with the thermoelement. The contacts have an included contact resistance.

The final test for the Sentaurus® simulation is under AC small signal conditions. In order to solve an AC small signal problem, Sentaurus® must use a mixed mode simulation. In mixed mode simulation, a circuit is created (see Fig. 5.3) and the stimuli are applied to nodes within the circuit. Using the *ACCoupled* command a 10 mV signal oscillates from 1 μHz to 1 MHz at the circuit node connecting to the cold contact. The same signal is applied in the equivalent circuit simulation (Appendix C.7). In mixed mode simulation, Sentaurus® automatically adds resistance to the contacts when they are connected to a circuit. By changing the default resistance, the shape of the Nyquist plot changes, as shown in Fig. 5.4. The added contact resistance must be subtracted from the real part of the impedance, but afterwards all Nyquist plots show the same high-frequency value of the electrical resistance of 0.06633 Ω, though as the frequency decreases the impedance spectra have large differences in both the real and imaginary components.

Using a contact resistance of 100 Ω/cm^2 (a total added resistance of 20000 Ω, the resistance doesn't need to be this large, but as shown in Fig. 5.4 too small of a
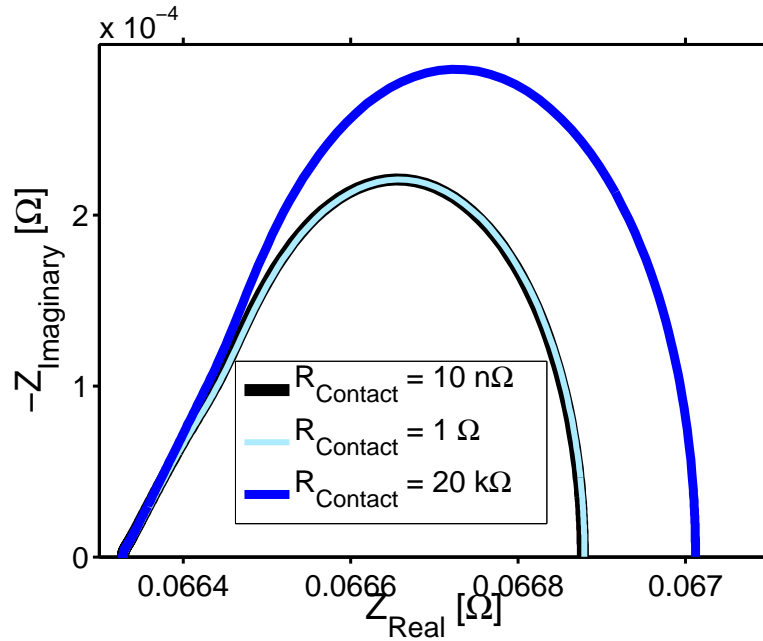
Fig. 5.4. A Nyquist plot comparison of how the contact resistance affects the shape of the impedance response in Sentaurus®. In a Nyquist plot the frequency increases from right to left.

resistance changes the shape of the impedance response) the Sentaurus® results look most similar to the equivalent circuit (See Fig. 5.5). In the high frequency regime (the left section of the plot), both simulations capture the same response (both find R = 0.06633 Ω), but as the frequency gets lower (moving from left to right in the plot) the equivalent circuit becomes larger in both real and imaginary magnitudes. At the low frequency real axis intercepts, the Nyquist plot is used to calculate the thermoelectric resistance, R_{TE} as defined in 4.4. The equivalent circuit calculates R_{TE} as 729.0 $\mu\Omega$, and the Sentaurus® simulation calculates R_{TE} as 684.2 $\mu\Omega$. The difference between the thermoelectric resistance in these two results is able to be explained with Eq. (4.29). The Sentaurus® simulation calculates the correct thermoelectric resistance if the Joule heating term is included, while the equivalent circuit is correct if the Joule heating term is neglected. It is yet unclear why this is the case, but is a question which is actively being examined.
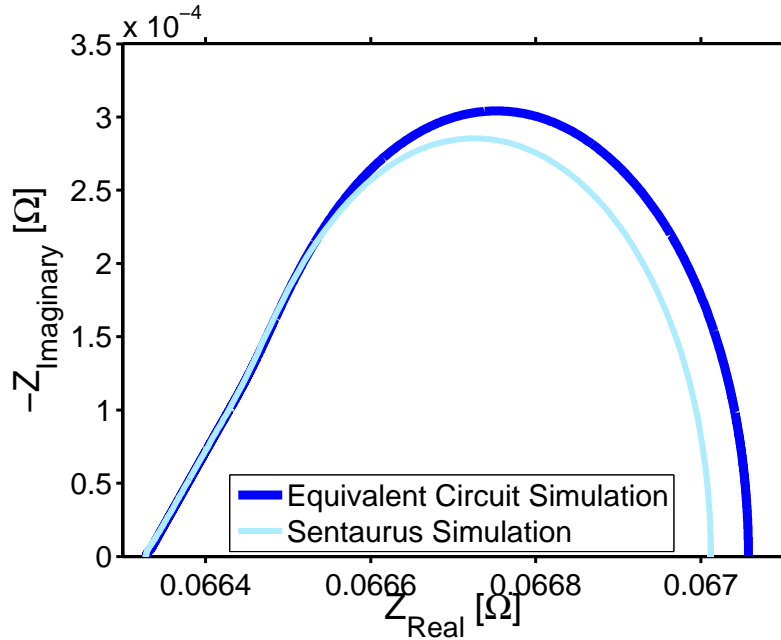
Fig. 5.5. A Nyquist plot comparison of the equivalent circuit and Sentaurus® simulations. The high frequency response is similar between the two, though at low frequencies the plots differ.

5.4 Conclusion

In this chapter a Sentaurus® simulation of a thermoelectric element was described and performed under a variety of operating conditions. The chapter began by describing how to set up the simulation such that the material parameters were constant and the device was similar to the equivalent circuit simulation. Then the equations solved in Sentaurus® were discussed, and shown to be the same as the equations discussed in Chapter 4. Finally the Sentaurus® simulation is performed under the same operating conditions as an equivalent circuit and the two are compared.

Under the DC case, the equivalent circuit and Sentaurus® simulations were exactly the same as the analytic results. For pulsed cooling, the two simulations were similar, though after the pulse ended there were slight differences, with the Sentaurus® simulation predicting a slightly larger $\Delta T_{PostPulse}$. The AC small signal simulation provided the largest difference between the two simulations. The Sentaurus® simulation

predicted the low frequency response including Joule heating, while the equivalent circuit predicted a result which did not include the changes due to Joule heating. This difference requires further investigation to reconcile.

Though this chapter was intended as a method of checking the equivalent circuit results, it also acts as a proof of concept for using Sentaurus® to model thermoelectric devices. The devices were simulated using Si, but in principle any thermoelectric material can be used. Since Sentaurus® contains a wide variety of options for simulations, there are many more areas that may be investigated for new materials than by just using an equivalent circuit simulation. More advanced simulations including recombination, generation, stress, and non uniform material parameters could be enabled with relative ease. In principle, many of the material parameters, and how they change with temperature and Fermi-level, could be known from LanTraP, and could be used in Sentaurus® to provide a straightforward way to examine a new material and easily perform simulation with that material.

6. CONCLUSIONS

The goal of this work has been to develop and test a physics-based, SPICE-compatible compact model for thermoelectric devices. The thesis began with an introduction to thermoelectrics, examining the history, effects, and potential uses. A discussion of thermoelectric transport theory followed where the Landauer approach was used to explain the thermoelectric transport parameters. The Landauer approach was then used as a basis for a tool LanTraP, which calculates the thermoelectric parameters of a material from a given dispersion relation for electrons and for phonons. This tool has been published on nanoHUB.org to serve as a resource for the thermoelectric community.

Next, an equivalent circuit for thermoelectric devices was presented and discussed. The required input parameters for the circuit model are the same as those that are output from LanTraP to provide a convenient means to assess the system level performance of new thermoelectric materials for which material parameter data is limited. Next, results from equivalent circuit simulations were compared to analytic, experimental, and other simulation results and was in good agreement in all cases. Finally thermoelements were simulated in Sentaurus®, a numerical simulation program that solves the thermoelectric equations was used as a computational benchmark for the equivalent circuit. The equivalent circuit is a simplified, lumped circuit representation of the real, distributed system that Sentaurus® simulated. DC and transient simulations using Sentaurus® were in good agreement with those obtained using the compact model. We did find, however, that the small-signal AC case did not match as well as other cases. This source of this difference is being investigated.

This thesis lays the groundwork for an end to end (atoms to applications) method for assessing the performance potential of thermoelectric devices made with new thermoelectric materials. For a new material, the thermoelectric transport parameters

can be calculated using LanTraP, and then directly input into the equivalent circuit. This capability should help transition new materials into real systems with the objective of realizing newer, more efficient devices.

Though the equivalent circuit compared well to previously published results, there are some areas that can be improved. As mentioned before, this work was focusing on simple cases and making assumptions that simplified the problem. In future work, these assumptions can be relaxed, and steps could be taken to work around them. Rather than assuming that the only resistances and capacitances were from the thermoelectric, it would be more accurate to add the external resistances and capacitances especially for the contacts and ceramic casing. It was also assumed that heat and current flowed parallel to each other, but that may not be the case. Heat sources from convection, as well as non-uniform heating may need to be considered. The temperature dependence of material parameters should also be considered, and could be easily added using LanTraP.

Sentaurus® was used in this thesis to benchmark the results of the equivalent circuit. There is a great deal of potential for improving Sentaurus® for use with thermoelectrics. For example, if Sentaurus® is to be used as a computational benchmark, some work to include the temperature dependence of thermoelectric transport parameters in Sentaurus® is needed. In addition, Sentaurus® had difficulties converging for high efficiency thermoelectrics due to large temperature changes. Sentaurus® is able to calculate many things that are not considered in the equivalent circuit. For example, with Sentaurus® mechanical stress and compositional grading can be included. The equivalent circuit is simpler to implement and faster to run, but the results should always be compared to an accurate and correct numerical simulation such as Sentaurus®.

In summary, in this thesis I have demonstrated an end to end method for developing new thermoelectric materials. The central part of the process is an accurate, physics-based compact model. Only simple examples have been considered in this thesis, but more complex and difficult possibilities (such as temperature dependence,

graded material profiles, and non-uniform heating) may be easily simulated in the same manner. This compact model should help make developing thermoelectric devices within electronic systems easier and help modern thermoelectric devices to find widespread use.

REFERENCES

REFERENCES

[1] J. P. Heremans, M. S. Dresselhaus, L. E. Bell, and D. T. Morelli, "When thermoelectrics reached the nanoscale," *Nat Nano*, vol. 8, no. 7, pp. 471–473, Jul. 2013. [Online]. Available: http://www.nature.com/nnano/journal/v8/n7/full/nnano.2013.129.html

[2] J. F. Munro, *The Story of Electricity.* New York: D. Appleton and Company, 1902. [Online]. Available: http://hdl.handle.net/2027/uc2.ark:/13960/t6f18tq1p

[3] A. F. Ioffe, *Semiconductor Thermoelements and Thermoelectric Cooling.* London: Infosearch Ltd., 1957.

[4] "History of thermoelectrics." [Online]. Available: http://www.thermoelectrics.caltech.edu/thermoelectrics/history.html

[5] A. Shakouri, "Recent developments in semiconductor thermoelectric physics and materials," *Annual Review of Materials Research*, vol. 41, no. 1, pp. 399–431, 2011. [Online]. Available: http://dx.doi.org/10.1146/annurev-matsci-062910-100445

[6] T. M. Tritt, "Thermoelectric phenomena, materials, and applications," *Annual Review of Materials Research*, vol. 41, no. 1, pp. 433–448, 2011. [Online]. Available: http://dx.doi.org/10.1146/annurev-matsci-062910-100453

[7] L. E. Bell, "Cooling, heating, generating power, and recovering waste heat with thermoelectric systems," *Science*, vol. 321, no. 5895, pp. 1457–1461, Sep. 2008. [Online]. Available: http://www.sciencemag.org/content/321/5895/1457

[8] M. V. Vedernikov and E. K. Iordanishvili, "A.f. ioffe and origin of modern semiconductor thermoelectric energy conversion," in *XVII International Conference on Thermoelectrics, 1998. Proceedings ICT 98*, May 1998, pp. 37–42.

[9] E. J. Sandoz-Rosado, S. J. Weinstein, and R. J. Stevens, "On the thomson effect in thermoelectric power devices," *International Journal of Thermal Sciences*, vol. 66, pp. 1–7, Apr. 2013. [Online]. Available: http://www.sciencedirect.com/science/article/pii/S129007291200292X

[10] M. Lundstrom and C. Jeong, *Near-Equilibrium Transport: Fundamentals and Applications*, ser. Lessons from Nanoscience: A Lecture Note Series. New Jersey: World Scientific, 2013, vol. 2.

[11] H. J. Goldsmid, *Introduction to Thermoelectricity.* New York: Springer, 2010.

[12] G. J. Snyder and E. S. Toberer, "Complex thermoelectric materials," *Nat Mater*, vol. 7, no. 2, pp. 105–114, Feb. 2008. [Online]. Available: http://www.nature.com/nmat/journal/v7/n2/full/nmat2090.html

[13] H. J. Goldsmid, "Timeliness in the development of thermoelectric cooling," in *XVII International Conference on Thermoelectrics, 1998. Proceedings ICT 98*, May 1998, pp. 25–28.

[14] A. Caponiti, "Power - mars science laboratory," http://mars.jpl.nasa.gov/msl/ mission/technology/technologiesofbroadbenefit/power/.

[15] P. Sucheski, "2012 10best: 10 most promising future technologies - 10best cars." [Online]. Available: http://www.caranddriver.com/features/ 2012-10best-10-most-promising-future-technologies-feature

[16] Alic Chen and Paul K Wright, "Medical applications of thermoelectrics," in *Modules, Systems, and Applications in Thermoelectrics*. CRC Press, Apr. 2012, pp. 1–22. [Online]. Available: http://www.crcnetbase.com/doi/abs/10. 1201/b11892-30

[17] L. Francioso, C. De Pascali, P. Siciliano, A. De Risi, S. D'Amico, C. Veri, and M. Pasca, "Thin film technology flexible thermoelectric generator and dedicated ASIC for energy harvesting applications," in *2013 5th IEEE International Workshop on Advances in Sensors and Interfaces (IWASI)*, Jun. 2013, pp. 104–107.

[18] U. E. I. Administration, "Annual energy review." [Online]. Available: http://www.eia.gov/totalenergy/data/annual/\#summary

[19] J. He, M. G. Kanatzidis, and V. P. Dravid, "High performance bulk thermoelectrics via a panoscopic approach," *Materials Today*, vol. 16, no. 5, pp. 166–176, May 2013. [Online]. Available: http://www.sciencedirect.com/science/ article/pii/S136970211300151X

[20] N. W. Ashcroft and N. D. Mermin, *Solid State Physics*.

[21] G. Nolas, G. Slack, J. Cohn, and S. Schujman, "The next generation of thermoelectric materials," in *XVII International Conference on Thermoelectrics, 1998. Proceedings ICT 98*, May 1998, pp. 294–297.

[22] L. D. Hicks and M. S. Dresselhaus, "Effect of quantum-well structures on the thermoelectric figure of merit," *Phys. Rev. B*, vol. 47, no. 19, pp. 12 727–12 731, May 1993. [Online]. Available: http://link.aps.org/doi/10.1103/PhysRevB.47. 12727

[23] L.-D. Zhao, S.-H. Lo, Y. Zhang, H. Sun, G. Tan, C. Uher, C. Wolverton, V. P. Dravid, and M. G. Kanatzidis, "Ultralow thermal conductivity and high thermoelectric figure of merit in SnSe crystals," *Nature*, vol. 508, no. 7496, pp. 373–377, Apr. 2014. [Online]. Available: http: //www.nature.com/nature/journal/v508/n7496/full/nature13184.html

[24] Z. Tian, S. Lee, and G. Chen, "A comprehensive review of heat transfer in thermoelectric materials and devices," *arXiv:1401.0749 [cond-mat]*, Jan. 2014, arXiv: 1401.0749. [Online]. Available: http://arxiv.org/abs/1401.0749

[25] G. D. Mahan and J. O. Sofo, "The best thermoelectric," *PNAS*, vol. 93, no. 15, pp. 7436–7439, Jul. 1996. [Online]. Available: http: //www.pnas.org/content/93/15/7436

[26] S. Datta, *Lessons from Nanoelectronics: A New Perspective on Transport*, ser. Lessons from Nanoscience: A Lecture Note Series. New Jersey: World Scientific, 2012, vol. 1.

[27] A. Shakouri, S. Datta, and M. Lundstrom, *Thermoelectricity: From Atoms to Systems*. nanoHUB-U. [Online]. Available: https://nanohub.org/courses/TEAS

[28] C. Jeong, R. Kim, M. Luisier, S. Datta, and M. Lundstrom, "On landauer versus boltzmann and full band versus effective mass evaluation of thermoelectric transport coefficients," *Journal of Applied Physics*, vol. 107, no. 2, p. 023707, Jan. 2010. [Online]. Available: http://scitation.aip.org/content/aip/journal/jap/107/2/10.1063/1.3291120

[29] R. Kim, S. Datta, and M. Lundstrom, "Influence of dimensionality on thermoelectric device performance," *Birck and NCN Publications*, Feb. 2009. [Online]. Available: http://docs.lib.purdue.edu/nanopub/539

[30] K. Conrad, J. Maassen, and M. Lundstrom, "LanTraP," 2014.

[31] A. Paul, S. Salamat, C. Jeong, G. Klimeck, and M. Lundstrom, "An efficient algorithm to calculate intrinsic thermoelectric parameters based on landauer approach," *Birck and NCN Publications*, Jan. 2011. [Online]. Available: http://docs.lib.purdue.edu/nanopub/792

[32] D. Mitrani, J. Salazar, A. Turó, M. J. García, and J. A. Chávez, "One-dimensional modeling of TE devices considering temperature-dependent parameters using SPICE," *Microelectronics Journal*, vol. 40, no. 9, pp. 1398–1405, Sep. 2009. [Online]. Available: http://www.sciencedirect.com/science/article/pii/S0026269208001766

[33] ——, "Transient distributed parameter electrical analogous model of TE devices," *Microelectronics Journal*, vol. 40, no. 9, pp. 1406–1410, Sep. 2009. [Online]. Available: http://www.sciencedirect.com/science/article/pii/S0026269208003133

[34] E. R. Keiter, T. Mei, T. V. Russo, R. L. Schiek, P. E. Sholander, H. K. Thornquist, J. C. Verley, and D. G. Baur, "Xyce parallel electronic simulator users' guide, version 6.2," Sep. 2014.

[35] W. Liu, K. C. Lukas, K. McEnaney, S. Lee, Q. Zhang, C. P. Opeil, G. Chen, and Z. Ren, "Studies on the bi2te3bi2se3bi2s3 system for mid-temperature thermoelectric energy conversion," *Energy Environ. Sci.*, vol. 6, no. 2, pp. 552–560, Jul. 2013. [Online]. Available: http://pubs.rsc.org.ezproxy.lib.purdue.edu/en/content/articlelanding/2013/ee/c2ee23549h

[36] "Encyclopedia of thermal packaging." [Online]. Available: http://www.worldscientific.com/worldscibooks/10.1142/7819-vol4

[37] G. J. Snyder, J.-P. Fleurial, T. Caillat, R. Yang, and G. Chen, "Supercooling of peltier cooler using a current pulse," *Journal of Applied Physics*, vol. 92, no. 3, pp. 1564–1569, Aug. 2002. [Online]. Available: http://scitation.aip.org.ezproxy.lib.purdue.edu/content/aip/journal/jap/92/3/10.1063/1.1489713

[38] A. Miner, A. Majumdar, and U. Ghoshal, "Thermoelectromechanical refrigeration based on transient thermoelectric effects," *Applied Physics Letters*, vol. 75, no. 8, pp. 1176–1178, Aug. 1999. [Online]. Available: http://scitation. aip.org.ezproxy.lib.purdue.edu/content/aip/journal/apl/75/8/10.1063/1.124634

[39] J. García-Cañadas and G. Min, "Impedance spectroscopy models for the complete characterization of thermoelectric materials," *Journal of Applied Physics*, vol. 116, no. 17, p. 174510, Nov. 2014. [Online]. Available: http://scitation.aip.org/content/aip/journal/jap/116/17/10.1063/1.4901213

[40] A. D. Marchi and V. Giaretto, "An accurate new method to measure the dimensionless figure of merit of thermoelectric devices based on the complex impedance porcupine diagram," *Review of Scientific Instruments*, vol. 82, no. 10, p. 104904, Oct. 2011. [Online]. Available: http://scitation.aip.org.ezproxy.lib. purdue.edu/content/aip/journal/rsi/82/10/10.1063/1.3656074

[41] J. García-Cañadas and G. Min, "Low frequency impedance spectroscopy analysis of thermoelectric modules," *Journal of Elec Materi*, vol. 43, no. 6, pp. 2411–2414, Jun. 2014. [Online]. Available: http://link.springer.com/article/10. 1007/s11664-014-3095-4

[42] Z. B. Q Zhou, "Pulsed cooling of inhomogeneous thermoelectric materials," *Journal of Physics D: Applied Physics*, vol. 40, no. 14, p. 4376, 2007.

[43] "Framework." [Online]. Available: http://www.synopsys.com/Tools/TCAD/ Pages/Framework.aspx

[44] N. Y. A. S. C. A. Gould, "A 3d TCAD simulation of a thermoelectric module configured for thermoelectric power generation, cooling and heating," pp. 65–68, 2012.

[45] C. Gould and N. Shammas, "Three dimensional TCAD simulation of a thermo-electric module suitable for use in a thermoelectric energy harvesting system," in *Small-Scale Energy Harvesting*, M. Lallart, Ed. InTech, Oct. 2012.

[46] *Sentaurus Structure Editor User Guide.* Synopsis, Inc., Jun. 2012, vol. Version G-2012.06.

[47] *Sentaurus Device User Guide.* Synopsis, Inc., Jun. 2012, vol. Version G-2012.06.

APPENDICES

A. LANTRAP USER MANUAL

This appendix includes the LanTraP user manual to describe how to use the tool. An updated version of this document may be found at https://nanohub.org/tools/lantrap where the tool may also be accessed. The tool is free to use online, and may also be downloaded as a MATLAB file from the website. Tutorial cases are also available for download, and a step by step guide is provided for every tutorial case.

LanTraP: User Manual

Kyle Conrad, Jesse Maassen, Mark Lundstrom

1. Introduction

LanTraP is an online tool aimed at assisting research and education. The tool allows for a .txt file containing band structure information to be uploaded, from which the thermoelectric (TE) transport coefficients for electrons and phonons can be calculated. LanTraP supports any general band structure, from simplified parabolic/linear disperions to accurate full band descriptions, to perform thermoelectric calculations within the Landauer formalism. In this manual, the basics of the calculation method are outlined and all of the input parameters are described. For more information about transport and the Landauer formalism, see *Near-Equilibrium Transport: Fundamentals and Applications,* by M. Lundstrom & C. Jeong (World Scientific, Singapore, 2013).

2. Input Parameters

There are a few ways to use LanTraP. By uploading a dispersion relation (E(k) for electrons or E(q) for phonons) the user may then decide to calculate (i) just the distribution of modes or (ii) calculate the distribution of modes and the transport coefficients simultaneously. Alternatively the user may upload a distribution of modes file and proceed to calculate the transport coefficients directly. When the calculation is complete, the tool produces plots and tables of the modes and transport coefficients (which are available for download).

2.1 Load Data

When starting LanTraP this is first slide the user will see. This slide will allow the user to upload the electron or phonon dispersion (to calculate the thermoelectric properties and/or the distribution of modes) or a pre-calculated distribution of modes (to calculate the TE properties only). The first input is the 'Upload' drop down box. This is where the input data (in a .txt file) is uploaded. From the drop down menu select

'upload'. This selection will prompt a pop up window allowing the user to select the desired file. After selecting the file and pressing upload the data will appear in the 'Data file' box.
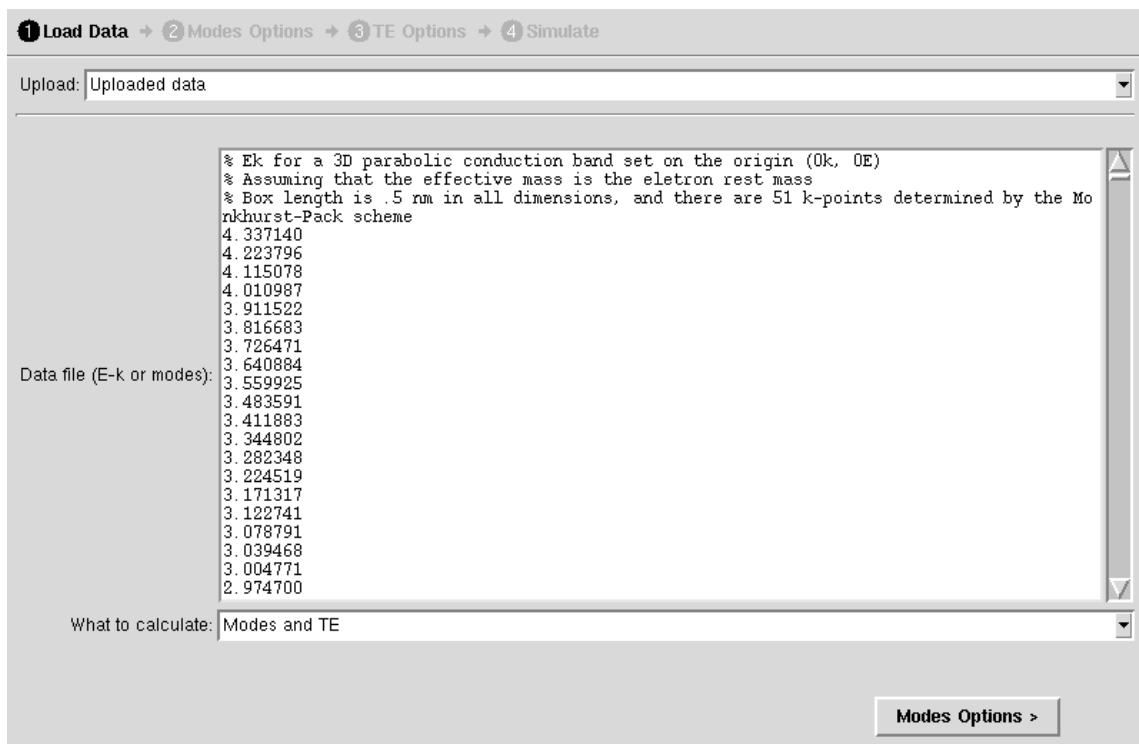
Figure 1: A screen shot of the 'Load Data' slide.

The 'Data file' text box shows what has been uploaded and allows the user to edit the file (for example to remove a header from the data). Note that the user can simply copy and paste data into the 'Data file' box. The uploaded data must have a specific format, depending on the data type (described below). The final option on this page is the 'What to calculate' drop down box. The options here are 'Modes', 'TE', and 'Modes and TE'. Depending on the data file, only certain options should be chosen. If an electron or phonon dispersion file has been uploaded choose either 'Modes' or 'Modes and TE' since a distribution of modes is required to calculate the transport coefficients. If the uploaded data was a pre-calculated distribution of modes, the user should only select

'TE'. Once completed, select the 'Modes Options' button in the bottom right corner to move to the next slide.

2.1.1 Format for the electron or phonon dispersion file

The basic format of a dispersion relation file is the following: each row vector lists the eigenvalues (in increasing order) corresponding to a specific k_x, k_y, k_z point, with the rows iterating over all the k-points in the Brillouin zone. The k-grid mesh must be uniform within the Brillouin zone along a given direction ($-\frac{\pi}{l}$ to $\frac{\pi}{l}$ where l is the box size in a given direction), but the density may be different along k_x, k_y and k_z. Note that the simulation box must be rectangular, with one direction corresponding to the transport direction. By labeling the k-points by the number from smallest to largest ($ik_x=1$ corresponding to the minimum k_x and $ik_x=n_x$ corresponding to the max k_x) the order of k-points in the dispersion file is as follows (see Figure 2):

- Each row corresponds to a list of eigenvalues.
- The rows iterate over all the k-points in the Brillouin zone.
- The sequence of k-points iterates over k_x, k_y, k_z (in this order).
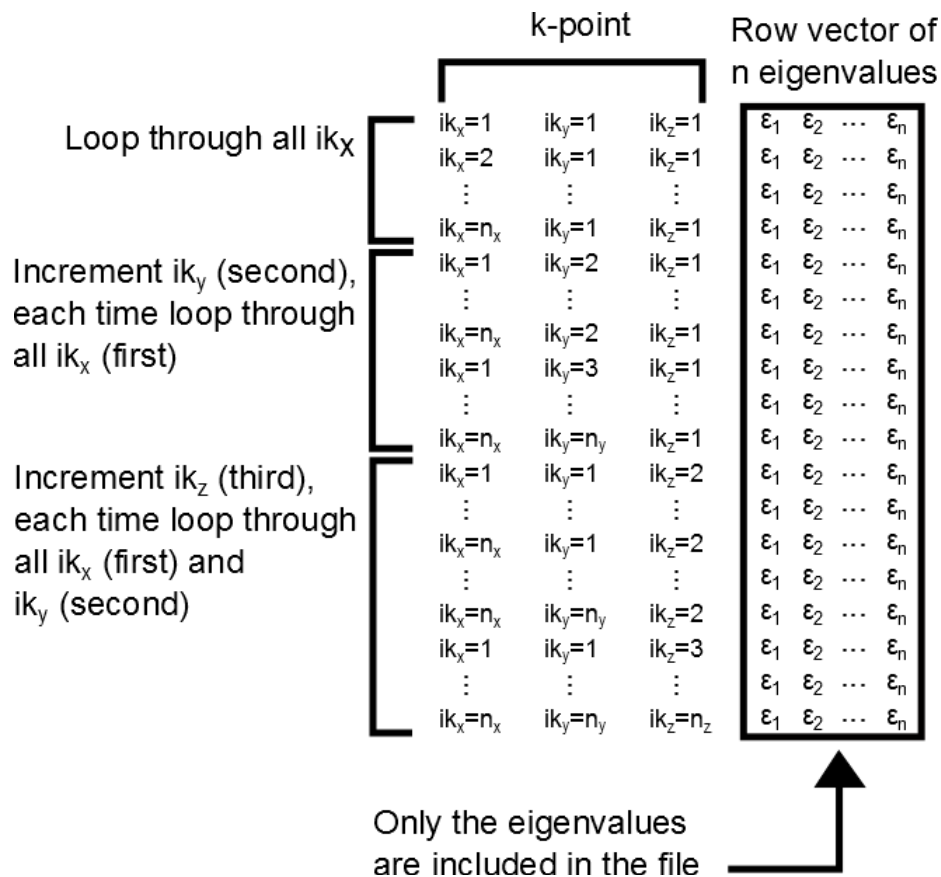
Figure 2: The proper format for an uploaded dispersion file.

2.1.2 Format for a distribution of modes file

For a pre-calculated distribution of modes the uploaded file has 2 columns, the first is an energy vector (in eV) in increasing order, and the second is the distribution of modes (in units of $m^{-(d-1)}$ where d is the dimensionality) at each energy. The output 'Modes Table' from the tool automatically has the correct format.

2.2 Modes Options

If on the 'Load Data' slide 'TE' was chosen from the 'What to calculate' drop down box, this slide has no options and prompts the user to select the 'TE Options' button. If from the 'What to calculate' drop down box either 'Modes' or 'Modes and TE' was selected the user will need to specify a number of parameters to calculate the modes, displayed on the 'Modes Options' slide.
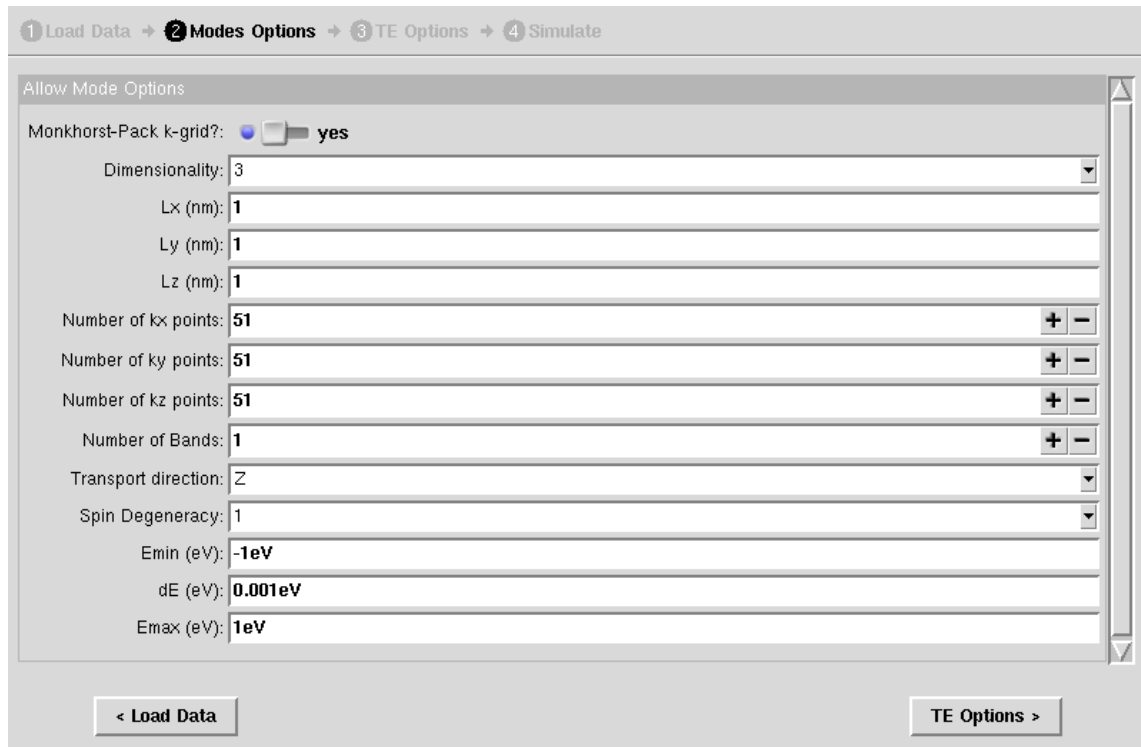
Figure 3: A screen shot of the 'Modes Options' slide.

- **'Monkhorst-Pack k-grid?'** (default = yes)

The 'Monkhorst-Pack k-grid?' boolean option allows for one of two uniformly spaced k-   grid organization schemes to be chosen. The Monkhorst-Pack k-grid is chosen so that   there are no duplicates in the Brillouin zone. If no is selected, the tool assumes that the first and last points of the k-grid are duplicates at the edge of the Brillouin zone, in k_x, k_y,   and k_z directions.

- **'Dimensionality'** (default = 3)

The user may select between 1, 2, and 3 dimensions from the drop down box. The   choice of dimensionality is important in determining the units of the distribution of modes   and the TE characteristics.

- **'Lx', 'Ly', and 'Lz'** (default = 1 nm)

These values correspond to the lengths of the simulation box used in creating the dispersion relation (in nm). If the user selects less than 3 dimensions, the tool will determine which lengths are used based on the number of k-points in each dimension,   with the largest numbers being the dimensions used.

- **'Number of k-points'** (default = 51 for k_x, k_y, and k_z)

  The 'Number of k-points' (for k_x, k_y, and k_z) are used to correctly interpret the uploaded file. If there is no periodicity along any of the directions, set the number of k-points along those directions to 1. Note that the distribution of modes may not be accurate if the k- grid is too coarse. By increasing the k-point density, eventually the modes will converge to the correct values and will no longer change with further increases in k-point density.

- **'Number of Bands'** (default = 1)

  Along with 'Number of k-points', 'Number of Bands' is used to correctly interpret the uploaded file. Note that the number of bands must be the same for all k-points.

- **'Transport direction'** (default = Z)

  The 'Transport direction' drop down menu is used to identify the transport direction, and assigns the other directions as perpendicular k-points when calculating modes.

- **'Spin Degeneracy'** (default = 2)

  The 'Spin Degeneracy' drop down box allows for either 1 or 2 to be chosen. The spin degeneracy parameter is set to 1 (2) when each band should only hold 1 (2) electron. This ensures that the calculated distribution of modes, for electrons, is per spin (i.e. identical spin-up and spin-down states will count as a single mode). In the case of phonons the 'Spin Degeneracy' should always be 2 (different by definition from electrons, the polarization of phonons is included in the calculation of the distribution of modes).

- **'Emin', 'dE', and 'Emax'** (default = -1eV, 0.001 eV, 1 eV respectively)

  The next 3 options are 'Emin', 'dE', and 'Emax' which allow any value to be entered in eV. These values determine the energy range (from 'Emin' to 'Emax') as well as the resolution ('dE') for which modes will be calculated. There will always be 0 modes where no band exists, so choose the energy range near the range of eigenvalues in the dispersion. Note that using a 'dE' that is too large may lead to significant errors. Thus, it is good practice to decrease 'dE' to ensure the distribution of modes is converged and accurate. Some suggested values are:

  - **Electrons** 'dE' should be in the range of 0.01 eV to 0.001 eV

▪ **Phonons** 'dE' should be in the range of 0.0001 eV to 0.000001 eV

After all of these options have been modified, the 'TE options' button in the lower right will move the tool onto the next slide.

2.3 TE Options

Figure 4: A screen shot of the 'TE Options' slide.

If on the 'Load Data' slide the user chose 'TE' or 'Modes and TE' this slide will have options, otherwise the slide will show a message that there are no options to modify.

- **'Particle'** (default = Electron)
  The 'Particle' drop down box has two options 'Electron' or 'Phonon'. This determines what properties are calculated.
- **'Temperature (K)'** (default = 300K)
  The lattice temperature (in K).
- **'Transport type'** (default = Ballistic)

'Transport type' is a drop down box with choices of 'Ballistic', 'Diffusive', and 'Quasi-Ballistic', where the last option allows the user to set the length of the transport region.

The choice of 'Particle' and 'Transport type' changes the options available, which are detailed below.

2.3.1 Ballistic Transport

Electrons

- **'Ef min'** (default = -0.5 eV)

    'Ef min' should be chosen such that 'Ef min' > 15 k_bT + Emin where Emin is the minimum   energy of the distribution of modes.

- **'delta Ef'** (default = 0.001 eV)

    The value of 'delta Ef' is the resolution of the Fermi energy range for which transport   coefficients are calculated over.

- **'Ef max'** (default = 0.5 eV)

    'Ef max' should be chosen such that 'Ef max' < Emax -15 k_bT where Emax is the maximum energy of the distribution of modes.

The reason for the restrictions on the Ef-grid is to insure the tool performs a proper integration. If the Fermi energy range is too wide, an error will occur and the calculation will stop without completion. For electron ballistic transport the tool will calculate electrical conductance, Seebeck coefficient, electron thermal conductance, power factor, and electronic zT (where K_L is assumed to be 0).

Phonons

For phonon ballistic transport there are no other options to modify and the tool will calculate the lattice thermal conductance.

2.3.2 Diffusive Transport

For diffusive transport there are more options, especially when the particle being considered is an electron. The tool allows for an energy dependent mean-free-path, with the form:

$$\lambda(E) = \lambda_0 \left(\frac{E_{ref}}{k_b T} \right)^r \tag{1}$$

where E_{ref} depends on the case considered and is defined below.

Electrons

For electron diffusive transport, all of the options for ballistic transport still need to be set in addition to the following scattering parameters:

- **'MFP CB'** (default = 10 nm)

  The mean-free-path of electrons in the conduction band (λ_0 in Equation (1)).

- **'CB scattering parameter'** (default = 0)

  The scattering exponent (r in Equation (1)) of the conduction band.

- **'Conduction Band Minimum'** (default = 0 eV)

  The minimum energy of the conduction band. For the conduction band, $E_{ref} = E - E_{CB}$ in Equation (1) where E_{CB} is the 'Conduction Band Minimum'.

- **'MFP VB'** (default = 10 nm)

  The mean-free-path of electrons in the valence band (λ_0 in Equation (1)).

- **'VB scattering parameter'** (default = 0)

  The scattering exponent (r in Equation (1)) of the valence band.

- **'Valence Band Maximum'** (default = -1 eV)

  The minimum energy of the valence band. For the valence band, $E_{ref} = E - E_{VB}$ in Equation (1) where E_{VB} is the 'Valence Band Maximum'. The 'Conduction Band Minimum' and 'Valence Band Maximum' are required to be different values, with 'Valence Band Maximum' being less than 'Conduction Band Minimum' for the calculation to occur.

For electrons the tool will calculate electrical conductivity, Seebeck coefficient, electron thermal conductivity, power factor, and electronic zT (where κ_L is assumed to be 0).

Phonons

For phonon diffusive transport, only a single mean-free-path and scattering parameter are required, since $E_{ref} = E$ in Equation (1).

- **'MFP Phonon'** (default = 10 nm)

  The mean-free-path of phonons (λ_0 in Equation (1)).
- **'Scattering Parameter'** (default = 0)

  The scattering exponent (r in Equation (1)) for phonons.

For phonons, the tool will calculate the lattice thermal conductivity.

2.3.3 Quasi-Ballistic Transport

For quasi-ballistic transport, the options are the same as diffusive transport (including the ballistic transport options for electrons), but with the following added parameter:

- **'Conductor length'** (default = 10 nm)

  This is the length of the material (in nm) along the transport direction.

The tool will calculate the same values as diffusive transport when quasi-ballistic transport is selected. However, transport in this case can be in between fully ballistic and fully diffusive.

3. Simulate

After the 'TE Options' slide, the calculation begins after pressing the simulate button in the lower right. On the screen, simulation information will appear, such as which calculation is being performed or any errors that may occur. Commonly the most time consuming part is the calculation of the distribution of modes. The computation time will increase with the size of the uploaded data file and the resolution of the Fermi energy

grid. The tool will typically run for anywhere between a few seconds to several minutes before completion.

Once the simulation is complete, the final slide will have a plot and the 'Result' drop down menu. From the drop down menu all of the calculated values can be selected to be plotted within the tool. If multiple simulations were run in the same instance of the tool, the results may be compared against each other. If an output was not calculated due to the choice of 'What to calculate' the plot will only contain one point at (0,0). As well, the 'Modes Table', 'TE Table', and 'Phonon Lattice Thermal Conductivity/Conductance' show the results in table form. Each output may be downloaded from the tool using the button next to the 'Result' drop down. The tables are designed to be downloaded and directly loaded into programs, such as MATLAB.
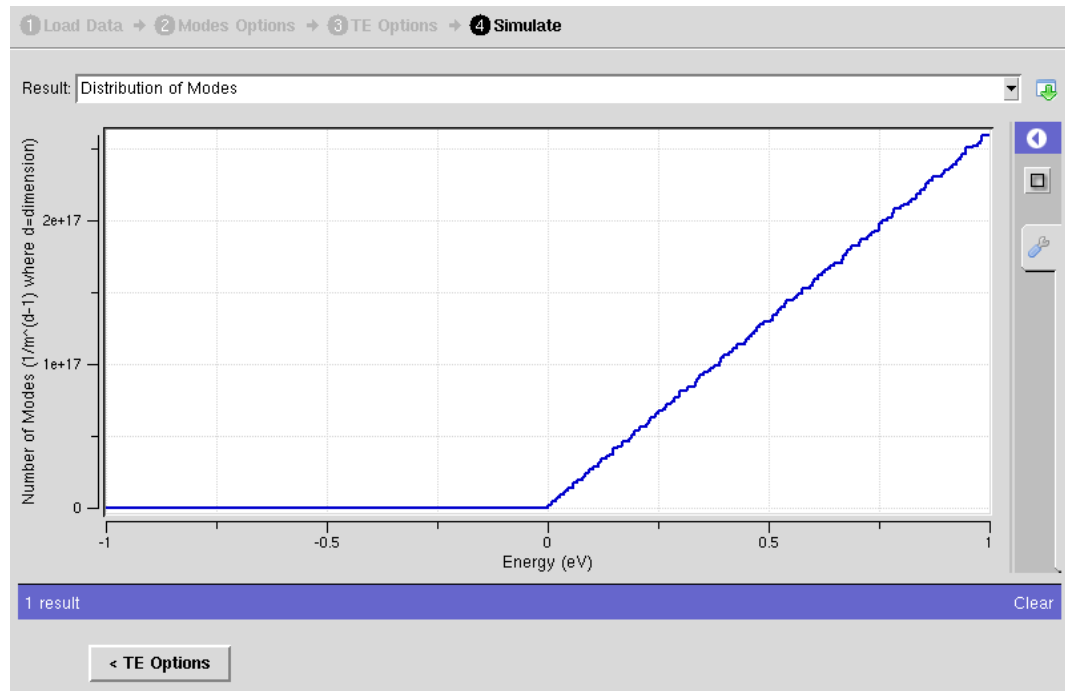
Figure 5: A screen shot of the 'Simulate' slide after calculation has completed.

B. BI$_2$TE$_3$ EQUIVALENT CIRCUIT NETLISTS

This appendix includes netlists for the test cases used in Chapter 4. Most of the netlists are using the same material parameters (see Table 4.2), and all that changes is the stimulus, Icool or Vcool, and the analysis performed. For more information on XYCE and understanding the netlists, see the XYCE User's Guide [34].

B.1   DC Lumped Model to Determine $T_{C,Min}$

```
*MATERIAL PARAMETERS***********
.PARAM S    =      0.000245        ;Seebeck  Coefficient                          [V/K]
.PARAM TK   =           1.4        ;Thermal  Conductivity                         [W/m–K]
.PARAM ER   =         2e−05        ;Electrical  Resistivity                       [Ohms/m]
.PARAM CP   =         0.158        ;Specific  Heat                                [J/kg–K]
.PARAM DEN  =      7.75e+06        ;Density                                       [kg/m^3]

*DEVICE PARAMETERS*************
.PARAM L    =         0.005        ;Device  Length                               [m]
.PARAM A    =         1e−06        ;Device  Area                                 [m^2]
.PARAM N    =             1        ;Number  of  Thermoelements

*SIMULATION PARAMETERS*********
.PARAM TAMB=            300        ;Ambient  Temperature                         [K]
.PARAM NDIS=              1        ;Number  of  Distributions

*CALCULATED PARAMETERS*********
.PARAM LE  = {L/NDIS}             ;Length  per  Distribution                     [m]
.PARAM SE  = {N*S}                ;Device  Seebeck                              [V/K]
.PARAM R   = {N*LE*ER/A}          ;Electrical  Resistance  per  Distribution     [Ohms]
.PARAM K   = {N*TK*A/LE}          ;Thermal  Conductance  per  Distribution       [W/K]
.PARAM Rth = {1/K}                ;Thermal  Resistance  per  Distribution        [K/W]
.PARAM Cth = {N*CP*DEN*A*LE}      ;Thermal  Capacitance  per  Distribution       [J/K]

*INPUT/MEASURING NODES*********
* Thermal (nodes 1−3)
IC 0 1 0                          ;Cold  side  heat  absorbed(QC = 0)
```

```
VCmeas 1 2 DC 0                    ;Measuring QC
VH 3 0 DC {TAMB}                   ;Hot side temperature (TH=Tamb from heat sink)
* Electrical (nodes 4−5)
Icool 0 4 DC 10                    ;Current Source to force cooling (will be swept)
VEmeas 4 5 0                       ;Measuring the electrical current


*THE CIRCUIT********************
BQPC 2 0 I={I(VEmeas)*SE*V(1)}            ;Peltier Cooling
X1 2 3 5 0 TEELEMENT
BQPH 0 3 I={I(VEmeas)*SE*V(3)}            ;Peltier Heating


*THERMOELECTRIC SUBCIRCUIT*****
* These nodes define the X elements
.SUBCKT TEELEMENT 11 13 15 18
CPC 11 0 {Cth/6}                          ;Cold side Peltier Capacitance
RCth 11 12 {.5/K}                         ;Cold side thermal resistance
BQJ 0 12 I={I(VESCmeas)*I(VESCmeas)*R}    ;Joule Heating
CJ 12 0 {2*Cth/3}                         ;Joule Heating Capacitance
RHth 12 13 {.5/K}                         ;Hot side thermal resistance
CPH 13 0 {Cth/6}                          ;Hot side Peltier capacitance
VESCmeas 15 16 0                          ;Measuring current through the subsection
RE 16 17 {R}                              ;Subsection resistance
BS 17 18 V={SE*V(13,11)}                  ;Seebeck Voltage
.ENDS


*ANALYSIS AND RESULTS**********
.DC Icool 0 20 .001
.OP
.PRINT DC I(VEmeas) V(1)
.END
```

B.2 DC Lumped Model to Determine $Q_{C,Max}$

```
*MATERIAL PARAMETERS***********
.PARAM S    =    0.000245      ;Seebeck Coefficient                          [V/K]
.PARAM TK   =        1.4       ;Thermal Conductivity                         [W/m–K]
.PARAM ER   =     2e−05        ;Electrical Resistivity                       [Ohms/m]
.PARAM CP   =       0.158      ;Specific Heat                                [J/kg–K]
.PARAM DEN  =    7.75e+06      ;Density                                      [kg/m^3]


*DEVICE PARAMETERS*************
.PARAM L    =       0.005      ;Device Length                                [m]
.PARAM A    =     1e−06        ;Device Area                                  [m^2]
.PARAM N    =          1       ;Number of Thermoelements


*SIMULATION PARAMETERS*********
.PARAM TAMB=          300      ;Ambient Temperature                          [K]
.PARAM NDIS=            1      ;Number of Distributions


*CALCULATED PARAMETERS*********
.PARAM LE  = {L/NDIS}          ;Length per Distribution                      [m]
.PARAM SE  = {N*S}             ;Device Seebeck                               [V/K]
.PARAM R   = {N*LE*ER/A}       ;Electrical Resistance per Distribution       [Ohms]
.PARAM K   = {N*TK*A/LE}       ;Thermal Conductance per Distribution         [W/K]
.PARAM Rth = {1/K}             ;Thermal Resistance per Distribution          [K/W]
.PARAM Cth = {N*CP*DEN*A*LE}   ;Thermal Capacitance per Distribution         [J/K]


*INPUT/MEASURING NODES*********
* Thermal (nodes 1−3)
VC 1 0 DC {TAMB}               ;Cold side temperature (ambient)
VCmeas 1 2 DC 0                ;Measuring QC
VH 3 0 DC {TAMB}               ;Hot side temperature (TH=Tamb from heat sink)
* Electrical (nodes 4−5)
Icool 0 4 DC 10                ;Current Source to force cooling (will be swept)
VEmeas 4 5 0                   ;Measuring the electrical current


*THE CIRCUIT*******************
BQPC 2 0 I={I(VEmeas)*SE*V(1)}          ;Peltier Cooling
X1 2 3 5 0 TEELEMENT
BQPH 0 3 I={I(VEmeas)*SE*V(3)}          ;Peltier Heating


*THERMOELECTRIC SUBCIRCUIT*****
* These nodes define the X elements
.SUBCKT TEELEMENT 11 13 15 18
CPC 11 0 {Cth/6}                        ;Cold side Peltier Capacitance
```

```
RCth 11 12 {.5/K}                          ;Cold side thermal resistance
BQJ 0 12 I={I(VESCmeas)*I(VESCmeas)*R}     ;Joule Heating
CJ 12 0 {2*Cth/3}                          ;Joule Heating Capacitance
RHth 12 13 {.5/K}                          ;Hot side thermal resistance
CPH 13 0 {Cth/6}                           ;Hot side Peltier capacitance
VESCmeas 15 16 0                           ;Measuring current through the subsection
RE 16 17 {R}                               ;Subsection resistance
BS 17 18 V={SE*V(13,11)}                   ;Seebeck Voltage
.ENDS


*ANALYSIS AND RESULTS**********
.DC Icool 0 20 .001
.OP
.PRINT DC I(VEmeas) V(1) I(VCmeas)
.END
```

B.3 DC Distributed Model Biased at $T_{C,Min}$

```
*MATERIAL PARAMETERS***********
.PARAM S    =      0.000245      ;Seebeck Coefficient                      [V/K]
.PARAM TK   =           1.4      ;Thermal Conductivity                     [W/m–K]
.PARAM ER   =         2e−05      ;Electrical Resistivity                   [Ohms/m]
.PARAM CP   =         0.158      ;Specific Heat                            [J/kg–K]
.PARAM DEN  =      7.75e+06      ;Density                                  [kg/mˆ3]


*DEVICE PARAMETERS*************
.PARAM L    =         0.005      ;Device Length                            [m]
.PARAM A    =         1e−06      ;Device Area                              [mˆ2]
.PARAM N    =             1      ;Number of Thermoelements


*SIMULATION PARAMETERS*********
.PARAM TAMB=            300       ;Ambient Temperature                     [K]
.PARAM NDIS=             10       ;Number of Distributions


*CALCULATED PARAMETERS*********
.PARAM LE  = {L/NDIS}           ;Length per Distribution                   [m]
.PARAM SE  = {N*S}              ;Device Seebeck                            [V/K]
.PARAM R   = {N*LE*ER/A}        ;Electrical Resistance per Distribution    [Ohms]
.PARAM K   = {N*TK*A/LE}        ;Thermal Conductance per Distribution      [W/K]
.PARAM Rth = {1/K}              ;Thermal Resistance per Distribution       [K/W]
.PARAM Cth = {N*CP*DEN*A*LE}    ;Thermal Capacitance per Distribution      [J/K]


*INPUT/MEASURING NODES*********
* Thermal (nodes 1−12)
IC 0 1 0                        ;Cold side heat absorbed(QC = 0)
VCmeas 1 2 DC 0                 ;Measuring QC
VH 12 0 DC {TAMB}                ;Hot side temperature (TH=Tamb from heat sink)
* Electrical (nodes 13−23)
Icool 0 13 DC 10                ;Current Source to force cooling (will be swept)
VEmeas 13 14 0                   ;Measuring the electrical current


*THE CIRCUIT*******************
BQPC 2 0 I={I(VEmeas)*SE*V(1)}          ;Peltier Cooling
X1 2 3 14 15 TEELEMENT
X2 3 4 15 16 TEELEMENT
X3 4 5 16 17 TEELEMENT
X4 5 6 17 18 TEELEMENT
X5 6 7 18 19 TEELEMENT
X6 7 8 19 20 TEELEMENT
X7 8 9 20 21 TEELEMENT
```

```
X8  9  10  21  22  TEELEMENT
X9  10  11  22  23  TEELEMENT
X10  11  12  23  0  TEELEMENT
BQPH  0  12  I={I(VEmeas)*SE*V(12)}              ;Peltier  Heating


*THERMOELECTRIC  SUBCIRCUIT*****
*  These  nodes  define  the  X  elements
.SUBCKT  TEELEMENT  20  22  24  27
CPC  20  0  {Cth/6}                      ;Cold  side  Peltier  Capacitance
RCth  20  21  {.5/K}                     ;Cold  side  thermal  resistance
BQJ  0  21  I={I(VESCmeas)*I(VESCmeas)*R}  ;Joule  Heating
CJ  21  0  {2*Cth/3}                     ;Joule  Heating  Capacitance
RHth  21  22  {.5/K}                     ;Hot  side  thermal  resistance
CPH  22  0  {Cth/6}                      ;Hot  side  Peltier  capacitance
VESCmeas  24  25  0                      ;Measuring  current  through  the  subsection
RE  25  26  {R}                          ;Subsection  resistance
BS  26  27  V={SE*V(22,20)}              ;Seebeck  Voltage
.ENDS


*ANALYSIS  AND  RESULTS**********
.DC  Icool  0  20  .001
.OP
.PRINT  DC  I(VEmeas)  V(1)  V(3)  V(4)  V(5)  V(6)  V(7)  V(8)  V(9)  V(10)  V(11)  V(12)
.END
```

B.4   DC Distributed Model Biased at $Q_{C,Max}$

```
*MATERIAL PARAMETERS***********
.PARAM S    =     0.000245        ;Seebeck Coefficient                             [V/K]
.PARAM TK   =           1.4       ;Thermal Conductivity                            [W/m–K]
.PARAM ER   =        2e−05        ;Electrical Resistivity                          [Ohms/m]
.PARAM CP   =         0.158       ;Specific Heat                                   [J/kg–K]
.PARAM DEN  =      7.75e+06       ;Density                                         [kg/m^3]


*DEVICE PARAMETERS*************
.PARAM L    =         0.005       ;Device Length                                   [m]
.PARAM A    =        1e−06        ;Device Area                                     [m^2]
.PARAM N    =             1       ;Number of Thermoelements


*SIMULATION PARAMETERS*********
.PARAM TAMB=            300        ;Ambient Temperature                            [K]
.PARAM NDIS=             10        ;Number of Distributions


*CALCULATED PARAMETERS*********
.PARAM LE  = {L/NDIS}            ;Length per Distribution                          [m]
.PARAM SE  = {N*S}               ;Device Seebeck                                   [V/K]
.PARAM R   = {N*LE*ER/A}         ;Electrical Resistance per Distribution           [Ohms]
.PARAM K   = {N*TK*A/LE}         ;Thermal Conductance per Distribution             [W/K]
.PARAM Rth = {1/K}               ;Thermal Resistance per Distribution              [K/W]
.PARAM Cth = {N*CP*DEN*A*LE}     ;Thermal Capacitance per Distribution             [J/K]


*INPUT/MEASURING NODES*********
* Thermal (nodes 1−12)
VC 1 0 DC {TAMB}                 ;Cold side temperature (ambient)
VCmeas 1 2 DC 0                  ;Measuring QC
VH 12 0 DC {TAMB}                ;Hot side temperature (TH=Tamb from heat sink)
* Electrical (nodes 13−23)
Icool 0 13 DC 10                 ;Current Source to force cooling (will be swept)
VEmeas 13 14 0                   ;Measuring the electrical current


*THE CIRCUIT*******************
BQPC 2 0 I={I(VEmeas)*SE*V(1)}            ;Peltier Cooling
X1 2 3 14 15 TEELEMENT
X2 3 4 15 16 TEELEMENT
X3 4 5 16 17 TEELEMENT
X4 5 6 17 18 TEELEMENT
X5 6 7 18 19 TEELEMENT
X6 7 8 19 20 TEELEMENT
X7 8 9 20 21 TEELEMENT
```

```
X8  9  10  21  22  TEELEMENT
X9  10  11  22  23  TEELEMENT
X10  11  12  23  0  TEELEMENT
BQPH  0  12  I={I(VEmeas)*SE*V(12)}              ;Peltier  Heating


*THERMOELECTRIC  SUBCIRCUIT*****
*  These  nodes  define  the  X  elements
.SUBCKT  TEELEMENT  20  22  24  27
CPC  20  0  {Cth/6}                              ;Cold  side  Peltier  Capacitance
RCth  20  21  {.5/K}                             ;Cold  side  thermal  resistance
BQJ  0  21  I={I(VESCmeas)*I(VESCmeas)*R}        ;Joule  Heating
CJ  21  0  {2*Cth/3}                             ;Joule  Heating  Capacitance
RHth  21  22  {.5/K}                             ;Hot  side  thermal  resistance
CPH  22  0  {Cth/6}                              ;Hot  side  Peltier  capacitance
VESCmeas  24  25  0                              ;Measuring  current  through  the  subsection
RE  25  26  {R}                                  ;Subsection  resistance
BS  26  27  V={SE*V(22,20)}                      ;Seebeck  Voltage
.ENDS


*ANALYSIS  AND  RESULTS**********
.DC  Icool  0  20  .001
.OP
.PRINT  DC  I(VEmeas)  V(1)  V(3)  V(4)  V(5)  V(6)  V(7)  V(8)  V(9)  V(10)  V(11)  V(12)
.END
```

B.5 Transient 25 Distribution Turn Off Biased at $T_{C,Min}$

```
*MATERIAL PARAMETERS***********
.PARAM S    =     0.000245      ;Seebeck Coefficient                          [V/K]
.PARAM TK   =          1.4      ;Thermal Conductivity                         [W/m–K]
.PARAM ER   =       2e−05       ;Electrical Resistivity                       [Ohms/m]
.PARAM CP   =        0.158      ;Specific Heat                                [J/kg–K]
.PARAM DEN  =     7.75e+06      ;Density                                      [kg/m^3]


*DEVICE PARAMETERS*************
.PARAM L    =        0.005      ;Device Length                                [m]
.PARAM A    =       1e−06       ;Device Area                                  [m^2]
.PARAM N    =            1      ;Number of Thermoelements


*SIMULATION PARAMETERS*********
.PARAM TAMB=          300       ;Ambient Temperature                          [K]
.PARAM IO   =       0.5852      ;The Initial current for a transient pulse    [A]
.PARAM IP   =            0      ;The Pulsed current for a transient pulse      [A]
.PARAM PW   =           60      ;The width of the current pulse               [s]
.PARAM NDIS=           25       ;Number of Distributions


*CALCULATED PARAMETERS*********
.PARAM LE  = {L/NDIS}           ;Length per Distribution                      [m]
.PARAM SE  = {N*S}              ;Device Seebeck                               [V/K]
.PARAM R   = {N*LE*ER/A}        ;Electrical Resistance per Distribution       [Ohms]
.PARAM K   = {N*TK*A/LE}        ;Thermal Conductance per Distribution         [W/K]
.PARAM Rth = {1/K}              ;Thermal Resistance per Distribution          [K/W]
.PARAM Cth = {N*CP*DEN*A*LE}    ;Thermal Capacitance per Distribution         [J/K]


*INPUT/MEASURING NODES*********
* Thermal (nodes 1−27)
IC 0 1 0                        ;Cold side heat absorbed(QC = 0)
VCmeas 1 2 DC 0                 ;Measuring QC
VH 27 0 DC {TAMB}               ;Hot side temperature (TH=Tamb from heat sink)
* Electrical (nodes 28−53)
Icool 0 28 PULSE({IO} {IP} 5 1us 1us {PW} 100)  ;Pulsed current source
VEmeas 28 29 0                  ;Measuring the electrical current


*THE CIRCUIT*******************
BQPC 2 0 I={I(VEmeas)*SE*V(1)}          ;Peltier Cooling
X1 2 3 29 30 TEELEMENT
X2 3 4 30 31 TEELEMENT
X3 4 5 31 32 TEELEMENT
X4 5 6 32 33 TEELEMENT
```

```
X5  6  7  33  34  TEELEMENT
X6  7  8  34  35  TEELEMENT
X7  8  9  35  36  TEELEMENT
X8  9  10  36  37  TEELEMENT
X9  10  11  37  38  TEELEMENT
X10  11  12  38  39  TEELEMENT
X11  12  13  39  40  TEELEMENT
X12  13  14  40  41  TEELEMENT
X13  14  15  41  42  TEELEMENT
X14  15  16  42  43  TEELEMENT
X15  16  17  43  44  TEELEMENT
X16  17  18  44  45  TEELEMENT
X17  18  19  45  46  TEELEMENT
X18  19  20  46  47  TEELEMENT
X19  20  21  47  48  TEELEMENT
X20  21  22  48  49  TEELEMENT
X21  22  23  49  50  TEELEMENT
X22  23  24  50  51  TEELEMENT
X23  24  25  51  52  TEELEMENT
X24  25  26  52  53  TEELEMENT
X25  26  27  53  0  TEELEMENT
BQPH  0  27  I={I(VEmeas)*SE*V(27)}          ;Peltier Heating

*THERMOELECTRIC SUBCIRCUIT*****
*  These nodes define the X elements
.SUBCKT TEELEMENT 35 37 39 42
CPC 35 0 {Cth/6}                            ;Cold side Peltier Capacitance
RCth 35 36 {.5/K}                           ;Cold side thermal resistance
BQJ 0 36 I={I(VESCmeas)*I(VESCmeas)*R}      ;Joule Heating
CJ 36 0 {2*Cth/3}                           ;Joule Heating Capacitance
RHth 36 37 {.5/K}                           ;Hot side thermal resistance
CPH 37 0 {Cth/6}                            ;Hot side Peltier capacitance
VESCmeas 39 40 0                            ;Measuring current through the subsection
RE 40 41 {R}                                ;Subsection resistance
BS 41 42 V={SE*V(37,35)}                    ;Seebeck Voltage
.ENDS

*ANALYSIS AND RESULTS**********
.TRAN 0.1 65 0ms 0.001s
.OP
.PRINT TRAN V(1)
.END
```

B.6 Pulsed Cooling with 25 Distributions

```
*******************************
*THERMOELECTRIC SPICE CIRCUIT**
***** Written 24-Dec-2014 *****
*******************************


*MATERIAL PARAMETERS***********
.PARAM S   =     0.000245       ;Seebeck Coefficient                       [V/K]
.PARAM TK  =          1.4       ;Thermal Conductivity                      [W/m-K]
.PARAM ER  =       2e-05        ;Electrical Resistivity                    [Ohms/m]
.PARAM CP  =        0.158       ;Specific Heat                             [J/kg-K]
.PARAM DEN =     7.75e+06       ;Density                                   [kg/m^3]


*DEVICE PARAMETERS*************
.PARAM L   =        0.005       ;Device Length                             [m]
.PARAM A   =       1e-06        ;Device Area                               [m^2]
.PARAM N   =            1       ;Number of Thermoelements


*SIMULATION PARAMETERS*********
.PARAM TAMB=          300       ;Ambient Temperature                       [K]
.PARAM IO  =       0.5852       ;The Initial current for a transient pulse [A]
.PARAM IP  =        1.463       ;The Pulsed current for a transient pulse  [A]
.PARAM PW  =       2.1305       ;The width of the current pulse            [s]
.PARAM NDIS=           25       ;Number of Distributions


*CALCULATED PARAMETERS*********
.PARAM LE  = {L/NDIS}           ;Length per Distribution                   [m]
.PARAM SE  = {N*S}              ;Device Seebeck                            [V/K]
.PARAM R   = {N*LE*ER/A}        ;Electrical Resistance per Distribution    [Ohms]
.PARAM K   = {N*TK*A/LE}        ;Thermal Conductance per Distribution      [W/K]
.PARAM Rth = {1/K}              ;Thermal Resistance per Distribution       [K/W]
.PARAM Cth = {N*CP*DEN*A*LE}    ;Thermal Capacitance per Distribution      [J/K]


*INPUT/MEASURING NODES*********
* Thermal (nodes 1-27)
IC 0 1 0                        ;Cold side heat absorbed(QC = 0)
VCmeas 1 2 DC 0                 ;Measuring QC
VH 27 0 DC {TAMB}               ;Hot side temperature (TH=Tamb from heat sink)
* Electrical (nodes 28-53)
Icool 0 28 PULSE({IO} {IP} 5 1us 1us {PW} 100)  ;Pulsed current source
VEmeas 28 29 0                  ;Measuring the electrical current


*THE CIRCUIT*******************
```

```
BQPC 2 0 I={I(VEmeas)*SE*V(1)}              ; Peltier  Cooling
X1 2 3 29 30 TEELEMENT
X2 3 4 30 31 TEELEMENT
X3 4 5 31 32 TEELEMENT
X4 5 6 32 33 TEELEMENT
X5 6 7 33 34 TEELEMENT
X6 7 8 34 35 TEELEMENT
X7 8 9 35 36 TEELEMENT
X8 9 10 36 37 TEELEMENT
X9 10 11 37 38 TEELEMENT
X10 11 12 38 39 TEELEMENT
X11 12 13 39 40 TEELEMENT
X12 13 14 40 41 TEELEMENT
X13 14 15 41 42 TEELEMENT
X14 15 16 42 43 TEELEMENT
X15 16 17 43 44 TEELEMENT
X16 17 18 44 45 TEELEMENT
X17 18 19 45 46 TEELEMENT
X18 19 20 46 47 TEELEMENT
X19 20 21 47 48 TEELEMENT
X20 21 22 48 49 TEELEMENT
X21 22 23 49 50 TEELEMENT
X22 23 24 50 51 TEELEMENT
X23 24 25 51 52 TEELEMENT
X24 25 26 52 53 TEELEMENT
X25 26 27 53 0 TEELEMENT
BQPH 0 27 I={I(VEmeas)*SE*V(27)}            ; Peltier  Heating


*THERMOELECTRIC SUBCIRCUIT*****
* These nodes define the X elements
.SUBCKT TEELEMENT 35 37 39 42
CPC 35 0 {Cth/6}                            ; Cold side Peltier Capacitance
RCth 35 36 {.5/K}                           ; Cold side thermal resistance
BQJ 0 36 I={I(VESCmeas)*I(VESCmeas)*R}      ; Joule Heating
CJ 36 0 {2*Cth/3}                           ; Joule Heating Capacitance
RHth 36 37 {.5/K}                           ; Hot side thermal resistance
CPH 37 0 {Cth/6}                            ; Hot side Peltier capacitance
VESCmeas 39 40 0                            ; Measuring current through the subsection
RE 40 41 {R}                                ; Subsection resistance
BS 41 42 V={SE*V(37,35)}                     ; Seebeck Voltage
.ENDS


*ANALYSIS AND RESULTS**********
.TRAN 0.0005s 450ms 0.01s
```

```
.OP
.PRINT  TRAN  V(1)
.END
```

B.7   AC Small Signal with 25 Distributions

```
*MATERIAL PARAMETERS***********
.PARAM S    =     0.000245      ;Seebeck Coefficient                          [V/K]
.PARAM TK   =          1.4      ;Thermal Conductivity                         [W/m–K]
.PARAM ER   =       2e−05       ;Electrical Resistivity                       [Ohms/m]
.PARAM CP   =        0.158      ;Specific Heat                                [J/kg–K]
.PARAM DEN  =     7.75e+06      ;Density                                      [kg/m^3]


*DEVICE PARAMETERS*************
.PARAM L    =        0.005      ;Device Length                                [m]
.PARAM A    =       1e−06       ;Device Area                                  [m^2]
.PARAM N    =            1      ;Number of Thermoelements


*SIMULATION PARAMETERS*********
.PARAM TAMB=          300       ;Ambient Temperature                          [K]
.PARAM NDIS=           25       ;Number of Distributions


*CALCULATED PARAMETERS*********
.PARAM LE  = {L/NDIS}           ;Length per Distribution                      [m]
.PARAM SE  = {N*S}              ;Device Seebeck                               [V/K]
.PARAM R   = {N*LE*ER/A}        ;Electrical Resistance per Distribution       [Ohms]
.PARAM K   = {N*TK*A/LE}        ;Thermal Conductance per Distribution         [W/K]
.PARAM Rth = {1/K}              ;Thermal Resistance per Distribution          [K/W]
.PARAM Cth = {N*CP*DEN*A*LE}    ;Thermal Capacitance per Distribution         [J/K]


*INPUT/MEASURING NODES*********
* Thermal (nodes 1−27)
IC 0 1 0                        ;Cold side heat absorbed(QC = 0)
VCmeas 1 2 DC 0                 ;Measuring QC
VH 27 0 DC {TAMB}               ;Hot side temperature (TH=Tamb from heat sink)
* Electrical (nodes 28−53)
Vcool 28 0 AC 10m               ;AC signal with 10mV amplitude
VEmeas 28 29 0                  ;Measuring the electrical current


*THE CIRCUIT*******************
BQPC 2 0 I={I(VEmeas)*SE*V(1)}          ;Peltier Cooling
X1 2 3 29 30 TEELEMENT
X2 3 4 30 31 TEELEMENT
X3 4 5 31 32 TEELEMENT
X4 5 6 32 33 TEELEMENT
X5 6 7 33 34 TEELEMENT
X6 7 8 34 35 TEELEMENT
X7 8 9 35 36 TEELEMENT
```

```
X8  9  10  36  37  TEELEMENT
X9  10  11  37  38  TEELEMENT
X10  11  12  38  39  TEELEMENT
X11  12  13  39  40  TEELEMENT
X12  13  14  40  41  TEELEMENT
X13  14  15  41  42  TEELEMENT
X14  15  16  42  43  TEELEMENT
X15  16  17  43  44  TEELEMENT
X16  17  18  44  45  TEELEMENT
X17  18  19  45  46  TEELEMENT
X18  19  20  46  47  TEELEMENT
X19  20  21  47  48  TEELEMENT
X20  21  22  48  49  TEELEMENT
X21  22  23  49  50  TEELEMENT
X22  23  24  50  51  TEELEMENT
X23  24  25  51  52  TEELEMENT
X24  25  26  52  53  TEELEMENT
X25  26  27  53  0  TEELEMENT
BQPH  0  27  I={I(VEmeas)*SE*V(27)}         ;Peltier Heating

*THERMOELECTRIC SUBCIRCUIT*****
* These nodes define the X elements
.SUBCKT TEELEMENT 35 37 39 42
CPC 35 0 {Cth/6}                            ;Cold side Peltier Capacitance
RCth 35 36 {.5/K}                           ;Cold side thermal resistance
BQJ 0 36 I={I(VESCmeas)*I(VESCmeas)*R}      ;Joule Heating
CJ 36 0 {2*Cth/3}                           ;Joule Heating Capacitance
RHth 36 37 {.5/K}                           ;Hot side thermal resistance
CPH 37 0 {Cth/6}                            ;Hot side Peltier capacitance
VESCmeas 39 40 0                            ;Measuring current through the subsection
RE 40 41 {R}                                ;Subsection resistance
BS 41 42 V={SE*V(37,35)}                    ;Seebeck Voltage
.ENDS

*ANALYSIS AND RESULTS**********
.AC DEC 500 1u 1MEG
.OP
.PRINT AC I(VEmeas) V(29)
.END
```

B.8   AC Small Signal of a 245 Leg TEM

```
*******************************
*THERMOELECTRIC SPICE CIRCUIT**
***** Written 09−Jan−2015 *****
*******************************

*MATERIAL PARAMETERS***********
.PARAM S   =       0.0002       ;Seebeck Coefficient                    [V/K]
.PARAM TK  =          1.5       ;Thermal Conductivity                   [W/m–K]
.PARAM ER  =     9.62e−06       ;Electrical Resistivity                 [Ohms/m]
.PARAM CP  =        0.158       ;Specific Heat                          [J/kg–K]
.PARAM DEN =      7.7e+06       ;Density                                [kg/m^3]

*DEVICE PARAMETERS*************
.PARAM L   =       0.0015       ;Device Length                          [m]
.PARAM A   =        1e−06       ;Device Area                            [m^2]
.PARAM N   =          254       ;Number of Thermoelements

*SIMULATION PARAMETERS*********
.PARAM TAMB=          300       ;Ambient Temperature                    [K]
.PARAM NDIS=           25       ;Number of Distributions

*CALCULATED PARAMETERS*********
.PARAM LE  = {L/NDIS}           ;Length per Distribution                [m]
.PARAM SE  = {N*S}              ;Device Seebeck                         [V/K]
.PARAM R   = {N*LE*ER/A}        ;Electrical Resistance per Distribution [Ohms]
.PARAM K   = {N*TK*A/LE}        ;Thermal Conductance per Distribution   [W/K]
.PARAM Rth = {1/K}              ;Thermal Resistance per Distribution    [K/W]
.PARAM Cth = {N*CP*DEN*A*LE}    ;Thermal Capacitance per Distribution   [J/K]

*INPUT/MEASURING NODES*********
* Thermal (nodes 1−27)
IC 0 1 0                        ;Cold side heat absorbed(QC = 0)
VCmeas 1 2 DC 0                 ;Measuring QC
VH 27 0 DC {TAMB}               ;Hot side temperature (TH=Tamb from heat sink)
* Electrical (nodes 28−53)
Vcool 28 0 AC 10m               ;AC signal with 10mV amplitude
VEmeas 28 29 0                  ;Measuring the electrical current

*THE CIRCUIT*******************
BQPC 2 0 I={I(VEmeas)*SE*V(1)}          ;Peltier Cooling
X1 2 3 29 30 TEELEMENT
X2 3 4 30 31 TEELEMENT
```

```
X3  4  5  31  32  TEELEMENT
X4  5  6  32  33  TEELEMENT
X5  6  7  33  34  TEELEMENT
X6  7  8  34  35  TEELEMENT
X7  8  9  35  36  TEELEMENT
X8  9  10  36  37  TEELEMENT
X9  10  11  37  38  TEELEMENT
X10  11  12  38  39  TEELEMENT
X11  12  13  39  40  TEELEMENT
X12  13  14  40  41  TEELEMENT
X13  14  15  41  42  TEELEMENT
X14  15  16  42  43  TEELEMENT
X15  16  17  43  44  TEELEMENT
X16  17  18  44  45  TEELEMENT
X17  18  19  45  46  TEELEMENT
X18  19  20  46  47  TEELEMENT
X19  20  21  47  48  TEELEMENT
X20  21  22  48  49  TEELEMENT
X21  22  23  49  50  TEELEMENT
X22  23  24  50  51  TEELEMENT
X23  24  25  51  52  TEELEMENT
X24  25  26  52  53  TEELEMENT
X25  26  27  53  0  TEELEMENT
BQPH  0  27  I={I(VEmeas)*SE*V(27)}          ;Peltier Heating


*THERMOELECTRIC SUBCIRCUIT*****
* These nodes define the X elements
.SUBCKT TEELEMENT 35 37 39 42
CPC  35  0  {Cth/6}                          ;Cold side Peltier Capacitance
RCth  35  36  {.5/K}                         ;Cold side thermal resistance
BQJ  0  36  I={I(VESCmeas)*I(VESCmeas)*R}    ;Joule Heating
CJ  36  0  {2*Cth/3}                         ;Joule Heating Capacitance
RHth  36  37  {.5/K}                         ;Hot side thermal resistance
CPH  37  0  {Cth/6}                          ;Hot side Peltier capacitance
VESCmeas  39  40  0                          ;Measuring current through the subsection
RE  40  41  {R}                              ;Subsection resistance
BS  41  42  V={SE*V(37,35)}                  ;Seebeck Voltage
.ENDS


*ANALYSIS AND RESULTS**********
.AC DEC 500 1u 1MEG
.OP
.PRINT AC I(VEmeas) V(29)
.END
```

C. SI SENTAURUS SIMULATION FILES

This appendix includes necessary for simulations used in Chapter 5. The first four files are used in the Sentaurus simulations, while the last three files are netlists used by XYCE for the equivalent circuit simulations.

C.1   Sentaurus Structure Editor Command File

```
( sde : clear )

; Creating rectangular regions
(sdegeo:create−rectangle (position 0 0 0) (position 5000 1000 0)
 "Silicon" "Channel")

; Contact definitions
(sdegeo:define−contact−set "Cold" 4.0  (color:rgb 1.0 1.0 0.0 ) "##" )
(sdegeo:define−contact−set "Hot"  4.0  (color:rgb 1.0 0.0 0.0 ) "||" )

; Contact assignments
(sdegeo:set−current−contact−set "Cold")
(sdegeo:define−2d−contact (find−edge−id (position 0 500 0) )
  (sdegeo:get−current−contact−set))
(sdegeo:set−current−contact−set "Hot")
(sdegeo:define−2d−contact (find−edge−id (position 5000 500 0) )
  (sdegeo:get−current−contact−set))

; Constant doping profile definions
(sdedr:define−constant−profile "Const.Bulk" "BoronActiveConcentration" 1e19)
(sdedr:define−constant−profile−region "PlaceCD.Bulk" "Const.Bulk" "Channel")

; Meshing strategies
(sdedr:define−refinement−window "RefWin.Channel" "Rectangle"
  (position 0 0 0) (position 5000 1000 0))
(sdedr:define−refinement−size "RefDef.Channel" 100 1000 50 500)
(sdedr:define−refinement−placement "RefPlace.Channel" "RefDef.Channel" "RefWin.Channel")

; Meshing structure
```

```
( sde : build −mesh  "snmesh"  ""  "n@node@" )
```

C.2   Sentaurus Device Command File

```
File{
  Grid     = "@tdr@"
  Plot     = "@tdrdat@"
  Current  = "@plot@"
  Output   = "@log@"
  Parameter = "@parameter@"
  * PMI path
  PMIPath = "/home/min/a/conrad14/RESEARCH/Sentaurus/TE_Si_All/sentaurus_seebeck"
}


Device "Thermoelement" {
  Electrode{
        { name="Cold"  Voltage=(0.0 at 0,
                 0.081 at 0.001, 0.081 at 0.1, 0.081 at 5,
                 0.2025 at 5.0001, 0.2025 at 5.0002, 0.2025 at 5.0271,
                 0.081 at 5.0272) DistResist=100 }
        { name="Hot"   Voltage=0 DistResist=100 }
  }


  Thermode{
        { name="Cold"  Temperature=300 Power=0 }
        { name="Hot"   Temperature=300 }
  }


  Physics(Electrode="Cold") {
                 MSPeltierHeat
  }


  Physics(Electrode="Hot") {
                 MSPeltierHeat
  }


  Physics(Material="Silicon") {
  }
}
* End Device Declaration

System {
        Vsource_pset dc_V (enode1 0) {dc = 0.01}
        "Thermoelement" leg ("Cold"=enode1 "Hot"=0)
        Plot "circuitplot" (v(enode1) i(enode1 leg))
}
```

```
Plot{
*−−Electrcal Information
  TotalCurrent/Vector eCurrent/Vector hCurrent/Vector
  TotalCurrentDensity eCurrentDensity hCurrentDensity
*−−Thermal Information
  Temperature
  lHeatFlux
  PeltierHeat
  eJouleHeat
  hJouleHeat
  ThomsonHeat
  RecombinationHeat
*−−NewPlots
  ElectricField
  Potential
  eCurrent hCurrent
  eDensity hDensity
  eHeatFlux hHeatFlux
  eMobility hMobility
  eQuasiFermiEnergy hQuasiFermiEnergy
  eQuasiFermi hQuasiFermi
  eThermoelectricPower hThermoelectricPower
  LatticeTemperature
  ThermalConductivity
  Current
  TotalHeat
  LatticeHeatCapacity
}

Physics{
        AreaFactor=1000
        Mobility(ConstantMobility)
        EffectiveIntrinsicDensity(NoBandGapNarrowing)
        Thermodynamic
        * PMI
        TEPower(pmi_seebeck)
}

Math{
        Extrapolate
        Derivatives
        RelErrControl
        Digits= 6
```

```
            Iterations= 500
            Method= Blocked
            RhsMin = 1e−15
            ExtendedPrecision
            ACMethod=Blocked  ACSubMethod=Super
            SubMethod= Super ∗was ParDiSo
            Spice_Temperature = 300
}


Solve {
  ∗Building initial Solution
  Poisson
  Coupled {Poisson Electron Hole}
  Coupled {Poisson Electron Hole Temperature}

  ∗Solving DC Voltage Sweep,sweeps the voltage at the node, not the contact
  Quasistationary (
        Goal {Node="enode1" Voltage=0.2}
        Minstep = 1e−5 Maxstep = 1e−2)
        {
        Coupled {Poisson Electron Hole Temperature}
        Plot ( FilePrefix = "Outputs/DCSweep/dc"
          Time = (Range = (0 1) Intervals =200) NoOverwrite)
        }
  ∗Solving AC, no plots saved as extraction_ac_des.plt
  ACCoupled (StartFrequency = 1e−6  EndFrequency = 1e6
        NumberOfPoints= 500 Decade
        Node("enode1")
        Exclude(dc_V)
        )
  {Poisson Electron Hole Temperature}

  ∗Solving Voltage Pulse
  Transient (
        InitialTime = 0.5 FinalTime = 7
        MinStep = 0.1e−10 Maxstep = 1)
        {Coupled {Poisson Electron Hole Temperature}
        Plot( FilePrefix = "Outputs/VoltagePulse/pulse"
        Time = (range = (0.50 4.90) intervals = 44;
                range = (4.99 5.09) intervals = 200;
                range = (5.09 7.00) intervals = 191)
                NoOverwrite)
        }
}
```

C.3 Sentaurus Modified Parameter File

The parameter file is very large, so only the parts that have been modified are included in this section.

```
*******************************************************************************
*                              Model Parameters:                             *
*******************************************************************************


*************************** Lattice Heat Capacity: ***************************
*******************************************************************************

LatticeHeatCapacity
{ *  lumped electron-hole-lattice heat capacity

  *  cv() = cv + cv_b * T + cv_c * T^2 + cv_d * T^3
        cv        = 1.63   # [J/(K cm^3)]
        cv_b      = 0.0000e+00     # [J/(K^2 cm^3)]
        cv_c      = 0.0000e+00     # [J/(K^3 cm^3)]
        cv_d      = 0.0000e+00     # [J/(K^4 cm^3)]
}


*************************** Thermal Conductivity: ***************************
*******************************************************************************

Kappa
{ *  Lattice thermal conductivity

  *  kappa(Si) = 1 / ( Si_a + Si_b * T + Si_c * T^2 )
        Si_a      = 0.03   # [K cm/W]
        Si_b      = 1.5600e-03     # [cm/W]
        Si_c      = 1.6500e-06     # [cm/(W K)]

  Formula = 1

  *  Formula = 0:
  *  kappa() = 1 / ( 1/kappa + 1/kappa_b * T + 1/kappa_c * T^2 )
        1/kappa = 0.03   # [K cm/W]
        1/kappa_b         = 1.5600e-03     # [cm/W]
        1/kappa_c         = 1.6500e-06     # [cm/(W K)]

  *  Formula = 1:
  *  kappa() = kappa + kappa_b * T + kappa_c * T^2
```

```
        kappa    = 1.5    #  [W/(K cm)]
        kappa_b = 0.0000e+00     #  [W/(K^2 cm)]
        kappa_c = 0.0000e+00     #  [W/(K^3 cm)]
}


****************************  Mobility Models:  ******************************
*  mu_lowfield^(-1) = mu_dop(mu_max)^(-1) + mu_Enorm^(-1) + mu_cc^(-1)        *
*  Variable = electron value ,   hole value      #  [units]                  *
******************************************************************************


ConstantMobility:
{  *  mu_const = mumax  (T/T0)^(-Exponent)
        mumax    = 1.4170e+03  ,   4.7050e+02         #  [cm^2/(Vs)]
        Exponent           = 0 ,    0         #  [1]
        mutunnel           = 0.05  ,         0.05     #  [cm^2/(Vs)]

}
```

C.4 Constant Seebeck Coefficient PMI

```
/* Copyright (C) 2013, Purdue University
 *
 * Thermoelectric Power calculation routine
 *
 * Written by Xufeng Wang (wang159@purdue.edu)
 *
 * This package is free software; you can redistribute it and/or modify
 * it under the terms of the GNU General Public License as published by
 * the Free Software Foundation; either version 2 of the License, or
 * (at your option) any later version.
 *
 * This package is distributed in the hope that it will be useful,
 * but WITHOUT ANY WARRANTY; without even the implied warranty of
 * MERCHANTABILITY or FITNESS FOR A PARTICULAR PURPOSE.  See the
 * GNU General Public License for more details.
 *
 * You should have received a copy of the GNU General Public License
 * along with this program; if not, write to the Free Software
 * Foundation, Inc., 59 Temple Place, Suite 330, Boston, MA  02111-1307  USA
 */

#include <stdlib.h>

#include <iostream>
#include <fstream>
#include <string>
#include <iterator>
#include <sstream>
#include <vector>

#include "PMI.h"

using namespace std;

double const_power;

// implementation of Thermoelectric power calculation using the PMI interface
class PMI_Constant_TEPower : public PMI_ThermoElectricPower {

  public:
    PMI_Constant_TEPower(const PMI_Environment& env, bool is_electron);
    virtual ~PMI_Constant_TEPower ();
```

```
    virtual void Compute_power(
      const double t,    // lattice temperature
      const double dens, // carrier density
      double& power);    // thermoelectric power


    virtual void Compute_dpowerdt(
      const double t,    // lattice temperature
      const double dens, // carrier density
      double& dpowerdt); // derivative of thermoelectric power
                         // with respect to lattice temperature


    virtual void Compute_dpowerddens(
      const double t,    // lattice temperature
      const double dens, // carrier density
      double& dpowerddens); // derivative of thermoelectric power
                            // with respect to carrier density
};


PMI_Constant_TEPower::
PMI_Constant_TEPower (const PMI_Environment& env, bool is_electron) :
  PMI_ThermoElectricPower (env)
{
  if (is_electron) {
    const_power = this->InitParameter("s_e", -.000270);
  } else {
    const_power = this->InitParameter("s_h", .000270);
  }
}


PMI_Constant_TEPower::
~PMI_Constant_TEPower ()
{
}


void PMI_Constant_TEPower::
Compute_power (const double t, const double dens, double& power)
{
  power = const_power;
}


void PMI_Constant_TEPower::
Compute_dpowerdt (const double t, const double dens, double& dpowerdt)
{
```

```
    dpowerdt = 0;
}


void PMI_Constant_TEPower ::
Compute_dpowerddens (const double t, const double dens, double& dpowerddens)
{
    dpowerddens = 0;
}


extern "C"
PMI_ThermoElectricPower* new_PMI_h_ThermoElectricPower
(const PMI_Environment& env)
{
    return new PMI_Constant_TEPower(env, false);
}


extern "C"
PMI_ThermoElectricPower* new_PMI_e_ThermoElectricPower
(const PMI_Environment& env)
{
    return new PMI_Constant_TEPower(env, true);
}
```

C.5 DC Si Equivalent Circuit Netlist

```
*MATERIAL PARAMETERS***********
.PARAM S    =       0.00027      ;Seebeck Coefficient                        [V/K]
.PARAM TK   =          150       ;Thermal Conductivity                       [W/m–K]
.PARAM ER   = 1.32657e−05        ;Electrical Resistivity                     [Ohms/m]
.PARAM CP   =        0.163       ;Specific Heat                              [J/kg–K]
.PARAM DEN  =        1e+07       ;Density                                    [kg/m^3]


*DEVICE PARAMETERS*************
.PARAM L    =        0.005       ;Device Length                              [m]
.PARAM A    =       1e−06        ;Device Area                                [m^2]
.PARAM N    =           1        ;Number of Thermoelements


*SIMULATION PARAMETERS*********
.PARAM TAMB=           300       ;Ambient Temperature                        [K]
.PARAM NDIS=            10       ;Number of Distributions


*CALCULATED PARAMETERS*********
.PARAM LE  = {L/NDIS}            ;Length per Distribution                    [m]
.PARAM SE  = {N*S}               ;Device Seebeck                             [V/K]
.PARAM R   = {N*LE*ER/A}         ;Electrical Resistance per Distribution     [Ohms]
.PARAM K   = {N*TK*A/LE}         ;Thermal Conductance per Distribution       [W/K]
.PARAM Rth = {1/K}               ;Thermal Resistance per Distribution        [K/W]
.PARAM Cth = {N*CP*DEN*A*LE}     ;Thermal Capacitance per Distribution       [J/K]


*INPUT/MEASURING NODES*********
* Thermal (nodes 1−12)
IC 0 1 0                         ;Cold side heat absorbed(QC = 0)
VCmeas 1 2 DC 0                  ;Measuring QC
VH 12 0 DC {TAMB}                ;Hot side temperature (TH=Tamb from heat sink)
* Electrical (nodes 13−23)
Vcool 13 0 DC 10                 ;Voltage Source to force cooling (will be swept)
VEmeas 13 14 0                   ;Measuring the electrical current


*THE CIRCUIT*******************
BQPC 2 0 I={I(VEmeas)*SE*V(1)}              ;Peltier Cooling
X1 2 3 14 15 TEELEMENT
X2 3 4 15 16 TEELEMENT
X3 4 5 16 17 TEELEMENT
X4 5 6 17 18 TEELEMENT
X5 6 7 18 19 TEELEMENT
X6 7 8 19 20 TEELEMENT
X7 8 9 20 21 TEELEMENT
```

```
X8  9  10  21  22  TEELEMENT
X9  10  11  22  23  TEELEMENT
X10  11  12  23  0  TEELEMENT
BQPH  0  12  I={I(VEmeas)*SE*V(12)}                    ;Peltier  Heating


*THERMOELECTRIC  SUBCIRCUIT*****
*  These  nodes  define  the  X  elements
.SUBCKT  TEELEMENT  20  22  24  27
CPC  20  0  {Cth/6}                          ;Cold  side  Peltier  Capacitance
RCth  20  21  {.5/K}                         ;Cold  side  thermal  resistance
BQJ  0  21  I={I(VESCmeas)*I(VESCmeas)*R}    ;Joule  Heating
CJ  21  0  {2*Cth/3}                         ;Joule  Heating  Capacitance
RHth  21  22  {.5/K}                         ;Hot  side  thermal  resistance
CPH  22  0  {Cth/6}                          ;Hot  side  Peltier  capacitance
VESCmeas  24  25  0                          ;Measuring  current  through  the  subsection
RE  25  26  {R}                              ;Subsection  resistance
BS  26  27  V={SE*V(22,20)}                  ;Seebeck  Voltage
.ENDS


*ANALYSIS  AND  RESULTS**********
.DC  Vcool  0  .5  .001
.OP
.PRINT  DC  I(VEmeas)  V(1)
.END
```

C.6 Pulsed Cooling Si Equivalent Circuit Netlist

```
*MATERIAL PARAMETERS***********
.PARAM S   =      0.00027     ;Seebeck Coefficient                          [V/K]
.PARAM TK  =          150     ;Thermal Conductivity                         [W/m–K]
.PARAM ER  = 1.32657e−05      ;Electrical Resistivity                       [Ohms/m]
.PARAM CP  =        0.163     ;Specific Heat                                [J/kg–K]
.PARAM DEN =        1e+07     ;Density                                      [kg/m^3]


*DEVICE PARAMETERS*************
.PARAM L   =        0.005     ;Device Length                                [m]
.PARAM A   =        1e−06     ;Device Area                                  [m^2]
.PARAM N   =            1     ;Number of Thermoelements


*SIMULATION PARAMETERS*********
.PARAM TAMB=          300     ;Ambient Temperature                          [K]
.PARAM IO  =        0.081     ;The Initial current for a transient pulse    [A]
.PARAM IP  =       0.2025     ;The Pulsed current for a transient pulse     [A]
.PARAM PW  =        0.027     ;The width of the current pulse               [s]
.PARAM NDIS=           50     ;Number of Distributions


*CALCULATED PARAMETERS*********
.PARAM LE  = {L/NDIS}         ;Length per Distribution                      [m]
.PARAM SE  = {N*S}            ;Device Seebeck                               [V/K]
.PARAM R   = {N*LE*ER/A}      ;Electrical Resistance per Distribution       [Ohms]
.PARAM K   = {N*TK*A/LE}      ;Thermal Conductance per Distribution         [W/K]
.PARAM Rth = {1/K}            ;Thermal Resistance per Distribution          [K/W]
.PARAM Cth = {N*CP*DEN*A*LE}  ;Thermal Capacitance per Distribution         [J/K]


*INPUT/MEASURING NODES*********
* Thermal (nodes 1−52)
IC 0 1 0                      ;Cold side heat absorbed(QC = 0)
VCmeas 1 2 DC 0               ;Measuring QC
VH 52 0 DC {TAMB}             ;Hot side temperature (TH=Tamb from heat sink)
* Electrical (nodes 53−103)
Vcool 53 0 PULSE({IO} {IP} 5 1us 1us {PW} 100)  ;Pulsed current source
VEmeas 53 54 0               ;Measuring the electrical current


*THE CIRCUIT*******************
BQPC 2 0 I={I(VEmeas)*SE*V(1)}          ;Peltier Cooling
X1 2 3 54 55 TEELEMENT
X2 3 4 55 56 TEELEMENT
X3 4 5 56 57 TEELEMENT
X4 5 6 57 58 TEELEMENT
```

```
X5  6  7  58  59  TEELEMENT
X6  7  8  59  60  TEELEMENT
X7  8  9  60  61  TEELEMENT
X8  9  10  61  62  TEELEMENT
X9  10  11  62  63  TEELEMENT
X10  11  12  63  64  TEELEMENT
X11  12  13  64  65  TEELEMENT
X12  13  14  65  66  TEELEMENT
X13  14  15  66  67  TEELEMENT
X14  15  16  67  68  TEELEMENT
X15  16  17  68  69  TEELEMENT
X16  17  18  69  70  TEELEMENT
X17  18  19  70  71  TEELEMENT
X18  19  20  71  72  TEELEMENT
X19  20  21  72  73  TEELEMENT
X20  21  22  73  74  TEELEMENT
X21  22  23  74  75  TEELEMENT
X22  23  24  75  76  TEELEMENT
X23  24  25  76  77  TEELEMENT
X24  25  26  77  78  TEELEMENT
X25  26  27  78  79  TEELEMENT
X26  27  28  79  80  TEELEMENT
X27  28  29  80  81  TEELEMENT
X28  29  30  81  82  TEELEMENT
X29  30  31  82  83  TEELEMENT
X30  31  32  83  84  TEELEMENT
X31  32  33  84  85  TEELEMENT
X32  33  34  85  86  TEELEMENT
X33  34  35  86  87  TEELEMENT
X34  35  36  87  88  TEELEMENT
X35  36  37  88  89  TEELEMENT
X36  37  38  89  90  TEELEMENT
X37  38  39  90  91  TEELEMENT
X38  39  40  91  92  TEELEMENT
X39  40  41  92  93  TEELEMENT
X40  41  42  93  94  TEELEMENT
X41  42  43  94  95  TEELEMENT
X42  43  44  95  96  TEELEMENT
X43  44  45  96  97  TEELEMENT
X44  45  46  97  98  TEELEMENT
X45  46  47  98  99  TEELEMENT
X46  47  48  99  100  TEELEMENT
X47  48  49  100  101  TEELEMENT
X48  49  50  101  102  TEELEMENT
```

```
X49  50  51  102  103  TEELEMENT
X50  51  52  103  0  TEELEMENT
BQPH  0  52  I={I(VEmeas)*SE*V(52)}          ;Peltier Heating

*THERMOELECTRIC SUBCIRCUIT*****
* These nodes define the X elements
.SUBCKT TEELEMENT 60 62 64 67
CPC  60  0  {Cth/6}                          ;Cold side Peltier Capacitance
RCth  60  61  {.5/K}                         ;Cold side thermal resistance
BQJ  0  61  I={I(VESCmeas)*I(VESCmeas)*R}    ;Joule Heating
CJ  61  0  {2*Cth/3}                         ;Joule Heating Capacitance
RHth  61  62  {.5/K}                         ;Hot side thermal resistance
CPH  62  0  {Cth/6}                          ;Hot side Peltier capacitance
VESCmeas  64  65  0                          ;Measuring current through the subsection
RE  65  66  {R}                              ;Subsection resistance
BS  66  67  V={SE*V(62,60)}                  ;Seebeck Voltage
.ENDS

*ANALYSIS AND RESULTS**********
.TRAN 0.01 6 4s 0.0001s
.OP
.PRINT TRAN V(1)
.END
```

C.7 AC Small Signal Si Equivalent Circuit Netlist

```
*MATERIAL PARAMETERS***********
.PARAM S   =      0.00027        ;Seebeck Coefficient                    [V/K]
.PARAM TK  =          150        ;Thermal Conductivity                   [W/m–K]
.PARAM ER  = 1.32657e−05         ;Electrical Resistivity                 [Ohms/m]
.PARAM CP  =        0.163        ;Specific Heat                          [J/kg–K]
.PARAM DEN =        1e+07        ;Density                                [kg/m^3]


*DEVICE PARAMETERS*************
.PARAM L   =        0.005        ;Device Length                          [m]
.PARAM A   =        1e−06        ;Device Area                            [m^2]
.PARAM N   =            1        ;Number of Thermoelements


*SIMULATION PARAMETERS*********
.PARAM TAMB=          300        ;Ambient Temperature                    [K]
.PARAM NDIS=           50        ;Number of Distributions


*CALCULATED PARAMETERS*********
.PARAM LE  = {L/NDIS}            ;Length per Distribution                [m]
.PARAM SE  = {N*S}               ;Device Seebeck                         [V/K]
.PARAM R   = {N*LE*ER/A}         ;Electrical Resistance per Distribution [Ohms]
.PARAM K   = {N*TK*A/LE}         ;Thermal Conductance per Distribution   [W/K]
.PARAM Rth = {1/K}               ;Thermal Resistance per Distribution    [K/W]
.PARAM Cth = {N*CP*DEN*A*LE}     ;Thermal Capacitance per Distribution   [J/K]


*INPUT/MEASURING NODES*********
* Thermal (nodes 1−52)
IC 0 1 0                         ;Cold side heat absorbed(QC = 0)
VCmeas 1 2 DC 0                  ;Measuring QC
VH 52 0 DC {TAMB}                ;Hot side temperature (TH=Tamb from heat sink)
* Electrical (nodes 53−103)
Vcool 53 0 AC 10m                ;AC signal with 10mV amplitude
VEmeas 53 54 0                   ;Measuring the electrical current


*THE CIRCUIT********************
BQPC 2 0 I={I(VEmeas)*SE*V(1)}        ;Peltier Cooling
X1 2 3 54 55 TEELEMENT
X2 3 4 55 56 TEELEMENT
X3 4 5 56 57 TEELEMENT
X4 5 6 57 58 TEELEMENT
X5 6 7 58 59 TEELEMENT
X6 7 8 59 60 TEELEMENT
X7 8 9 60 61 TEELEMENT
```

```
X8  9  10  61  62  TEELEMENT
X9  10  11  62  63  TEELEMENT
X10  11  12  63  64  TEELEMENT
X11  12  13  64  65  TEELEMENT
X12  13  14  65  66  TEELEMENT
X13  14  15  66  67  TEELEMENT
X14  15  16  67  68  TEELEMENT
X15  16  17  68  69  TEELEMENT
X16  17  18  69  70  TEELEMENT
X17  18  19  70  71  TEELEMENT
X18  19  20  71  72  TEELEMENT
X19  20  21  72  73  TEELEMENT
X20  21  22  73  74  TEELEMENT
X21  22  23  74  75  TEELEMENT
X22  23  24  75  76  TEELEMENT
X23  24  25  76  77  TEELEMENT
X24  25  26  77  78  TEELEMENT
X25  26  27  78  79  TEELEMENT
X26  27  28  79  80  TEELEMENT
X27  28  29  80  81  TEELEMENT
X28  29  30  81  82  TEELEMENT
X29  30  31  82  83  TEELEMENT
X30  31  32  83  84  TEELEMENT
X31  32  33  84  85  TEELEMENT
X32  33  34  85  86  TEELEMENT
X33  34  35  86  87  TEELEMENT
X34  35  36  87  88  TEELEMENT
X35  36  37  88  89  TEELEMENT
X36  37  38  89  90  TEELEMENT
X37  38  39  90  91  TEELEMENT
X38  39  40  91  92  TEELEMENT
X39  40  41  92  93  TEELEMENT
X40  41  42  93  94  TEELEMENT
X41  42  43  94  95  TEELEMENT
X42  43  44  95  96  TEELEMENT
X43  44  45  96  97  TEELEMENT
X44  45  46  97  98  TEELEMENT
X45  46  47  98  99  TEELEMENT
X46  47  48  99  100  TEELEMENT
X47  48  49  100  101  TEELEMENT
X48  49  50  101  102  TEELEMENT
X49  50  51  102  103  TEELEMENT
X50  51  52  103  0  TEELEMENT
BQPH  0  52  I={I(VEmeas)*SE*V(52)}          ;Peltier  Heating
```

```
*THERMOELECTRIC SUBCIRCUIT*****
* These nodes define the X elements
.SUBCKT TEELEMENT 60 62 64 67
CPC 60 0 {Cth/6}                                   ;Cold side Peltier Capacitance
RCth 60 61 {.5/K}                                  ;Cold side thermal resistance
BQJ 0 61 I={I(VESCmeas)*I(VESCmeas)*R}   ;Joule Heating
CJ 61 0 {2*Cth/3}                                  ;Joule Heating Capacitance
RHth 61 62 {.5/K}                                  ;Hot side thermal resistance
CPH 62 0 {Cth/6}                                   ;Hot side Peltier capacitance
VESCmeas 64 65 0                                   ;Measuring current through the subsection
RE 65 66 {R}                                       ;Subsection resistance
BS 66 67 V={SE*V(62,60)}                           ;Seebeck Voltage
.ENDS

*ANALYSIS AND RESULTS**********
.AC DEC 500 1u 1MEG
.OP
.PRINT AC I(VEmeas) V(54)
.END
```